BILINGUAL PUBLISHING GROUP

Journal of Geographical Research

Volume 6 • Issue 3 • July 2023
ISSN 2630-5070(Online)

Volume 6 Issue 3 • July 2023 • ISSN 2630-5070 (Online)

Journal of Geographical Research

BILINGUAL PUBLISHING GROUP

BILINGUAL PUBLISHING GROUP

Volume 6 | Issue 3 | July 2023 | Page1-80

Journal of Geographical Research

Contents

Articles

BILINGUAL PUBLISHING GROUP

Journal of Geographical Research

https://journals.bilpubgroup.com/index.php/jgr

ARTICLE

Combating Climate Change and Global Warming for a Sustainable Living in Harmony with Nature

V. Balaram

CSIR—National Geophysical Research Institute, Hyderabad, 500007, India

ABSTRACT

As humanity has been polluting the atmosphere with greenhouse gases, the planet is getting warmed up which is triggering the frequency and the intensity of extreme events like heat waves, dry conditions, wildfires, cyclones, tornadoes, lightning, and massive flooding all over the planet Earth. There is considerable evidence that the concentration of greenhouse gases, especially that of CO_2 has steadily increased in the atmosphere as a result of the indiscriminate use of fossil fuels around the world particularly during the last 70 years. The glaciers in the high mountain and polar regions are diminishing fast, sea levels are rising, and food production is being affected severely in certain parts of the world. In fact, the changing climate has currently become one of the major threats to the survival of civilization. The world scientific communities are warning of a climate emergency and requesting the decision makers to promptly respond and act to sustain life on planet Earth. To deliver net zero emissions by the year 2050, the whole world must phase out the technologies such as coal-powered thermal plants and diesel/petrol/gasoline-powered vehicles which release abundant amounts of CO_2 and other greenhouse gases into the atmosphere and invest in the development of clean energies such as hydel, wind, solar, space-solar, and nuclear energies. This transition to a low-carbon economy with the help of these technologies together with other technologies such as hydrogen fuel, fuel cells, electric vehicles, and massive plantations is expected to take our planet Earth to a safe zone in the coming 20-30 years.

Keywords: Greenhouse gases; Ocean acidification; Diminishing of glaciers; Sea level rise; Carbon capture; Direct air capture; Critical minerals in deep-sea

*CORRESPONDING AUTHOR:

Balaram, V., CSIR—National Geophysical Research Institute, Hyderabad, 500007, India; Email: balaram1951@yahoo.com

ARTICLE INFO

Received: 17 April 2023 | Revised: 19 June 2023 | Accepted: 25 June 2023 | Published Online: 29 June 2023

DOI: https://doi.org/10.30564/jgr.v6i3.5706

CITATION

Balaram, V., 2023. Combating Climate Change and Global Warming for a Sustainable Living in Harmony with Nature. Journal of Geographical Research. 6(3): 1-17. DOI: https://doi.org/10.30564/jgr.v6i3.5706

1. Introduction

Our planet is very complex and delicate in several ways, without taking proper steps to preserve its ecosystem related to life on Earth would not sustain itself. Currently, global warming is one of the biggest threats to the survival of the natural environment and humans with disastrous consequences such as long-term shifts in global weather patterns and temperatures (https://news.un.org/en/story/2022/05/1117842). In fact, the whole world is waging a war against nature for which man himself is responsible. Ever since the industrial revolution started about 150 years back, human activities especially related to power generation and various other industries, transportation, and agriculture have indiscriminately released huge amounts of major greenhouse gases (GHGs) such as carbon dioxide (CO_2), methane (CH_4), and nitrous oxide (N_2O) into the environment disrupting the natural phenomenon and the delicate ecosystem of the planet (https://www.epa.gov/ghgemissions/overview-greenhouse-gases). Concentrations of these GHGs are currently more abundant in the earth's atmosphere than at any time in the last 800,000 years. In 2021 our planet Earth reached a dark milestone of hitting over 150% of CO_2 value in the atmosphere compared to that of the pre-industrial times (https://www.noaa.gov/news-release/carbon-dioxide-now-more-than-50-higher-than-pre-industrial-levels). According to the National Oceanic and Atmospheric Administration (NOAA), the average surface temperature across land and ocean in 2021 was 0.86 °C warmer than the twentieth-century average of 13.9 °C, and 1.06 °C warmer than the pre-industrial period (https://www.climate.gov/news-features/understanding-climate/climate-change-global-temperature). In fact, the experiments conducted by the scientific community even in the 1800s gave hints of human-induced climate change as CO_2 and other gases are capable of altering the earth's climate. But by the 1950s, the subsequently generated data supported the global warming theory [1].

Carbon dioxide and other GHGs were found to be responsible for the increase in the average temperatures of the surface of the earth as well as oceans and their projected continuation due to the greenhouse effect. Further deeper studies indicated that the other general processes such as variations in solar radiation, deviations in the Earth's orbit, volcanic eruptions, mountain-building and continental drift, and changes in GHG concentrations are responsible for changes in the Earth's climate (https://www.bgs.ac.uk/discovering-geology/climate-change/what-causes-the-earths-climate-to-change/). On the other hand, the increased water stress, a rise in the frequency of extreme events such as heatwaves, floods, cyclones, snowstorms, poor agricultural productivity, drought conditions, extinction of different forms of fauna and flora, spreading of new diseases, etc., are the key indicators of climate change (https://climate.ec.europa.eu/climate-change/consequences-climate-change_en). Climate-related studies indicated that increased GHGs concentrations, land and ocean surface temperatures, sea level rise, and ocean acidification are the key indicators of climate change during the past few decades (**Figure 1**). The Intergovernmental Panel on Climate Change (IPCC) is a United Nations body set up in 1988 to assess the science around climate change, and to provide governments with scientific information which can be used to develop policies on reducing global warming. IPCC's 6th Assessment Report (AR6), which details the devastating consequences of GHG emissions around the world, was released in March 2023. It also identifies available, and cost-effective solutions to reduce GHG emissions to secure a safe, liveable future. The average increase in global temperatures is now about 1.1 °C above pre-industrial levels according to the IPCC (2023). To safeguard the Paris Agreement, there is a need to limit global warming to well below 2 °C, and if necessary drastic actions are required to pursue efforts to limit it to 1.5 °C. For example, the Himalayan ecosystem is very delicate and even the slightest changes in the climate can have long-lasting effects on such vulnerable regions [2]. The average global temperature across the year was around 14.9 °C, putting it around 1.2 °C rise above the average (**Figure 2**). The planet Earth

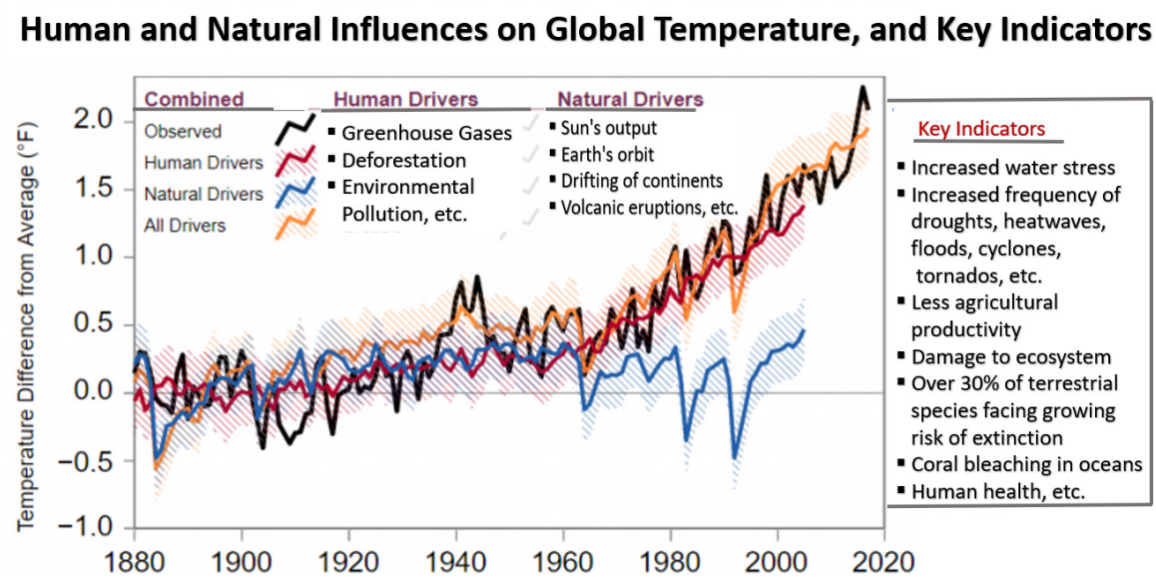

Figure 1. Natural and human factors are responsible for the earth's climate, and key indicators.

Source: Modified after U.S. Global Change Research Program, Fourth National Climate Assessment, Chapter 2: Our Changing Climate, 2017.

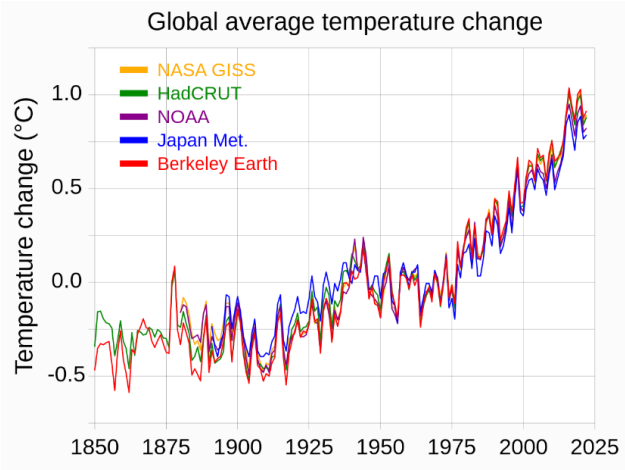

Figure 2. The increase in Earth's average surface temperature with time (from Wikipedia, 2023).

is neither too close nor too far away from the Sun and lies in a "Goldilocks zone" which is just right to support life—not too hot, not too cold with the planet's average surface temperature at 14.9 °C [3]. But currently, with remarkable changes in our climate, a lot of questions are arising. A recent study on a 300-foot-long core of mud from a lakebed high in the Peruvian Andes was found to preserve the history of the deformation and flow of glaciers for more than 700,000 years. This is one of the longest records of historical climate revealing the variations in temperature and precipitation based on geochemical and magnetic studies of the sediment [4]. Human activities such as industries, electric power generation by coal, agriculture, and transportation are the four top sources of GHGs which are responsible for almost all of the increase in greenhouse gases in the atmosphere over the last 150 years [5]. More pieces of evidence are seen in recent times about human-induced climate change [6]. Deforestation, agriculture, and the use of fossil fuels are the primary sources of CO_2. China, India, the US, Russia, and Japan are the biggest emitters of CO_2 in the world today.

2. Greenhouse effect

Between the year 1870 (the first industrial revolution) and today, the increase in global temperature is due to more fossil fuel burning (petroleum oil, natural gas, coal), which also increased the CO_2 levels from 280 ppm in preindustrial time to 423.46 ppm in June 2023 (NOAA, 2023 & https://www.co2.earth/daily-co2). The burning of fossil fuels and indiscriminate cutting of forests increases CO_2 in the atmosphere (15-35 km above the Earth's surface), and the increase in CO_2 causes more heat to be trapped in the Earth's atmosphere as CO_2 has the ability to absorb infrared radiation. As a result, global temperatures are rising. The Earth receives radiation during the

daytime from the Sun which is a flow of infrared radiation. Part of this is reflected back into space by the atmosphere, while the rest warms the planet during the day and is radiated back into space at night (https://earthobservatory.nasa.gov/features/EnergyBalance). During this delicate balance that prevailed in preindustrial times, the incoming heat was exactly offset by the amount lost to space, ensuring average global temperatures remained constant. But unfortunately, today, due to the drastic increase in GHGs, this balance is lost because some of the heat that should be radiated back into space gets trapped inside the atmosphere. Thus, the temperature is constantly rising as the concentrations of CO_2 which has about 82% share among greenhouse gases, along with other greenhouse gases such as CH_4, N_2O, and O_3, increase in the atmosphere. This is known as the greenhouse effect and these gases are trapping the infrared radiation and making the Earth warmer which is also called global warming [7]. In order to combat this phenomenon and to prevent the worst effects of climate change, humans must reduce the release of CO_2 and other GHGs into the atmosphere and this is the only option available for humanity. The rising temperatures could have catastrophic effects on ecosystems if these trends continue to persist. The rapid increase in temperature would wipe out species not able to adapt quickly enough to this warming environment which is already visible all across the planet. Polar ice caps could melt raising the sea levels and causing flooding of coastal cities. A number of pieces of evidence are being gathered on how human interference in the Earth's climate continues to impact global warming. Europe, the western US, and Canada lived through the warmest summer temperature records during the last 3-4 years due to extreme wildfires which burnt several towns to the ground and killed hundreds (https://climate.ec.europa.eu/climate-change/consequences-climate-change_en). In 2023 some of the European countries like Spain recorded the highest temperature of the season (https://www.worldweatherattribution.org/extreme-april-heat-in-spain-portugal-morocco-algeria-almost-impossible-without-climate-change/).

3. Rise in methane gas in the environment

The latest report from the IPCC leaves no doubt about the rising levels of CO_2 and the powerful link between methane (CH_4) and climate change has also been established already. Methane with more heat absorbing capacity has more warming potential and is 84 times stronger than CO_2 on a 20-year horizon [8]. Emissions of heat-trapping methane are rising all over the world, mostly due to agriculture, and intense fossil fuel use [9,10], with the current concentration of methane reporting at 1909 ppb against a pre-industrial time concentration of 722 ppb. The IPCC also highlighted the problem posed by methane, which has contributed as much as 0.5 °C of warming since preindustrial times, second only to CO_2 [11]. Last year, about 111 countries that were responsible for nearly half of the methane emissions promised to cut down methane emissions by 2030 at COP26 in 2021 (https://www.iea.org/reports/global-methane-tracker-2022/the-global-methane-pledge). Methane usually leaks from oil and gas pipelines during maintenance operations which is evidenced by the huge methane plumes from oil and gas seen on satellite maps. It is also produced by landfill, agriculture, and in coal production. Zhou et al. [12] evaluated the scale of methane emissions from the U.S. ammonia fertilizer industry and found that the majority of methane gets into the atmosphere through leakage only. At the same time, the methane emissions from the industrial sector have been vastly underestimated and are significantly higher. Recently Lauvaux et al. [13] focused their studies on detecting oil and gas leaks that can be plugged if companies want to invest in prevention. In addition, about 2% of the atmospheric methane is from the seafloor methane seepage due to the gas hydrate dissociation activity contributed by climate change [14,15]. Despite these recent studies, an appropriate understanding of the interplay between methane sources and sinks is not completely known.

4. Where from GHGs come and where do they go?

GHGs including CO_2 come from almost every human activity such as the burning of fossil fuels for transportation, electricity generation and running several industries, agriculture, land-use, and residential and commercial activities. In 2014, the top CO_2 emitters were China, the United States, the European Union, India, the Russian Federation, and Japan (https://www.epa.gov/ghgemissions/global-greenhouse-gas-emissions-data). Apart from coal-powered thermal power stations, transport, and several other industries, volcanic eruptions all over the world are some of the major sources of CO_2 (https://www.climate.gov/news-features/climate-qa/which-emits-more-carbon-dioxide-volcanoes-or-human-activities). Over the geological times, before the pre-industrial times, variations in atmospheric CO_2 depended mainly on volcanic emissions, which were difficult to estimate. For example, the Etna volcano in Italy releases an exceptional amount of CO_2 (9083 t/day) and contributes to 10% of global volcanic emissions [16]. But CH_4 and N_2O, mostly come from agriculture, and waste, and also from industries. For example, adipic acid is used in the production of industrial products such as nylon and polyurethanes and it is one of the largest sources of N_2O emissions [17]. China alone accounts for 94% of global annual N_2O emissions. Major contributors to GHG emissions in the USA in 2019 are shown in **Figure 3**. Only about 50% of the CO_2 from industrial emissions remains in the atmosphere. The remainder is approximately equally divided between uptake into the land biosphere and into the ocean. Most of the CO_2 is absorbed by the plants, trees, minerals, and microbes in the soils on the land, and oceans absorb a major portion, and the rest remains in the atmosphere (https://www.energy.gov/science/doe-explains-the-carbon-cycle).

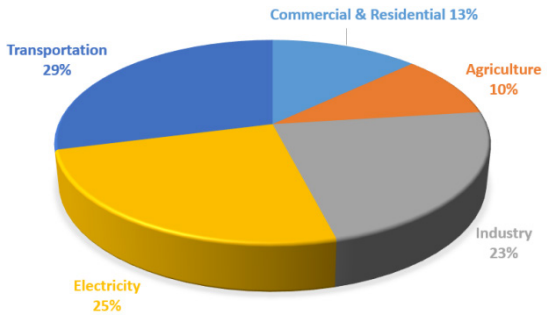

Figure 3. Approximate global GHG emissions from different sources in the US. Total emissions are 6,558 million metric tons of CO_2 equivalent.

Source: Modified after US EPA, 2019.

5. Increase in the frequency of extreme events

The devastating effects of climate change and nature's fury are visible in many forms such as higher average temperatures especially in colder regions, hotter summers even in regions such as Siberia, melting sea ice in places like Arctic and Antarctic regions, severe droughts, more wildfires, more powerful hurricanes, and stronger winter storms. These frequent and more intense extreme events are already signaling our planet's uncertain future. As a result, currently, millions of lives, and homes are destroyed in droughts and floods, and millions of people are dislocated and facing hunger in certain parts of the world as more than 3 billion people are living in highly vulnerable areas. These developments warrant more serious investigations. New data show, that the number of flooding and other hydrological events all over the world has quadrupled since 1980 and doubled since 2004 the world over [18]. Goswami et al. [19] reported that there is a significant rise in the trend of extreme rain events and extreme heat waves all over India in a warming environment. Extreme heat waves and wildfires are wreaking havoc around the globe every year, and these wildfires usually send plumes of smoke into the higher reaches of our atmosphere, where smoke particles interact with ozone. There is growing evidence that bushfire smoke reduces the concentration of ozone in the stratosphere (20-25 km from the Earth's surface), as the tiny carbon particles originating from these fires carry some chemical compounds containing chlorine which react with ozone, depleting its concentration [20]. Ozone is highly effective at blocking

damaging ultraviolet rays from the sun. Without this layer, many plants would die, while humans and other animals would be afflicted with skin cancers [21]. But it also contributes to the trapping of heat in the troposphere. The drought-hit countries like Kenya, Somalia, and Ethiopia in Africa have seen thousands of families being displaced from their homes whilst livestock losses have been huge. A small shift in the center means that more of the curve touches the extremes (**Figure 4**) and so heatwaves become more frequent and extreme as experienced, for example, in western Canada and the US in 2021. In recent years, the world has witnessed numerous wildfires in countries such as Turkey, Greece, Italy, Spain, Portugal, and France. The UK recorded over 40 ºC for the first time in history in 2022. In the usual weather cycle, hot weather creates more moisture and the water vapor in the air turns into droplets to create rain. The warmer it becomes, however, the more vapor there is in the atmosphere, resulting in more droplets and heavier rainfall, sometimes in a shorter space of time and over smaller areas such as experienced by the historic flooding in certain parts of China, Germany, Belgium, and the Netherlands in 2021, and Pakistan in 2022. Cyclones in ice-covered areas such as Greenland and Russia in the Arctic which can destroy sea ice and threaten people living in these regions are becoming more intense and frequent [22]. In fact, the polar regions and countries such as Britain, Spain, and Italy in Europe were hit hardest by global warming in 2022. Apart from Europe, there were significant heat record events in the Middle East, Central Asia, China, Pakistan, and parts of India. A comprehensive worldwide assessment of heatwaves down to regional levels has revealed that heatwaves have been increasing in frequency and duration since the 1950s in nearly every part of the world [23]. The extreme meteorological surface air temperatures recorded to date are –89.2 ºC in Antarctica, and 56.7 ºC in Death Valley, California [24]. Australia recorded the hottest day in 62 years as the temperature rose to 50.7 ºC in the coastal town of Onslow Western Australia in January 2022. Churu in Rajasthan, India recorded the highest temperature in the country in 2019 at 50.8 ºC, nine degrees above normal. In addition, the number of extremely hot days every year when the temperature reaches 50 ºC has doubled since the 1980s. India recorded its highest temperature in February in 2023 with an average maximum temperature was 29.54 ºC since recording began in 1901. Several other countries particularly in Asia and Europe are currently experiencing very high temperatures and severe dry conditions as rivers and freshwater lakes are getting dried up affecting their hydropower generation and agriculture leading to severe drought and global food crisis. Millions of fish are dying in some rivers in Europe and Australia due to ongoing heatwaves in addition to toxic algal blooms. Hotter temperatures are speeding up evaporation leading to increased salt levels in the surface water. Warmer water holds less oxygen than cold water leading to hypoxia conditions as fish require more oxygen in warmer conditions for their survival [25]. Sometimes the countries which are facing water stress are often accompanied by additional exposure to flooding (like India, and Pakistan) which have witnessed devastating rains and flooding with one-third of Pakistan under water in 2022 [26]. IPCC (2023) report says that the frequency and the intensity of those extreme events being witnessed these days are a result of global warming which will become more frequent and severe in the future as the planet continues to warm.

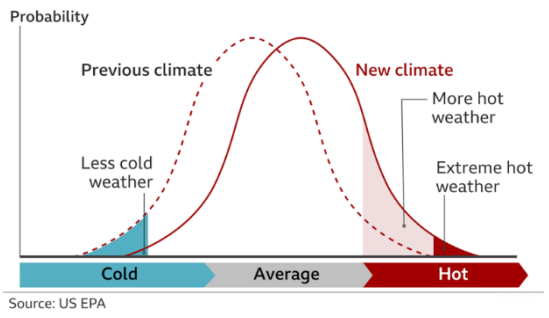

Figure 4. A small shift in climate can make a big difference in the weather conditions (US EPA).

6. Glaciers are shrinking and vanishing

Northern Alaska, Canada, Northern Europe, Northern Russia, Himalayas are melting faster at

the glacier bottom, shortening the glacier and reducing its mass, and the melt line moves upwards. A team of researchers [27] extracted ice cores from the glaciers on Mt. Hunter, in Alaska, and showed that the amount of water that melts currently is 60 times greater than it was prior to 1850. These studies are revealing that global temperatures are rising and in places like Greenland, the ice is vanishing and the destruction of coral reefs and other climate-related damages are hitting the world at an unprecedented rate. Satellite monitoring studies revealed that the overall rate of ice loss from Western Antarctica has increased five-fold over a 25-year period. It is interesting to note that Northern Hemisphere lost more ice (58%) in the past compared to that (42%) of the Southern Hemisphere [28]. Relatively a smaller number of studies were carried out on Himalayan glaciers due to problems with accessing remote and high-elevation glaciers, in politically unstable regions such as Nepal, Pakistan, China, and India, making these mountains difficult places to work especially for foreign scientists. In fact, Himalayan glaciers, are also showing increasing extreme temperatures and precipitation events, accelerating glacier-ice mass loss, permafrost degradation, frequent landslides, and a substantial shift in the seasonal riverine water supply. Terrestrial water storage and glacier show decreasing trends in most mountain regions across the planet and will have a greater influence on glaciers, groundwater, soil water, reservoirs, and lakes [29]. In addition, glacial lake outburst floods represent a major hazard in countries such as India, Pakistan, Peru and China where over 15 million people live in high mountain areas and are exposed to these risks [30]. Shukla and Sen [31], recommend satellite-based, real-time monitoring to develop a strong network of early flood warning systems in the Himalayas in order to check the devastating flash floods which are occurring in higher regions of the Himalayan mountains more frequently in recent times.

7. Sea levels rise and their impact on coastal zones

Climate-induced sea-level rises recorded along entire coastlines in different parts of the world have been a primary scientific focus in climate change studies for the past two decades as sea level rise is one of the primary indicators. The melting of global ice sheets is one of the primary causes of sea level rise, which has accelerated over recent decades. Since 1993, the global sea level has risen 4.3 cm (1.7 inches), 60% coming from the expansion of ocean water as its temperature rise, and 40% from melting glaciers. In coastal areas where 40% of the world's population lives, rising sea levels can increase the risk of flooding and endanger water sources. Pacific Island nations are already facing this threat, where people are being continuously displaced from their homes. Parts of cities such as Shanghai and Mumbai which are located in coastal areas are already experiencing flooding due to global warming, and the rise in sea levels along the coast (https://climate-adapt.eea.europa.eu/en/metadata/publications/ranking-of-the-worlds-cities-to-coastal-flooding/11240357). According to some studies, the global sea level is not rising steadily, rather it is getting faster every year. The global-mean sea level reconstruction shows a trend of 1.5 ± 0.2 mm/year from 1958 to 2014 [32]. Globally, the sea level has risen about eight inches (20 cm) since the beginning of the 20th century and more than two inches (5 cm) in the last 20 years alone. IPCC projections for 2100 range from 9 to 88 cm. Antarctica is covered by an up to 4 km thick ice layer and contains about 90% of fresh water on the surface of the Earth. This ice sheet in Antarctica is even shrinking in response to climate change and has lost over 3,000 billion tons of ice over 25 years [33]. Global sea level rise is 3 mm per year which is quite significant [34]. The rise in sea level not only encroaches on territories of coastal communities but also contributes to seawater intrusion on freshwater systems in coastal areas. Coastal wetlands are critical to Earth's ecosystem which is becoming increasingly vulnerable in the face of rising sea levels [6]. Recently, at the COP26 meeting in Glasgow, representatives of some 1.2 billion people, from the Climate Vulnerable Forum (CVF) consisting of countries from Latin America, Africa, Asia, the Caribbean, and the Pacific

were pushing the rest of the world to accept the idea of keeping the rise in global temperatures to under 1.5 ºC. Currently, the world's ocean surface heat is at record-breaking levels and its impacts are potentially catastrophic [35]. The vast amount of Arctic ice helps to cool the planet by reflecting the majority of the Sun's radiation back into space. But unfortunately, since the mid-1990s, there has been a marked decrease in sea ice cover in the Arctic Ocean [36] and there is a fear among the scientific communities that most of it could be gone in the coming 30 years [37]. According to some estimates, rising seas could submerge Jakarta (by 2100), Rio, and low-lying islands like those of the Maldives, where half a million people live barely a meter above the Indian Ocean, are under threat of rising sea levels driven by global warming. As a result, Indonesia is currently shifting its capital from Jakarta to the island of Borneo. The Mediterranean Sea level rise by 2100 will lead to a potential loss of about 192 km^2 of land along a coastline length of about 400 km of locations of tourist resorts, railways, airports, and heritage sites belonging to France, Spain, Tunisia, and Cyprus [38]. Coming to the Indian Ocean, the sea level rise is seen along the entire Indian coast and is rising faster than the global average [39,40].

8. Ocean acidification

Oceans cover over 70% of the Earth's surface and play a crucial role in sequestering significant quantities of CO_2 from the atmosphere. The free-floating algae called phytoplankton and tiny planktonic animals called zooplankton in oceans play a major role in the absorption of CO_2 and transfer of it to the ocean floor. The rise in CO_2 levels has led to more absorption and thereby more acidification of the oceans, leading to the weakening of the shells and skeletons of animals living in the sea. Concentrations of elements such as Mo, B, V, Cr, U, and Se and their isotopes in seawater and marine animals allow an understanding of ancient ocean chemistry and the ocean acidification process [41]. The replenishment of fish populations is threatened by ocean acidification caused by the uptake of additional CO_2 at the ocean surface which affects the marine ecosystem [42]. Ocean water's acidity level becomes higher when more CO_2 dissolves in the water, although some CO_2 returns to the atmosphere from the oceans and land reservoirs due to the outgassing effect. This makes it difficult for corals to build their skeleton [43] and coral reefs are under constant threat as the atmospheric CO_2 increases. In fact, both ocean warming and acidification are two of the greatest global threats to the persistence of coral reefs [44]. In addition, if the International Seabed Authority (ISA) gives permission to the mining of the seafloor for critical mineral resources, the disturbance to the ocean's ecosystems can also reduce their ability to absorb carbon to keep climate change under check [45].

9. Water scarcity

Groundwater has been extensively exploited worldwide during the last several decades. As a result, problems such as groundwater decline, and contamination are being currently confronted, and there is a definite threat to its sustainable use as a clean water source in the coming future unless proper early actions are taken. In addition, safeguarding groundwater quality is an essential part of sustainable water management and taking care of human health [25,46]. This deficiency of water is prevailing currently in several countries such as Madagascar, Yemen, India, and China, and in many European countries for several years across the globe. This situation has posed more serious questions about the disparity of rainfall caused by climate change and global warming, and over 4 billion people in the world are currently facing water scarcity [47]. At present, the whole world is suffering from the spread of new viral diseases such as COVID-19 and its several variants, monkeypox, and tomato flu, threatening the health of people the world over. According to Lim et al. [48], there is a threat of increased infectious disease risk likely in the future.

10. Effect on food production

As the global land surface temperature is on the

rise, our key food and fuel cropping systems are expected to affect our food production. In general, the increase in CO_2 concentrations together with the increase in global temperatures theoretically produces greater yields in crops. However, the majority of studies have shown that crop yields are downward trending due to the increase in the frequency of extreme weather events [49]. At temperatures above 40 °C, the photosynthesis rate slows down because the enzymes involved in the chemical reactions of photosynthesis are temperature sensitive and get destroyed at greater warming conditions. Excessive heat also can reduce the efficiency of enzymes that drive photosynthesis and can hinder plants' ability to regulate CO_2 uptake and water loss [50]. Hence with more and more global warming in the future, there is a definite threat to food production worldwide.

11. The sixth mass extinction?

There have been five mass biodiversity extinction events in the 4.54 billion years of the history of the Earth, all caused by dramatic and extreme natural phenomena such as prolonged ice age, sea-level changes, asteroid impacts, and voluminous volcanic eruptions in certain parts of the world. The massive volcanic eruptions leading to the formation of the Siberian Traps, and the enormous amounts of CO_2 led to the wiping out of 90% of all marine life during the largest extinction event (Permian-Triassic) in Earth's history [51]. Today, there is mounting evidence that the Earth is at the start of, or perhaps in the midst of the sixth mass extinction crisis which is underway with 7.5%-13% of species lost over the last 500 years, entirely caused by human activities [52]. Even if such an eventuality is unavoidable, some countries can most likely survive a global societal collapse and maintain their complex way of life according to a study by King and Jones [53]. For this study, five island nations, including Ireland and New Zealand were chosen as they could remain habitable through agriculture because of their vast land area for a small group of people they have, relatively cool temperatures, low weather variability, and other factors that make them more resistant to climate change. With favorable conditions such as a low population, large amounts of good quality agricultural land, and reliable domestic energy, New Zealand is expected to hold up the best, compared to others. So, even if climate change triggers a catastrophic global civilization collapse, humans will likely be able to keep going, at least, in some parts of the world. Coming to animals, polar bears are some of the largest terrestrial carnivores on Earth, but their fate is intimately tied to what happens to the Arctic's sea ice. Most polar bears are expected to struggle to survive in the Arctic by 2100 as the Arctic is continuously losing its ice. Standing almost four feet tall and weighing around 40 kg, emperor penguins in Antarctica are the world's largest penguins which need sea ice for their survival. A recent study estimates that 98% of colonies will be quasi-extinct by 2100 unless the world drastically reduces its greenhouse gas emissions [54]. Bumble bees which depend on wildflowers for their survival can also be affected as extremely high temperatures have negatively impacted most species of them over the past 120 years [55]. If greenhouse gas emissions and warmer temperatures are not controlled, some researchers estimate that life in oceans could be depleted severely within the coming 150 years [56]. The risk of species loss depends on how far global temperatures rise in the future.

12. Current, and upcoming technologies to limit warming, and steps to net zero

Cutting down CO_2 emissions to control climate change and reach net zero by 2050 is possible but not easy. So far, we have failed to reverse the 150-year trend of rising greenhouse gas emissions even after repeated warnings by the scientific communities for more than 30 years (IPCC, 2023). The UN secretary general is calling for countries to bring forward their plans for the effective reduction of GHG emissions for net zero by a decade or at least as close as possible to 2040. Innovative technologies such as solar-driven hydrogen production and fuel cell technologies [57,58], and space-solar power are likely to help to achieve sustainable goals and

for environmental planning by fulfilling the requirement of energy if they are technically feasible [59]. NASA and European Space Agency (ESA) are of the opinion that space-based solar power technology has the ability to increase energy independence and reduce greenhouse gas emissions. In addition, several countries have recognized the potential of wave power that could tackle the global energy crisis, support economic growth, and provide green energy [60]. Several studies are also currently focused on more efficient solar panels reaching efficiency levels nearing 50%. Four pioneering scientists who built more efficient electricity-generating silicon solar cells (from around 16-18% efficiency to about 25%) have won Queen Elizabeth Prize for Engineering in 2023. This is an example of the intensive efforts towards the development of technologies for tackling climate change, and the recognition and encouragement of the technologists and scientists who achieve stunning successes in this direction. The estimates of some scientists suggest that by the 2030s, solar will have more installed capacity than coal, oil, gas, nuclear, and hydro put together. Switching over to battery-powered electric vehicles or vehicles based on hydrogen fuel or using hydrogen fuel cells in the coming years will certainly help to reduce CO_2 and tackle climate change, despite the fact that there are also large uncertainties around the emissions associated with electric vehicle battery production. However, according to Plötz [61], fuel-cell electric vehicle technology will not play a major role in sustainable road transport in the future. The CO_2 concentration of about 425 ppm poses a difficult situation for high CO_2 capture capacities using sorption-desorption processes [62]. The magnitude of this crisis is gigantic, with about 40 gigatons/year of global CO_2 emission with no signs of shrinking [63]. Out of several technologies, technologies like direct air capture (DAC) which uses a 10% solution of KOH to capture CO_2 from the atmosphere, and carbon capture and storage (CCS) have emerged as indispensable tools in combating climate change and reaching their goal of net zero emissions. A lot of meetings and summits are being organized to discuss the latest developments by different international firms during the last couple of years. Unfortunately, the implementation of these and a few other critical and proven technologies has been very slow and inadequate [64]. Geological CCS technology involves the injection of CO_2 underground for long-term geological storage. It can help fight climate change by lowering industrial emissions [65]. Carbon dioxide would be injected into the ground for sequestration and geological medium like igneous and metamorphic rocks through a process known as carbon mineralization are needed for keeping the CO_2 underground [66] (**Figure 5**). In this context, olivine mineral is found to be very efficient in absorbing CO_2 and this process is also up-scalable [67].

Figure 5. Concept of carbon capture and storage.

Source: Modified after Schiermeier et al. [68].

Net zero emissions target means reducing carbon emissions to the greatest extent possible, by phasing out coal-powered thermal stations, switching over to alternate renewable energies such as hydro, solar, nuclear, hydrogen, and wave, and removing the remaining unavoidable emissions via removal technologies. Planting more and more trees is seen as a good option to tackle climate change. Replacing conventional fossil fuel vehicles with electric

vehicles which run on batteries would also significantly reduce CO_2 in the atmosphere improving air quality and human health [69]. Every nation on Earth understood the science behind climate change and the catastrophic consequences the people have to face if man does not act promptly to keep the rise in global temperatures well below 2 ºC by the end of this century and pursue efforts to keep it under 1.5 ºC. Several countries in Europe including the UK have already cut down the use of coal. India has set a target to ensure that 50% of its energy will be from renewable energy sources by 2030 and also to achieve net zero emissions latest by 2070 as per the declaration at the COP26 summit in Glasgow last year. In the meantime, a lot of studies are going on with regard to the reduction of CO_2 and converting it into useful products such as fuels, and chemicals which also contribute to the reduction of CO_2 levels and avoid catastrophic temperature rises across the world [70]. The easiest way to cut down the release of carbon is by using alternative ways to generate electricity such as the use of hydropower, nuclear fission, fusion (future), biomass, wind, geothermal, solar, hydrogen, and ocean energy [69,71]. Already some countries such as the UK are producing more electricity for the first time by using renewable sources such as wind power. At present, energy-efficient lighting is saving up to 75% of the energy currently used to light our homes, thanks to the invention of LED bulbs. In 2022, net fusion power was achieved for the first time, and some countries like the US, EU, UK, and Japan are heavily investing in nuclear-fusion power which is clean power and a breakthrough can be expected at any time in the near future [72].

Supply of critical metals required for green technology applications

For the whole world to deliver net zero by 2050, large-scale mining is more critical for metals such as Li, Cu, Ni, Co, Pt, Pd, REE, Ga, W, Te, and In, as these metals are essential for green technology applications such as making wind turbines, solar panels, fuel-cells, electric vehicles, and data storage systems required to transition to a low-carbon economy and for a sustainable energy future. Since land-based mineral deposits are dwindling fast, sea-bed resources are seen as a new resource frontier for mineral exploration and extraction [73-75]. As the land ore deposits are becoming scarce for some of these critical metals, there is an urgent need to look for alternative resources [76]. As vast mineral wealth is available in the seabed, the demand for exploiting critical minerals in the deep sea is rising in recent times. But what about the ecological and environmental consequences of mining the ocean which covers 71% of the planet's surface, and in turn is the habitat of the vast majority (97%) of living organisms? [45,77]. The oceans are an essential part of the biosphere, influencing several areas such as climate, food, health, and overall well-being.

13. United and rigorous global efforts only can resolve this crisis!

Many nations are not able to achieve their sustainable development goals such as poverty alleviation, quality healthcare, and economic growth due to climate change-driven lethal heatwaves and other climate change-driven extreme events [78]. Unfortunately, each country takes a different track toward the efforts for the mitigation of climate change. The big oil companies obtain approvals and licenses with the promise that they store huge amounts of CO_2 underground by CCS technology but fail to reach the promised storage goals. The EU targets to cut down all greenhouse gases by 2050. China's net-zero plan focuses on balancing CO_2 emissions by 2060. The UK announced that it would reach net zero greenhouse-gas emissions by 2050. Top oil exporter Saudi Arabia targets net zero by 2060, and Australia pledges to reach net zero emissions by 2050. But without more clear strategies by different countries behind achieving net zero targets, it's very difficult to evaluate the impact. However, according to Rogelj et al. [11] the current pledges and actions by different governments together with technological advancements, the world will be able to witness the decline of GHG only after 2050 through united and rigorous global efforts (**Figure 6**).

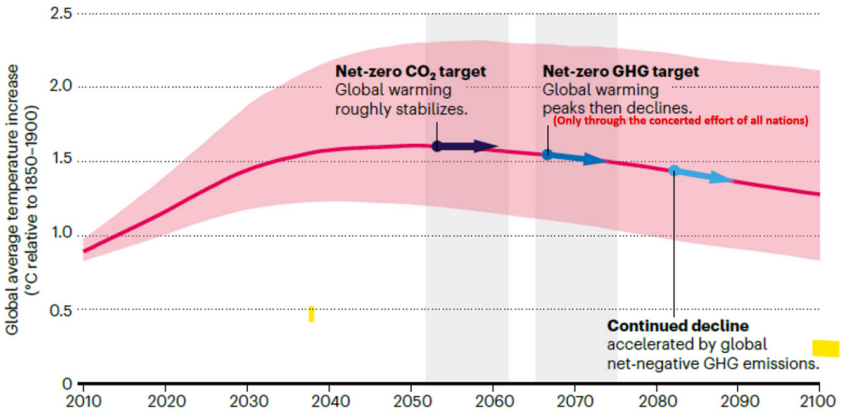

Figure 6. Estimated global temperature peaks (in pink) and declines (arrows) under net-zero GHG emissions.

Source: Modified after [11].

14. Conclusions and future

At the recent 26th United Nations Climate Change Conference of the Parties (COP26), over 127 countries committed to net zero targets which will limit global warming to 1.5 ºC above pre-industrial levels. Several scientists believe that the Paris Climate Agreement's goal to limit global warming in this century to 2 ºC is certainly within reach. All governmental bodies are making climate emergency declarations. It is possible to reach net zero carbon emissions, but it is not going to be easy and there is a long road ahead to net zero. With available emission budgets defined by the 2 ºC target itself looked challenging, the goal of achieving 1.5 ºC looks certainly harder unless united and rigorous global efforts are made. A coordinated effort of all nations is required to switch over from fossil fuels to renewable energy systems such as solar, wind, and nuclear for electricity generation (**Figure 6**). The necessary technologies have to be developed to remove excess CO_2 and other GHGs, and particulate pollution from the atmosphere, and limit CO_2 emissions by planting more and more trees. Every individual must understand the severity of this situation and contribute toward tackling climate change. Children should be taught the cause, effects, and how to combat climate change in depth even from high school. Any further delay in concerted global action will miss a brief and rapidly closing window to secure a liveable future. In fact, all of us can be very optimistic about the restoration of the natural climatic conditions as targeted, just as the notable recovery of the protective ozone layer in the upper stratosphere has been observed in recent times due to the complete ban on ozone-depleting substances. The UN Secretary-General António Guterres also said that the restoration of the ozone layer was "an encouraging example of what the world can achieve when we work together".

Conflict of Interest

There is no conflict of interest.

Acknowledgement

The author thanks Dr. Prakash Kumar, Director of CSIR-NGRI, Hyderabad, for his support and encouragement. The contents of this manuscript were presented in part by the author at > 70 INSPIRE Science Camps organized by the Department of Science and Technology (DST), New Delhi, Government of India, in different Universities and Academic Institutions across the country, during the last ~15 years, and also at the Trent Lott Geospatial and Visualization Research Center, and the Department of Chemistry, Jackson State University, Jackson, MS, USA in 2010.

References

[1] Le Treut, H., Somerville, R., Cubasch, U., et al.,

2007. Historical overview of climate change. Climate change 2007: The physical science basis. Contribution of Working Group I to the Fourth Assessment Report of the Intergovernmental Panel on Climate Change. Cambridge University Press: Cambridge, United Kingdom and New York, NY, USA.

[2] Kc, K.B., Tzadok, E., Pant, L., 2022. Himalayan ecosystem services and climate change driven agricultural frontiers: A scoping review. Discover Sustainability. 3(1), 35.
DOI: https://doi.org/10.1007/s43621-022-00103-9

[3] Isokangas, E., Rozanski, K., Rossi, P.M., et al., 2015. Quantifying groundwater dependence of a sub-polar lake cluster in Finland using an isotope mass balance approach. Hydrology and Earth System Sciences. 19(3), 1247-1262.

[4] Rodbell, D.T., Hatfield, R.G., Abbott, M.B., et al., 2022. 700,000 years of tropical Andean glaciation. Nature. 607(7918), 301-306.
DOI: https://doi.org/10.1038/s41586-022-04873-0

[5] Perera, F., 2018. Pollution from fossil-fuel combustion is the leading environmental threat to global pediatric health and equity: Solutions exist. International Journal of Environmental Research and Public Health. 15(1), 16.
DOI: https://doi.org/10.3390/ijerph15010016

[6] Weston, N.B., Rodriguez, E., Donnelly, B., et al., 2023. Recent acceleration of wetland accretion and carbon accumulation along the US East Coast. Earth's Future. 11(3), e2022EF003037.
DOI: https://doi.org/10.1029/2022EF003037

[7] Gadani, H., Vyas, A., 2011. Anesthetic gases and global warming: Potentials, prevention and future of anesthesia. Anesthesia, Essays and Researches. 5(1), 5.
DOI: https://doi.org/10.4103/0259-1162.84171

[8] Zhang, Z., Poulter, B., Feldman, A.F., et al., 2023. Recent intensification of wetland methane feedback. Nature Climate Change. 13(5), 430-433.
DOI: https://doi.org/10.1038/s41558-023-01629-0

[9] Jackson, R.B., Saunois, M., Bousquet, P., et al., 2020. Increasing anthropogenic methane emissions arise equally from agricultural and fossil fuel sources. Environmental Research Letters. 15(7), 071002.
DOI: https://doi.org/10.1088/1748-9326/ab9ed2

[10] Cheng, C.H., Redfern, S.A., 2022. Impact of interannual and multidecadal trends on methane-climate feedbacks and sensitivity. Nature Communications. 13(1), 3592.
DOI: https://doi.org/10.1038/s41467-022-31345-w

[11] Rogelj, J., Geden, O., Cowie, A., et al., 2021. Net-zero emissions targets are vague: Three ways to fix. Nature. 591(7850), 365-368.
DOI: https://doi.org/10.1038/d41586-021-00662-3

[12] Zhou, X., Passow, F.H., Rudek, J., et al., 2019. Estimation of methane emissions from the US ammonia fertilizer industry using a mobile sensing approach. Elementa: Science of the Anthropocene. 7, 19.
DOI: https://doi.org/10.1525/elementa.358

[13] Lauvaux, T., Giron, C., Mazzolini, M., et al., 2022. Global assessment of oil and gas methane ultra-emitters. Science. 375(6580), 557-561.
DOI: https://doi.org/10.1126/science.abj4351

[14] Ruppel, C.D., Kessler, J.D., 2017. The interaction of climate change and methane hydrates. Reviews of Geophysics. 55(1), 126-168.
DOI: https://doi.org/10.1002/2016RG000534

[15] Clemens, S.C., Thirumalai, K., Oppo, D., 2023. Indian margin methane hydrate dissociation recorded in the carbon isotopes of benthic (Miliolida) foraminifera. Earth and Planetary Science Letters. 609, 118101.
DOI: https://doi.org/10.1016/j.epsl.2023.118101

[16] Bragagni, A., Mastroianni, F., Münker, C., et al., 2022. A carbon-rich lithospheric mantle as a source for the large CO_2 emissions of Etna volcano (Italy). Geology. 50(4), 486-490.
DOI: https://doi.org/10.1130/G49510.1

[17] Wu, T., Niu, Z., Feng, L., et al., 2021. Performance analysis of VPSA process for separating N_2O from adipic acid tail gas. Separation and Purification Technology. 256, 117750.
DOI: https://doi.org/10.1016/j.seppur.2020.117750

[18] Cai, W., Wang, G., Santoso, A., et al., 2015.

Increased frequency of extreme La Niña events under greenhouse warming. Nature Climate Change. 5(2), 132-137.
DOI: https://doi.org/10.1038/nclimate2492

[19] Goswami, B.N., Venugopal, V., Sengupta, D., et al., 2006. Increasing trend of extreme rain events over India in a warming environment. Science. 314(5804), 1442-1445.
DOI: https://doi.org/10.1126/science.1132027

[20] Solomon, S., Dube, K., Stone, K., et al., 2022. On the stratospheric chemistry of midlatitude wildfire smoke. Proceedings of the National Academy of Sciences. 119(10), e2117325119.
DOI: https://doi.org/10.1073/pnas.2117325119

[21] Lucas, R.M., Norval, M., Neale, R.E., et al., 2015. The consequences for human health of stratospheric ozone depletion in association with other environmental factors. Photochemical & Photobiological Sciences. 14(1), 53-87.
DOI: https://doi.org/10.1039/c4pp90033b

[22] Zhang, X., Tang, H., Zhang, J., et al. (editors), 2022. Continuing intensification of arctic cyclone activity. AGU Fall Meeting; 2022 Dec 12-16; Chicago, IL.

[23] Perkins-Kirkpatrick, S.E., Lewis, S.C., 2020. Increasing trends in regional heat waves. Nature Communications. 11, 3357.
DOI: https://doi.org/10.1038/s41467-020-16970-7

[24] Andrew, C., 2017. Global temperature and life. Principles of thermal ecology: Temperature, energy, and life. Oxford University Press: Oxford. pp. 308-328.
DOI: https://doi.org/10.1093/oso/9780199551668.003.0014

[25] Balaram, V., Copia, L., Kumar, U.S., et al., 2023. Pollution of water resources, causes, application of ICP-MS techniques in hydrological studies, monitoring, and management. Geosystems and Geoenvironment. 2(4), 100210.
DOI: https://doi.org/10.1016/j.geogeo.2023.100210

[26] Warren, R., Andrews, O., Brown, S., et al., 2022. Quantifying risks avoided by limiting global warming to 1.5 or 2 °C above pre-industrial levels. Climatic Change. 172, 39.
DOI: https://doi.org/10.1007/s10584-021-03277-9

[27] Winski, D., Osterberg, E., Kreutz, K., et al., 2018. A 400-year ice core melt layer record of summertime warming in the Alaska Range. Journal of Geophysical Research: Atmospheres. 123(7), 3594-3611.
DOI: https://doi.org/10.1002/2017JD027539

[28] Slater, T., Lawrence, I.R., Otosaka, I.N., et al., 2021. Earth's ice imbalance. The Cryosphere. 15(1), 233-246.
DOI: https://doi.org/10.5194/tc-15-233-2021

[29] Li, X., Wang, L., Hu, B., et al., 2023. Contribution of vanishing mountain glaciers to global and regional terrestrial water storage changes. Frontiers in Earth Science. 11, 1134910.
DOI: https://doi.org/10.3389/feart.2023.1134910

[30] Taylor, C., Robinson, T.R., Dunning, S., et al., 2023. Glacial lake outburst floods threaten millions globally. Nature Communications. 14, 487.
DOI: https://doi.org/10.1038/s41467-023-36033-x

[31] Shukla, T., Sen, I.S., 2021. Preparing for floods on the Third Pole: Satellite-based real-time monitoring is needed for Himalayan glacial catchments. Science. 372(6539), 232-234.
DOI: https://doi.org/10.1126/science.abh3558

[32] Frederikse, T., Jevreva, S., Riva, R.E.M., et al., 2018. Consistent sea-level reconstruction and its budget on basin and global scales over 1958-2014. American Meteorological Society. 31(3), 1267-1280.
DOI: https://doi.org/10.1175/JCLI-D-17-0502.1

[33] Davison, B.J., Hogg, A.E., Rigby, R., et al., 2023. Sea level rise from West Antarctic mass loss significantly modified by large snowfall anomalies. Nature Communications. 14, 1479.
DOI: https://doi.org/10.1038/s41467-023-36990-3

[34] Wilson, D.J., Bertram, R.A., Needham, E.F., et al., 2018. Ice loss from the East Antarctic Ice Sheet during late Pleistocene inter-glacials. Nature. 561, 383-386.
DOI: https://doi.org/10.1038/s41586-018-0501-8

[35] Cheng, L., Abraham, J., Trenberth, K.E., et al., 2023. Another year of record heat for the oceans. Advances in Atmospheric Sciences. 40(6), 963-

974.
DOI: https://doi.org/10.1007/s00376-023-2385-2

[36] Ivanov, V., 2023. Arctic sea ice loss enhances the oceanic contribution to climate change. Atmosphere. 14(2), 409.
DOI: https://doi.org/10.3390/atmos14020409

[37] Hu, A., Meehl, G.A., Han, W., et al., 2009. Transient response of the MOC and climate to potential melting of the greenland ice sheet in the 21st century. Geophysical Research Letters. 36(10).
DOI: https://doi.org/10.1029/2009GL037998

[38] Antonioli, F., Falco, G.D., Presti, V.L., et al., 2020. Relative sea-level rise and potential submersion risk for 2100 on 16 coastal plains of the Mediterranean Sea. Water. 12(8), 2173.
DOI: https://doi.org/10.3390/w12082173

[39] Unnikrishnan, A.S., Nidheesh, A.G., Lengaigne, M., 2015. Sea-level-rise trends off the Indian coasts during the last two decades. Current Science. 108(10), 966-971.

[40] Krishnan, R., Sanjay, J., Gnanaseelan, C., et al., 2021. Assessment of climate change over the Indian Region. A report of the Ministry of Earth Sciences (MoES), Government of India. Springer Nature: Switzerland AG.
DOI: https://doi.org/10.1007/978-981-15-4327-2

[41] Balaram, V., Rahaman, W., Roy, P., 2022. Recent advances in MC-ICP-MS applications in Earth and environmental sciences: Challenges and solutions. Geosystems and Geoenvironment. 1(2), 100019.
DOI: https://doi.org/10.1016/j.geogeo.2021.100019

[42] Munday, P.L., Dixson, D.L., McCormick, M.I., et al., 2010. Replenishment of fish populations is threatened by ocean acidification. Proceedings of the National Academy of Sciences. 107(29), 12930-12934.
DOI: https://doi.org/10.1073/pnas.1004519107

[43] Sulpis, O., Boudreau, B.P., Mucci, A., et al., 2018. Current $CaCO_3$ dissolution at the seafloor caused by anthropogenic CO_2. Proceedings of the National Academy of Sciences. 115(46), 11700-11705.
DOI: https://doi.org/10.1073/pnas.1804250115

[44] Cornwall, C.E., Comeau, S., Putnam, H., et al., 2022. Impacts of ocean warming and acidification on calcifying coral reef taxa: Mechanisms responsible and adaptive capacity. Emerging Topics in Life Sciences. 6(1), 1-9.
DOI: https://doi.org/10.1042/ETLS20210226

[45] Balaram, V., 2023. Deep-sea mineral deposits as a future source of critical metals, and environmental issues—a brief review. Minerals and Mineral Materials. 2(2), 5.
DOI: https://doi.org/10.20517/mmm.2022.12

[46] Balaram, V., Rani, A., Rathore, D.P.S., 2022. Uranium in groundwater in parts of India and world: A comprehensive review of sources, impact to the environment and human health, analytical techniques, and mitigation technologies. Geosystems and Geoenvironment. 1(2), 100043.
DOI: https://doi.org/10.1016/j.geogeo.2022.100043

[47] Mekonnen, M.M., Hoekstra, A.Y., 2016. Four billion people facing severe water scarcity. Science Advances. 2(2), e1500323.
DOI: https://doi.org/10.1126/sciadv.1500323

[48] Lim, D.K., Kim, J.W., Kim, J.K., 2022. Effects of climatic factors on the prevalence of influenza virus infection in Cheonan, Korea. Environmental Science and Pollution Research. 29(39), 59052-59059.
DOI: https://doi.org/10.1007/s11356-022-20070-y

[49] Mirón, I.J., Linares, C., Díaz, J., 2023. The influence of climate change on food production and food safety. Environmental Research. 216, 114674.
DOI: https://doi.org/10.1016/j.envres.2022.114674

[50] Moore, C.E., Hensold, K.M., Lemonnier, P., et al., 2021. The effect of increasing temperature on crop photosynthesis: From enzymes to ecosystems. Journal of Experimental Botany. 72(8), 2822-2844.
DOI: https://doi.org/10.1093/jxb/erab090

[51] Penn, J.L., 2022. Avoiding ocean mass extinction from climate warming. Science. 376(6592), 524-526.
DOI: https://doi.org/10.1126/science.abe9039

[52] Cowie, R.H., Bouchet, P., Fontaine, B., 2022.

The sixth mass extinction: Fact, fiction or speculation? Biological Reviews. 97(2), 640-663. DOI: https://doi.org/10.1111/brv.12816

[53] King, N., Jones, A., 2021. An analysis of the potential for the formation of 'nodes of persisting complexity'. Sustainability. 13(15), 8161. DOI: https://doi.org/10.3390/su13158161

[54] Jenouvrier, S., Che-Castaldo, J., Wolf, S., et al., 2021. The call of the emperor penguin: Legal responses to species threatened by climate change. Global Change Biology. 27(20), 5008-5029. DOI: https://doi.org/10.1111/gcb.15806

[55] Jackson, M.H., Johnson, S.A., Morandin, L.A., et al., 2022. Climate change winners and losers among North American bumblebees. Biology Letters. 18(6), 071002 DOI: https://doi.org/10.1098/rsbl.2021.0551

[56] Crichton, K.A., Wilson, J.D., Ridgwell, A., et al., 2023. What the geological past can tell us about the future of the ocean's twilight zone. Nature Communications. 14, 2376. DOI: https://doi.org/10.1038/s41467-023-37781-6

[57] Song, H., Luo, S., Huang, H., et al., 2022. Solar-driven hydrogen production: Recent advances, challenges, and future perspectives. ACS Energy Letters. 7(3), 1043-1065. DOI: https://doi.org/10.1021/acsenergylett.1c02591

[58] Kastell, D., 2022. Hydrogen storage technology for aerial vehicles. Fuel cell and hydrogen technologies in aviation. Springer Nature: Switzerland AG.

[59] Dakora, J.D., Davidson, I.E., Sharma, G. (editors), 2020. Review of modern solar power satellite and space rectenna systems. 2020 International Conference on Artificial Intelligence, Big Data, Computing and Data Communication Systems (icABCD); 2020 Aug 6-7; Durban, South Africa. New York: IEEE. DOI: https://doi.org/10.1109/icabcd49160.2020.9183884

[60] Jin, S., Greaves, D., 2021. Wave energy in the UK: Status review and future perspectives. Renewable and Sustainable Energy Reviews. 143, 110932. DOI: https://doi.org/10.1016/j.rser.2021.110932

[61] Plötz, P., 2022. Hydrogen technology is unlikely to play a major role in sustainable road transport. Nature Electronics. 5, 8-10.

[62] Chen, H., Dong, H., Shi, Z., et al., 2023. Direct air capture (DAC) and sequestration of CO_2: Dramatic effect of coordinated Cu (II) onto a chelating weak base ion exchanger. Science Advances. 9(10), eadg1956. DOI: https://doi.org/10.1126/sciadv.adg1956

[63] Friedlingstein, P., O'Sullivan, M., Jones, M.W., et al., 2022. Global carbon budget 2022. Earth System Science Data. 14(11), 4811-4900. DOI: https://doi.org/10.5194/essd-14-4811-2022

[64] Morrow, D.R., 2021. Is there a role for carbon capture and storage in a just transition? One Earth. 4(11), 1546-1547. DOI: https://doi.org/10.1016/j.oneear.2021.10.022

[65] Meckel, T.A., Bump, A.P., Hovorka, S.D., et al., 2021. Carbon capture, utilization, and storage hub development on the Gulf Coast. Greenhouse Gases: Science and Technology. 11(4), 619-632. DOI: https://doi.org/10.1002/ghg.2082

[66] Shaw, R., Mukherjee, S., 2022. The development of carbon capture and storage (CCS) in India: A critical review. Carbon Capture Science & Technology. 2, 100036. DOI: https://doi.org/10.1016/j.ccst.2022.100036

[67] Vink, J.P., Knops, P., 2023. Size-fractionated weathering of olivine, its CO_2-sequestration rate, and ecotoxicological risk assessment of nickel release. Minerals. 13(2), 235. DOI: https://doi.org/10.3390/min13020235

[68] Schiermeier, Q., Tollefson, J., Scully, T., et al., 2008. Energy alternatives: Electricity without carbon. Nature. 454, 816-823. DOI: https://doi.org/10.1038/454816a

[69] Balaram, V., 2020. Environmental impact of Pt, Pd and Rh emissions from autocatalytic converters—A brief review of the latest developments. Handbook of environmental materials management. Springer Nature: Switzerland AG. pp. 1-37.

[70] Yao, B., Xiao, T., Makgae, O.A., et al., 2020.

Transforming carbon dioxide into jet fuel using an organic combustion-synthesized Fe-Mn-K catalyst. Nature Communications. 11(1), 6395. DOI: https://doi.org/10.1038/s41467-020-20214-z

[71] Yadav, K., Sircar, A., 2021. Geothermal energy provinces in India: A renewable heritage. International Journal of Geoheritage and Parks. 9(1), 93-107. DOI: https://doi.org/10.1016/j.ijgeop.2020.12.002

[72] Betti, R., 2023. A milestone in fusion research is reached. Nature Reviews Physics. 5(1), 6-8. DOI: https://doi.org/10.1038/s42254-022-00547-y

[73] Hein, J.R., Mizell, K., Koschinsky, A., et al., 2013. Deep-ocean mineral deposits as a source of critical metals for high-and green-technology applications: Comparison with land-based resources. Ore Geology Reviews. 51, 1-14. DOI: http://dx.doi.org/10.1016/j.oregeorev.2012.12.001

[74] Balaram, V., 2019. Rare earth elements: A review of applications, occurrence, exploration, analysis, recycling, and environmental impact. Geoscience Frontiers. 10(4), 1285-1303. DOI: https://doi.org/10.1016/j.gsf.2018.12.005

[75] Balaram, V., 2023. Potential future alternative resources for rare earth elements: Opportunities and challenges. Minerals. 13(3), 425. DOI: https://doi.org/10.3390/min13030425

[76] Toro, N., Galvez, E., Saldana, M., et al., 2022. Submarine mineral resources: A potential solution to political conflicts and global warming. Minerals Engineering. 179, 107441. DOI: https://doi.org/10.1016/j.mineng.2022.107441

[77] Turner, P.J., 2019. Deep-sea mining and environmental management. Encyclopedia of Ocean Sciences, 3rd Edition. 6, 507-515. DOI: https://doi.org/10.1016/B978-0-12-409548-9.11106-6

[78] Debnath, R., Bardhan, R., Bell, M.L., 2023. Lethal heatwaves are challenging India's sustainable development. PLOS Climate. 2(4), e0000156. DOI: https://doi.org/10.1371/journal.pclm.0000156

BILINGUAL PUBLISHING GROUP

Journal of Geographical Research

https://journals.bilpubgroup.com/index.php/jgr

ARTICLE

Spatiotemporal Analysis of Land Use Land Cover Mapping and Change Detection in Dambatta Local Government Area

***David Sesugh Aule*[1*], *Mamman Saba Jibril*[1], *Ali Hussain Idris*[2]**

[1] *Department of Geography, Nigerian Defence Academy, Kaduna, PMB 2109, Nigeria*

[2] *Nigerian Airforce Headquarters, Abuja, PMB 0244, Nigeria*

ABSTRACT

This research studied the spatiotemporal changes in land use (LU)/land cover (LC) in Dambatta local government area, with a view to identifying the effect arising from the observable changes in land use patterns. The imageries used in the study were obtained from the National Space Research and Development Agency (NARSDA), Abuja. Spatial analytical techniques and descriptive statistical techniques were employed to analyze the data. The results showed 66.8% reduction in agricultural lands, 45.5% reduction in vegetation cover, 223.2% increase in built-up areas, 269.1% increase in bare lands and 70% increase in water bodies within the 20 years. Spatio-temporal analysis of the three imageries revealed that agricultural lands were largely been taken over by urbanization while vegetation had rapidly given way to bare lands within the 20 years. It was observed that these changes resulted from anthropogenic activities, environmental factors and climate change. These result in the loss of farmlands, inadequate food supply, unemployment, inadequate industrial raw materials, reduction in revenue generated, forest depletion, desertification, wildlife extinction and temperature increase. While it is recommended that reforestation, land reclamation and irrigation agriculture should be promoted in the area, it is also suggested that further research should focus on the impact of climate change on land cover change in the area.

Keywords: Dambatta; GIS; Land cover; Land use; Spatio-temporal changes

1. Introduction

Most often, land use and land cover are used interchangeably, however, there is a clear difference between them. Land cover refers to those things that cover part of the earth's surface like grassland and

*CORRESPONDING AUTHOR:
David Sesugh Aule, Department of Geography, Nigerian Defence Academy, Kaduna, PMB 2109, Nigeria; Email: auleds@yahoo.com

ARTICLE INFO
Received: 6 May 2023 | Revised: 21 June 2023 | Accepted: 27 June2023 | Published Online: 17 July 2023
DOI: https://doi.org/10.30564/jgr.v6i3.5707

CITATION
Aule, D.S., Jibril, M.S., Idris, A.H., 2023. Spatiotemporal Analysis of Land Use Land Cover Mapping and Change Detection in Dambatta Local Government Area. Journal of Geographical Research. 6(3): 18-28. DOI: https://doi.org/10.30564/jgr.v6i3.5707

forest. Land use on the other hand refers to the manner in which the land is utilized. Land uses include activities such as wildlife management, agricultural practices, urbanization, recreation, etc. [1,2]. A given land use may take place on one, or more than one piece of land and several land uses may occur on the same piece of land [3]. Changes in land cover may occur when one type of land cover is totally replaced by another, while changes in land use may result from the modification of land cover types [4-6]. The predominant drivers of these scenarios include anthropogenic activities causing land subsidence, storms and sea level rise [7-10].

Remote sensing techniques and geographic information system (GIS) can be integrated into a single tool to perform different tasks including detecting land use and land cover changes [11-13]. Many researchers have studied the relationship between land surface temperature and land use/land cover NDVI using remote sensing and geographic information system (GIS). Amongst these, Campbell [14] studied the impact of urbanization on the thermal environment of the Bangkok Metropolitan Area. The study used normalized difference vegetation index (NDVI) to extract land use/land cover information from remote sensing images of different time periods and then analyzed the surface temperature retrieved from the thermal infrared band. The results showed that urban/built-up areas expanded dramatically with equally decreasing agricultural land. Moreover, temperature differences between the urban/built-up and the surrounding rural areas significantly widened. Similar studies with related results were conducted [15-20].

The use of remotely sensed data in the form of satellite imagery as a source of reliable information for surveying, classification, mapping and monitoring cannot be over-emphasized. Land use/cover mapping is one of the commonest uses of remotely sensed data. It has been extensively used in supervised image classification where a prior knowledge of all cover types to be mapped within the classified scene is assumed [1]. Other variants of supervised classification developed in recent years include decision trees [21-24]. It seems evident that when one knows what classes are desired and where they occur (at least a sample), supervised classification strategies are preferable. Due to its architecture, planting date, growing period and plant density, each crop has a unique spectral signature [1,25]. This is used during classification, crop identification and discrimination. In areas where land is scarce, the need to maintain food production with growing demand is achieved via technological changes in land use accomplishing higher returns per area of land [25]. In places of abundance, land conservation is the main strategy used. A better understanding of land use changes is essential to assess and predict its effects on ecosystems and society [26].

In Dambata LGA, it is revealed that the productivity of the land has declined by about 12% . This is mostly due to land degradation which translates to an economic loss of about ₦18 million [27,28]. It is the loss of agricultural land with consequent productivity reduction and economic loss that has necessitated this study. The study employed contemporary methods to detect and also analyze the rate of land use and land cover changes in the area. Thus, this research made use of land cover (LC) data of Dambatta LGA as it checked integrally, the spatial and temporal changes in land use and the rate of land cover change by analyzing the satellite images of 1997, 2007, and 2017 and also checking the vegetation dynamics within the study area. It is on this basis that the research work identified the spatio-temporal changes in land use and land cover (LULC) that occurred in Dambatta LGA between 1997 and 2017.

2. Materials and methods

2.1 Study area

Dambatta Local Government Area is positioned in the Northern part of Kano State. The approximate geographic location of the study area is between latitude 12°25’59” N and 12°30’00” N of the equator and longitude 8°30’00” E and 8°50’00” E of the Greenwich Meridian [27,28] (**Figure 1**). It has a total land area of 732 km^2 and lies within the “wet and dry”

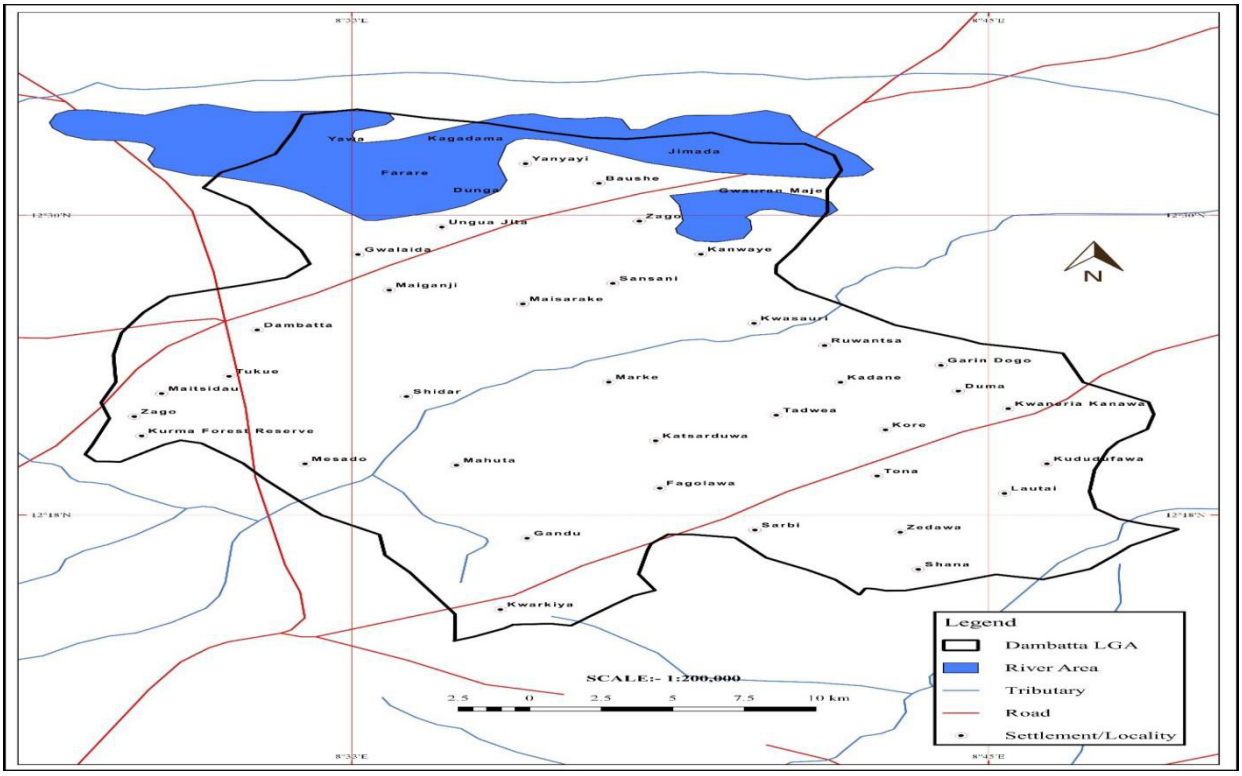

Figure 1. Dambatta LGA showing its localities.

Source: Researchers' field work.

climate with more dry months than wet months [29,30]. The climate of the study area is categorized under tropical savanna in Koppen's classification. The study area falls within the Sudan savannah as well as the chad formation underlain by sedimentary rocks of criterion origin. Agriculture forms the dominant land use.

2.2 Data collection techniques

The coordinates of the control points were obtained from a field survey using GPS device (GPSMap 76 CSx), while the spatial data was obtained from NASRDA, Abuja. These data sets were captured as shown in **Table 1**. Landsat imageries were chosen for this study because of their wider swath width which is required to display a larger area of Dambatta LGA in a single footprint. Hence, the number of footprints required for the study (per year) was reduced to two.

2.3 Image classification

A supervised classification procedure was used in the analysis of data. False color composites were developed for the individual images using three out of the respective bands in accordance with Jibril et al. [27,28]. These composites were used to separately classify 1997, 2007 and 2017 images. Sample sets were created for the individual land cover classes, using

Table 1. Landsat imageries for the study period.

Landsat imageries					
Sensor	Date	Resolution	Source	Path/Row	Satellite
MSS/TM	21st December, 1997	30 m	NARSDA	188/050 188/051	Landsat5
ETM+	4th November, 2007	30 m	NARSDA	188/050 188/051	Landsat7
OLI	24th November, 2017	30 m	NARSDA	188/050 188/051	Landsat8

Source: Authors' fieldwork (2018).

the 'create' icon on the sub-set image of the study area. The supervised approach was found useful in selecting the calibrated pixels. Training sets were cross-checked in the field to validate the various land cover classes for change detection assigned to each training sample set on the image. Thus, a classification scheme was developed for this research.

Subsequently, a maximum likelihood classifier (MLC) was used in this study because it uses a probability density function which enables it to accurately classify land cover categories that have residual ambiguity existing between overlapping classes in the measurement space. This ensured accurate classification in the analysis. Thus, the applied MLC in ILWIS academy software assumed that the image data exhibits normal distribution and thus, pixels should be made up of a single land use type. MLC allocates pixels in the image [31].

2.4 Accuracy assessment and field validation

The accuracy of classification is a function of the number of GCPs used for training. A useful rule of thumb is 30*n (n = number of bands) [32]. The rule was applied in this study and sampling was done using stratified random technique on the LC maps. The accuracy of the classification exercise was measured by analyzing both *commission* and *omission* errors that were supposed to have occurred during image classification. Out of the 700 GCPs, 400 were used for the accuracy assessment. It was assessed for each land cover type separately using an accuracy index (AI) that incorporated both omission and commission error into a single summary value: $AI = ((n\text{-}o\text{-}c)/n) \times 100$.

2.5 Data analysis

Data processing was conducted using post-classification change detection technique in Integrated Land and Water Information System ILWIS 5.2, and later converted to shape files which was imported to Arc Map 10.2 GIS software. Landsat images of 30 metres resolution covering the study area in 1997, 2007, and 2017 were used for land cover classification to identify the spatio-temporal changes in land use (LU) land cover (LC) of Dambatta LGA between 1997-2017. Finally, descriptive statistical tools were used to analyze the spatio-temporal changes identified.

3. Results

The results of the analyses were corroborated by the ground truthing exercise and the satellite images of 1997, 2007, and 2017. Consequently, some maps were achieved and illustrated with Landsat MSS as of 1997, Landsat ETM+ as of 2007 and Landsat OLI as of 2017 respectively (**Figure 2**). **Figure 2** also shows the standard color code used to represent the five (5) LU LC classes. The green color represents agricultural land and the light green represents vegetation cover. The brown color represents a developed area, the milk color represents bare land while blue represents the water body.

3.1 Temporal analysis of land use land cover change in Dambatta LGA between 1997 and 2017

Land use (LU) land cover (LC) levels in Damnatta LGA in 1997

The agricultural land as at 1997 covered an estimate of about 51.7% of the lands in the area which was the highest spatial coverage, followed by vegetation cover at about 27.5%, developed area covered about 13.5%, bare land stood at 5.7%; while water body took 1.3% of the total land area (**Table 2**). This implies that, as at 1997, the level of anthropogenic disturbance in Dambatta LGA was minimal, and land degradation was very low with abundant agricultural farmlands and vegetation cover in virtually all corners of the LGA as shown by the statistical distribution of LU/LC. This, however, is an estimate and therefore not very suitable for conclusions, generalizations and decision making. A confusion matrix was created and used to assess the accuracy of image classification (**Table 3**).

It should be noted that, during classification, one-pixel value can enter another. Therefore, no image classification can be 100% accurate. This is why **Table 4** was created to establish the accuracy or oth-

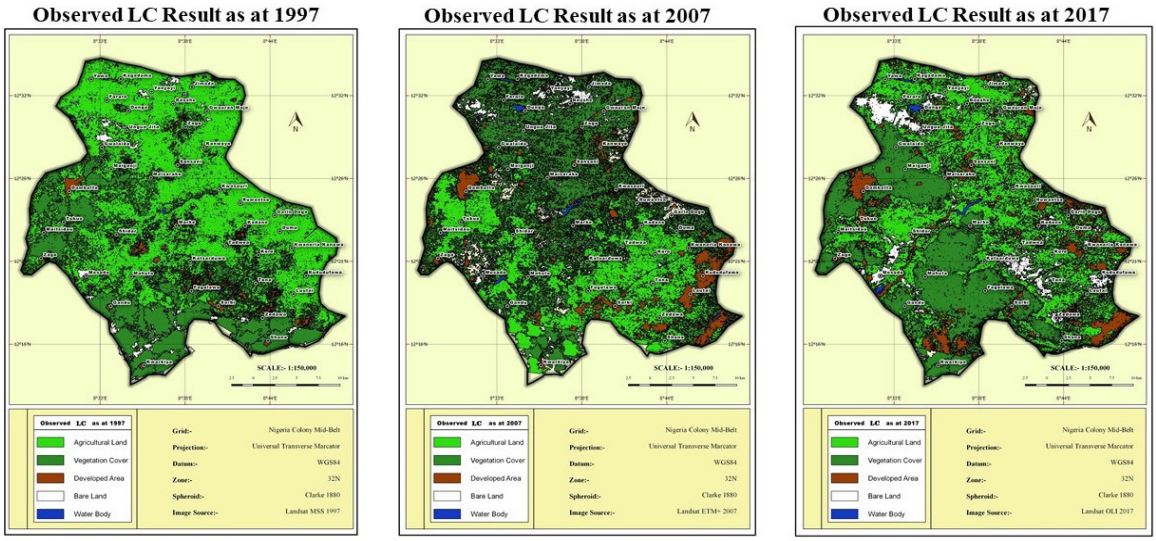

Figure 2. Land cover changes in Dambatta LGA between 1997-2017.

Source: Authors' fieldwork (2018).

erwise of the classification.

The diagonal columns in **Table 3** were added to obtain 340. The rows and columns numbers were also summed up to obtain 400. Therefore, the overall accuracy was computed as (340/400 × 100) 85%. This level of accuracy is indicative of an effective classification result. This method was repeated for 2007 and 2017 image classification.

Table 2. Estimated LU/LC distribution as of 1997.

S/No	LC observed	1997(km^2)	%
1	Agricultural land	379	51.7
2	Vegetation cover	202	27.5
3	Developed area	99	13.5
4	Bare land	42	5.7
5	Water body	10	1.3
	Total	732	100

Source: Authors' fieldwork (2018).

Land use (LU) land cover (LC) change in Dambatta LGA between 1997 and 2007

The land cover distribution as spatially displayed in **Figure 2** was represented in percentages in **Table 5**. The geospatial analysis of the classified Landsat ETM + image as at 2007 shows that vegetation cover occupied 25.1% of the total land in the study area. This was followed by agricultural land at about 24.5%, developed area had increased significantly to 33.4%, bare land had also increased to 13.7% while water body covered 3% of the total land mass as at 2007.

It was also observed that within a period of 10 years (1997 to 2007), agricultural land had decreased significantly by over 50%, while vegetal cover decreased by 10%. Developed area and bare land have increased by 147% and 140% respectively. This

Table 3. Error (confusion) matrix for landsat MSS 1997.

Classified data	Referenced data					
	Agricultural land	Vegetation cover	Developed area	Bare land	Water body	Total
Agricultural land	**182**	5	0	1	2	**190**
Vegetation cover	5	**42**	1	1	1	**50**
Developed area	4	10	**50**	6	0	**70**
Bare land	9	4	1	**31**	0	**45**
Water body	7	3	0	0	**35**	**45**
Total	**207**	**64**	**52**	**39**	**38**	**400**

Source: Authors' fieldwork (2018).

Table 4. Accuracy assessment for landsat MSS 1997.

Class name	Producer's accuracy	User's accuracy
Agricultural land	95.7%	87.9%
Vegetation cover	84%	65.6%
Developed area	68.8%	96.1%
Bare land	71.1%	79.4%
Water body	77.7%	92.1%
Overall accuracy	85%	

Source: Authors' fieldwork (2018).

Table 5. Land cover distribution as of 2007.

S/NO	LC observed	2007 (km^2)	Percentage (%)
1	Agricultural land	180	24.5
2	Vegetation cover	184	25.1
3	Developed area	245	33.4
4	Bare land	101	13.7
5	Water body	22	3.0
Total	732		100

Source: Authors' fieldwork (2018).

depicts that agricultural land and vegetal cover are giving way for built-up areas and bare lands.

It could be deduced from the observations that built-up areas are increasing obviously as a result of anthropogenic activities, while bare lands could be increasing as a result of anthropogenic activities or environmental factors like drought, less rainfall, wind and temperature. This, however, is an estimation based on observation. **Table 6** reveals the quality of the digital classification of the landsat imagery of the study area as at 2007. Producer's accuracy vis-à-vis user's accuracy was employed to arrive at the overall accuracy to ascertain the strength of the classification. Therefore, the overall accuracy of 93.7% was computed. This level of accuracy is indicative of an effective classification result (**Table 7**).

Land use (LU) land cover (LC) change in Dambatta LGA between 2007 and 2017

Supervised classification was also carried out on the Landsat OLI satellite image of 2017 as shown in **Figure 2**. The spatial distribution of land cover features resulting from the supervised classification of Landsat OLI satellite image of 2017 is shown in **Table 8**. On the basis of the digital image classification of Dambatta LGA as of 2017, bare land has increased progressively over time alongside built-up areas, while agricultural land and natural vegetation cover have continuously decreased over time. The implication of this result is that anthropogenic activities and environmental factors like drought, less rainfall, wind and temperature have increased over time and have affected vegetal cover in the environment leading to an increase in bare land and a consequential effect of land degradation. This has further led to a reduction in agricultural land. The accuracy assessment of the 2017 Landsat OLI satellite image computed is 83.25% (See **Tables 9 and 10**). This result is indicative of an accurate and effective classification process.

Table 6. Error (confusion) matrix for landsat ETM + 2007.

Classified data	Referenced data					
	Agricultural land	Vegetation cover	Developed area	Bare land	Water body	Total
Agricultural land	**90**	8	0	1	1	**100**
Vegetation cover	5	**68**	1	1	1	**76**
Developed area	0	2	**20**	0	0	**22**
Bare land	0	2	0	**99**	1	**102**
Water body	1	1	0	0	**98**	**100**
Total	**96**	**81**	**21**	**101**	**101**	**400**

Source: Authors' fieldwork (2018).

Table 7. Accuracy assessment for landsat ETM + 2007.

Class name	Producer's accuracy	User's accuracy
Agricultural land	90.0%	93.7%
Vegetation cover	89.4%	83.9%
Developed area	90.9%	95.2%
Bare land	97.0%	98.0%
Water body	98.0%	97.0%
Overall accuracy	93.7%	

Source: Authors' fieldwork (2018).

Table 8. Land cover distribution as of 2017.

S/NO	LC observed	2017 (km^2)	Percentage (93.7%)
1	Agricultural land	130	17.7
2	Vegetation cover	110	15.0
3	Developed area	320	43.7
4	Bare land	155	21.1
5	Water body	17	2.3
Total	732		100

Source: Authors' fieldwork (2018).

3.2 Spatial analysis of land use land cover change in Danbatta LGA between 1997 and 2017

Table 2 shows that Dambatta LGA had 732 km^2 of land in 1997. It also presents the result of spatial variation and distribution of land use land cover categories within the spatio-temporal frame from 1997 to 2017. **Table 11** shows that bare land and built-up areas witnessed remarkable increase which were also concentrated at the western and eastern parts (**Figure 2**). While bare lands occupied 5.7% of the land area in 1997, 13.7% in 2007 and 21.1% in 2017, built up areas had 13.5% of the total land area in 1997, 33.4% in 2007 and 43.7% in 2017 (**Table 12**). This means that bare lands had positive change differentials of 8% between 1997 and 2007, and 7.4% between 2007 and 2017. The built-up areas on the other hand had positive change differentials of 19.9% between 1997 and 2007 and 10.3% between 2007 and 2017. Generally, bare lands had increased by 269.1%, built-up areas had increased by 223.2%, and water bodies had increased by 70% within the 20 years. The implication is that the bare lands and built-up areas were increasing continuously throughout the period of the study. The increase in both bare lands and developed areas is not concentrated in one part of the area. The proportion covered by bare lands and built-up areas increased northwards of the southern part of the area and southwards of the northern part with few concentrations in the centre of the area (**Figure 2**). Very few water bodies were found around the central region of the imageries in 1997. A few more channels of water were found around the western, north western and south eastern regions besides the initial streams of the central region in 2007. The waters of the south western part of the land, however, disappeared in 2017. Thus, the water bodies in the area appear to be increasing and decreasing from 1997 to 2017.

Table 9. Error (confusion) matrix for landsat OLI 2017.

Classified data	Referenced data					
	Agricultural land	Vegetation cover	Developed area	Bare land	Water body	Total
Agricultural land	**80**	20	2	5	3	**110**
Vegetation cover	10	**40**	1	1	3	**55**
Developed area	0	8	**89**	3	0	**100**
Bare land	2	8	1	**39**	0	**50**
Water body	0	0	0	0	**85**	**85**
Total	**92**	**76**	**93**	**48**	**91**	**400**

Source: Authors' fieldwork (2018).

Table 10. Accuracy assessment for landsat OLI 2017.

Class name	Producer's accuracy	User's accuracy
Agricultural land	72.7%	86.9%
Vegetation cover	72.7%	52.6%
Developed area	89.0%	95.6%
Bare land	78.0%	78.0%
Water body	100%	100%
Overall accuracy	83.25%	

Source: Author's fieldwork (2018).

Agricultural land and vegetation cover decreased significantly over the period of study and were scattered around the study area. Agricultural lands occupied 51.7% of the total land area in 1997, 24.5% in 2017 and 17.7% in 2017 while vegetation cover had 27.5% in 1997, 25% in 2007 and 15% in 2017 (**Table 12**). The water bodies in the local government area took 1.3% of the total land area in 1997, 3.0% in 2007 and 2.3% in 2017. The comparison of the three satellite imageries (1997, 2007 and 2017) revealed a variation in the pattern of land cover. In 2007, the proportion covered by bare land increased southward of the northern area and northward of southern axis with few concentrations at the center when compared to 1997 with just a few scattered bare lands and more of vegetation cover with agricultural land (**Figure 2**). Less vegetation and agricultural land were visible in 2007 and the vegetation located in the northern and southern area of the study area had been lost to bare land and built-up area in 2007. In 2017, the area covered by vegetation decreased in both axis of the study area when compared to 2007. Generally, agricultural lands reduced by 66.8% and vegetation cover reduced by 45.5% within the 20 years.

4. Discussion

The spatio-temporal analysis reveals a number of changes. Initially (1997), the proportions of the land area were used in order of magnitude between agriculture, vegetation, urbanization, bare lands and water bodies. However, the year 2007 had a remarkable change, bringing the order to developed areas, vegetation, agricultural land, bare lands and water bodies. It means that development in the area had rapidly taken away almost half of the agricultural lands between 1997 and 2007. For example, the agricultural land left for cultivation is not enough to

Table 11. Land cover changes in Dambatta LGA between 1997-2017.

LULC types	1997 (km^2)	2007 (km^2)	2017 (km^2)	Changed area (km^2) 1997-2007	Changed area (km^2) 2007-2017	Overall change (km^2) 1997-2017
Agricultural land	379	180	130	–199	–50	–249
Vegetation cover	202	184	110	–18	–74	–92
Developed area	99	245	320	+146	+75	+221
Bare land	42	101	155	+59	+54	+113
Water body	10	22	17	+12	–5	+7

Source: Authors' fieldwork (2018).

Table 12. Percentage of land cover changes in Dambatta LGA between 1997-2017.

LC types	1997 (km^2)	%	2007 (km^2)	%	2017 (km^2)	%
Agricultural land	379	51.7	180	24.5	130	17.7
Vegetation cover	202	27.5	184	25	110	15.0
Developed area	99	13.5	245	33.4	320	43.7
Bare land	42	5.7	101	13.7	155	21.1
Water body	10	1.3	22	3.0	17	2.3
Total	732	100	732	100	732	100

Source: Author's wield work (2018).

produce food in quantities that are enough to feed all the people in the study area. The implication of this result is that most people in the area may partly depend on imported food for survival. This may result in famine due to the economic status of the people. Furthermore, the reduction in agricultural land has negative economic implications for the populace. A greater number of farmers would have been left jobless. The government would also record a huge reduction in revenue generated from the sale of farm produce. Industries that depend on agricultural products as raw materials for their products would rather have to import such raw materials in the midst of the scarcity created by agricultural land inadequacy. This will lead to a consequent rise in the prices of products in the market.

In 2017, there were still further changes, bringing the order to developed areas, bare lands, agriculyural land, vegetation and water bodies. This time, bare lands had taken over the lands previously occupied by vegetation cover. The implication is that the land has been exposed to erosion and its attendant consequences. This explains why there is much land left unoccupied in the midst of rapid development. Sand mining for building activities would have also exposed the land to erosion leaving a large portion of the land almost useless. In fact, continuous erosion on the exposed soil surfaces is more likely to displace settlers on such lands. Loss of vegetation cover implies loss of timber, wildlife, fire wood, medicine, employment and increased temperature. The loss of vegetal cover and developed areas are likely to generate high temperatures which can promote climate change. This is likely to be the reason why the rivers and streams in the area continue to increase and decrease over the years.

5. Conclusions

The study showed evidence of changes between 1997 and 2017. Spatiotemporal analysis of the three imageries showed that agricultural lands were largely been taken over by urbanization while vegetation areas had rapidly given way to bare lands. The study reached the conclusion that these changes are evident in almost all parts of Danbatta Local Government area, especially the northwestern, central and south eastern parts.

The strong and consistent occurrence of the changes is most likely due to anthropogenic activities like deforestation, urbanization, and environmental factors like drought, less rainfall, wind, temperature, erosion and climate change consequently. These results no doubt have negative implications for farmers, ruler dwellers, urban development boards, forest reserves and other policy-makers. This paper, therefore, suggests that further research should be conducted focusing on the impact of climate change on land cover change in the area. It also suggests that reforestation; land reclamation and irrigation agriculture should be promoted in the area.

Author Contributions

David Sesugh Aule: Besides serving as the corresponding author, David Sesugh Aule performed the analysis, wrote the abstract and introduction. He also did much of the discussion ensuring the application of the results to the study area in various ways.

Mamman Saba Jibril: Mamman Saba Jibril performed the supervisory role. He guided the ideas that culminated in the production of this paper from the beginning to the end. The methodology of this publication is his brainchild entirely.

Ali Husein Idris: Ali Husein Idris worked on data collection, processing and spatial analysis. He also produced the maps that are used in this study.

Conflict of Interest

The authors declare that they have no conflicts of interest regarding the publication of this paper.

Acknowledgement

Our profound gratitude and appreciation go to members of the research team for giving precious contributions towards the completion of this research. We also acknowledge members of our various families who supported and encouraged us

throughout this study. We are most grateful to God, for giving us guidance and knowledge as well as good health in constructing this research work. The support of Professor Mamman Saba Jibril who financed this work for publication is equally acknowledged.

References

[1] Sesha Sai, M.V., Ramana, K.V., Hebbar, R. (editors), 2007. Satellite remote sensing for efficient coastal agriculture. International Symposium on Management of Coastal Ecosystems; 2007 Oct 27-30; Kolkata.

[2] Stroosnijder, L., Fresco, L.O., Duiker, S.W., 1994. Imaginable futures, a contribution to thinking about land use planning. The future of land: Mobilizing and integrating knowledge for land use options. John Wiley and Sons: Chichester. pp. 1-8.

[3] Kebede, G., 2010. GIS Based Surface Irrigation Potential Assessment of River Catchment for Irrigation Development in Dale Woreda, Sidama Zone, SNNP, School of Natural Resource and Environmental Engineering, Haramaya University

[4] Turner, I.I., Ross, R.H., Skole, O.L., 1993. Relating Land Use and Global Land-Cover Change: A Proposal for an IGBP-HDP Core Project [Internet]. A Report from the IGBP/HDP Working Group on Land-Use/Land-Cover Change. Available from: http://ciesin.org/docs/008-105/008-105.html

[5] Lillesand, T., Kiefer, R.W., Chipman, J., 2015. Remote sensing and image interpretation, 7th Edition. John Willey and Sons: New York. pp. 804.

[6] Obiahu, O.H., Yan, Z., Uchenna, U.B., 2021. Spatiotemporal analysis of land use land cover changes and built-up expansion projection in predominantly dystric nitosol of Ebonyi state, Southeastern, Nigeria. Environmental Challenges. 4, 100145.
DOI: https://doi.org/10.1016/j.envc.2021.100145

[7] Keogh, M.E., Törnqvist, T.E., 2019. Measuring rates of present-day relative sea-level rise in low-elevation coastal zones: A critical evaluation. Ocean Science. 15(1), 61-73.
DOI: https://doi.org/10.5194/os-15-61-2019

[8] Hoegh-Guldberg, O., Masson-Delmotte, V., Zhai, P., et al., 2018. Impacts of 1.5°C Global Warming on Natural and Human Systems [Internet]. Available from: http://hdl.handle.net/10138/311749

[9] Mentaschi, L., Vousdoukas, M.I., Pekel, J.F., et al., 2018. Global long-term observations of coastal erosion and accretion. Scientific Reports. 8(1), 12876.
DOI: https://doi.org/10.1038/s41598-018-30904-w

[10] Pendergrass, A.G., 2018. What precipitation is extreme?. Science. 360(6393), 1072-1073.
DOI: https://doi.org/10.1126/science.aat1871

[11] Jadkowski, M.A., Howard, R.R., Brostuen, D.E., 1990. Application of SPOT data for regional growth analysis and local planning. Photogrammetric Engineering and Remote Sensing. 56(2), 175-180.

[12] Treitz, P.M., Howard, P.J., Gong, P., 1992. Application of satellite and GIS technologies for land-cover and land-use mapping at the rural-urban fringe: A case study. Journal of Photogrammetric Engineering and Remote Sensing. 58, 439-448.

[13] Dangulla, M., Abd Munaf, L., Mohammad, F.R., 2020. Spatio-temporal analysis of land use/land cover dynamics in Sokoto Metropolis using multi-temporal satellite data and land change modeller. The Indonesian Journal of Geography. 52(3), 306-316.

[14] Campbell, J.B., Wynne, R.H., 2002. Introduction to remote sensing, 3rd edition. The Guilford Press: New York. pp. 621.

[15] Star, J.L., Estes, J.E., 1993. Remote Sensing and GIS Integration: Towards a Prioritized Research Agenda (93-4) [Internet] [cited 2021 Mar 21]. Available from: https://escholarship.org/uc/item/675609bw

[16] Focardi, S., Loiselle, S.A., Mazzuoli, S., et al., 2008. Satellite-based indices in the analysis of

land cover for municipalities in the province of Siena, Italy. Journal of Environmental Management. 86(2), 383-389.

[17] Cihlar, J., 2000. Land cover mapping of large areas from satellites: Status and research priorities. International Journal of Remote Sensing. 21(6-7), 1093-1114.

[18] Jansen, L.J., Di Gregorio, A., 2002. Parametric land cover and land-use classifications as tools for environmental change detection. Agriculture, Ecosystems & Environment. 91(1-3), 89-100.

[19] Rogan, J., Chen, D., 2004. Remote sensing technology for mapping and monitoring land-cover and land-use change. Progress in Planning. 61(4), 301-325.

[20] Weng, Q., 2009. Thermal infrared remote sensing for urban climate and environmental studies: Methods, applications, and trends. ISPRS Journal of Photogrammetry and Remote Sensing. 64(4), 335-344.

[21] Hansen, M.C., DeFries, R.S., Townshend, J.R., et al., 2000. Global land cover classification at 1 km spatial resolution using a classification tree approach. International Journal of Remote Sensing. 21(6-7), 1331-1364.

[22] Foody, G.M., 1998. Sharpening fuzzy classification output to refine the representation of sub-pixel land cover distribution. International Journal of Remote Sensing. 19(13), 2593-2599.

[23] Mannan, B., Roy, J., Ray, A.K., 1998. Fuzzy ARTMAP supervised classification of multi-spectral remotely-sensed images. International Journal of Remote Sensing. 19(4), 767-774.

[24] Van Der Meer, F., 1995. Spectral unmixing of landsat thematic mapper data. International Journal of Remote Sensing. 16(16), 3189-3194.

[25] Raji, B.A., 2004. Agricultural land use planning and management in Kadawa irrigation scheme, Kano State. Paper presented at the National Workshop on Satellite Remote Sensing (NigeriaSat-1) and GIS: A Solution to Sustainable National Development Challenges; 2004 Jun 15-17.

[26] Dolman, A.J., Moors, E.J., Elbers, J.A., 2002. The carbon uptake of a mid latitude pine forest growing on sandy soil. Agricultural and Forest Meteorology. 111(3), 157-170.

[27] Jibril, M.S., Aule, D.S., Idris, A.H., 2022. Land cover changes in Danbatta local government area of Kano State, Nigeria. AFRIGIST Journal of Land Administration and Environmental Management. 2(1), 27-38.

[28] Jibril, M.S., Aule, D.S., Idris, A.H., 2022. Assessment of land degradation in Dambatta local government area using remote sensing techniques. Advances in Remote Sensing. 11(4), 167-181.
DOI: https://doi.org/10.4236/ars.2022.114010

[29] Mohammed, M. A., 2015. Impact of Soil Microbial Respiration on Atmospheric Carbon Under Different Land Use in Part of Kano State, Northern Nigeria. International Journal of Animal Biology. Vol. 1, No. 5, 2015, pp. 158-164.

[30] Olofin, E.A., 1987. Some effects of Tiga Dam on the environmental downstream in Kano River Basin [Ph.D. thesis]. Zaria: Department of Geography, A.B.U.

[31] Smith, D.R., Chandra, S., Barth, R.F., et al., 2001. Quantitative imaging and microlocalization of boron-10 in brain tumors and infiltrating tumor cells by SIMS ion microscopy: Relevance to neutron capture therapy. Cancer Research. 61(22), 8179-8187.

[32] Jensen, J.R., 1996. Introductory digital image processing: A remote sensing perspective, 2nd Edition. Prentice Hall, Inc.: Upper Saddle River, NJ.

BILINGUAL PUBLISHING GROUP

Journal of Geographical Research

https://journals.bilpubgroup.com/index.php/jgr

ARTICLE

Application of Vegetation Indices for Detection and Monitoring Oil Spills in Ahoada West Local Government Area of Rivers State, Nigeria

Jonathan Lisa Erebi* , ***Egirani E. Davidson***

Department of Geology, Niger Delta University, Wilberforce Island, Bayelsa State, 560103, Nigeria

ABSTRACT

The study evaluated the environmental effects of an oil spill in Joinkrama 4 and Akimima Ahoada West LGA, Rivers State, Nigeria, using various vegetation indices. Location data for the spill were obtained from the Nigeria Oil Spill Detection and Response Agency, and Landsat imagery was acquired from the United States Geological Survey. Three soil samples were collected from the affected area, and their analysis included measuring total petroleum hydrocarbons (TPH), total hydrocarbons (THC), and polycyclic aromatic hydrocarbons (PAH). The obtained data were processed with ArcGIS software, utilizing different vegetation indices such as the Normalized Difference Vegetation Index (NDVI), Atmospheric Resistant Vegetation Index (ARVI), Soil Adjusted Vegetation Index (SAVI), Green Short Wave Infrared (GSWIR), and Green Near Infrared (GNIR). Statistical analysis was performed using SPSS and Microsoft Excel. The results consistently indicated a negative impact on the environment resulting from the oil spill. A comparison of spectral reflectance values between the oil spill site and the non-oil spill site showed lower values at the oil spill site across all vegetation indices (NDVI 0.0665-0.2622, ARVI –0.0495-0.1268, SAVI 0.0333-0.1311, GSWIR –0.183-0.0517, GNIR –0.0104-–0.1980), indicating damage to vegetation. Additionally, the study examined the correlation between vegetation indices and environmental parameters associated with the oil spill, revealing significant relationships with TPH, THC, and PAH. A t-test with a significance level of $p < 0.05$ indicated significantly higher vegetation index values at the non-oil spill site compared to the oil spill site, suggesting a potential disparity in vegetation health between the two areas. Hence, this study emphasizes the harmful effect of oil spills on vegetation and highlights the importance of utilizing vegetation indices and spectral reflectance analysis to detect and monitor the impact of oil spills on vegetation.

Keywords: Vegetation indices; TPH; PAH; THC; Oil spill; Impact; Rivers State; Nigeria

*CORRESPONDING AUTHOR:

Jonathan Lisa Erebi, Department of Geology, Niger Delta University, Wilberforce Island, Bayelsa State, 560103, Nigeria; Email: jonathanlisa788@gmail.com

ARTICLE INFO

Received: 28 June 2023 | Revised: 27 July 2023 | Accepted: 1 August 2023 | Published Online: 7 August 2023

DOI: https://doi.org/10.30564/jgr.v6i3.5817

CITATION

Erebi, J.L., Davidson, E.E., 2023. Application of Vegetation Indices for Detection and Monitoring Oil Spills in Ahoada West Local Government Area of Rivers State, Nigeria. Journal of Geographical Research. 6(3): 29-41. DOI: https://doi.org/10.30564/jgr.v6i3.5817

1. Introduction

Oil spills in the Niger Delta, particularly in Joinkrama 4 and Akinima, have emerged as a critical global issue with far-reaching consequences for ecosystems, wildlife, and human livelihoods [1] The discovery of crude oil in Oloibiri in 1956 marked the beginning of a series of oil spill incidents, both intentional and unintentional, which have led to the devastation of rivers, seas, and marshes, posing significant environmental hazards [2]. The Niger Delta, acknowledged as one of the world's ten most important wetlands and marine ecosystems, has suffered extensive environmental ramifications due to the presence of numerous oil industries [3]. While these industries have contributed to the growth and development of the region, they have also resulted in adverse impacts. The relentless activities of restless youths who vandalize pipelines and the rising number of illegal refineries in oil-producing areas have substantially amplified environmental contamination [1]. The sensitivity of vegetation to hydrocarbons varies depending on the type and quantity of chemicals involved, as well as the type of vegetation [4]. The impact of oil spills poses a significant threat to the environment in Nigeria, especially in the Niger Delta. If not effectively managed, it could lead to the complete destruction of ecosystems in the region where oil spills have become alarmingly frequent [5]. Communities in this area suffer from the degrading effects of oil spills, as the once-vibrant mangroves that provided fuelwood and habitat for biodiversity have been depleted and rendered lifeless due to oil toxicity. Marine life has also been adversely affected by oil spills, resulting in contaminated seafood and subsequent health risks associated with human consumption. The oil leak has had a significant influence on the health, social, and economic aspects of the affected communities, emphasizing the importance of effective steps to avoid and handle oil disasters in Nigeria's Niger Delta region [6]. Farmlands and sources of potable water are destroyed, further impacting coastal fishing activities. The recurrent incidents of oil spills in the Niger Delta have created significant tension between the local population and multinational oil companies operating in the region. Technological advancements, particularly vegetation spectral indices and remote sensing, offer valuable tools for detecting and monitoring the impacts of oil spills in these environments [7]. Remote sensing techniques, including vegetation spectral indices, have proven effective in detecting and monitoring the effects of hydrocarbon leaks on vegetation health [8]. Changes in leaves, stems, and trunks serve as indicators of plant responses to oil contamination or stress [9]. Continuous monitoring of pipelines and oil leaks at oil production sites is crucial to mitigate oil contamination in rivers, seas, oceans, and marshes.

2. Material and methods

2.1 Location of the study area

The research focuses on the settlements of Joinkrama 4 and Akinima in Rivers State, Nigeria's Ahoada West Local Government Area. These towns are located on the eastern bank of the Orashi River, a significant Niger Delta river (**Figure 1**). Joinkrama 4 is located at roughly 4.8265° N, 6.0665° E, whereas Akinima is located at approximately 5.1046° N, 6.4529° E. The area's geographical location is largely flat, with heights varying from below sea level in the southwest to roughly 39 meters inland [10]. The region is easily accessible by road and footpath, and it has multiple hydrocarbon flow stations operated by Shell Petroleum Development Company (SPDC) and Nigeria Agip Oil Company (NAOC) [10]. The region is drained by various tributaries and creeks, including Kolo Creek and Taylor Creek, which are connected to the Orashi River.

2.2 The geology of the area

The research area is geologically located on the south-western side of the Niger Delta region, which was produced by a failed rift junction between the South American and African plates. The rifting occurred between the late Jurassic and mid-Cretaceous periods [11]. The Niger Delta Basin has an area of more than 105,000 km^2 [12]. The Akata For-

mation, Agbada Formation, and Benin Formation are among the geological formations studied in the area. According to Short and Stauble [13], the Akata Formation, which ranges in age from the Paleocene to the Holocene, is the Niger Delta region's base lithostratigraphic unit. It is made up of thick shales, turbidite sands, and traces of silt and clay. Near the interface with the underlying Agbada Formation, the formation comprises high-pressure, low-density deep marine deposits containing plant remains. It has a varied microfauna, with planktonic foraminifera accounting for a sizable percentage, indicating a shallow maritime shelf depositional environment [14]. The sand and silt streaks inside the formation provide evidence of high-energy deposition as the delta moved into the sea. The Akata Formation extends in thickness from 0 to 6,000 meters and is mostly underwater, not visible at the seashore [15].

2.3 Data collection for oil spill

The satellite data were collected from the United States Geological Survey (USGS). The data includes Landsat-5 acquired on September 12, 1990, with a spatial resolution of 30 meters, and Landsat-8 acquired on December 12, 2021, with a similar spatial resolution. The source for both datasets is the USGS Earth Explorer website. Additionally, oil spill records and corresponding GPS locations from November 2020 to April 2021 were obtained from the Nigeria Oil Spill Detection and Response Agency (NOSDRA) archives, available at https://oilspillmonitor.ng/#/.

2.4 Collection of data for soil

A total number of three (3) soil samples were collected with the aid of a hand auger two were collect-

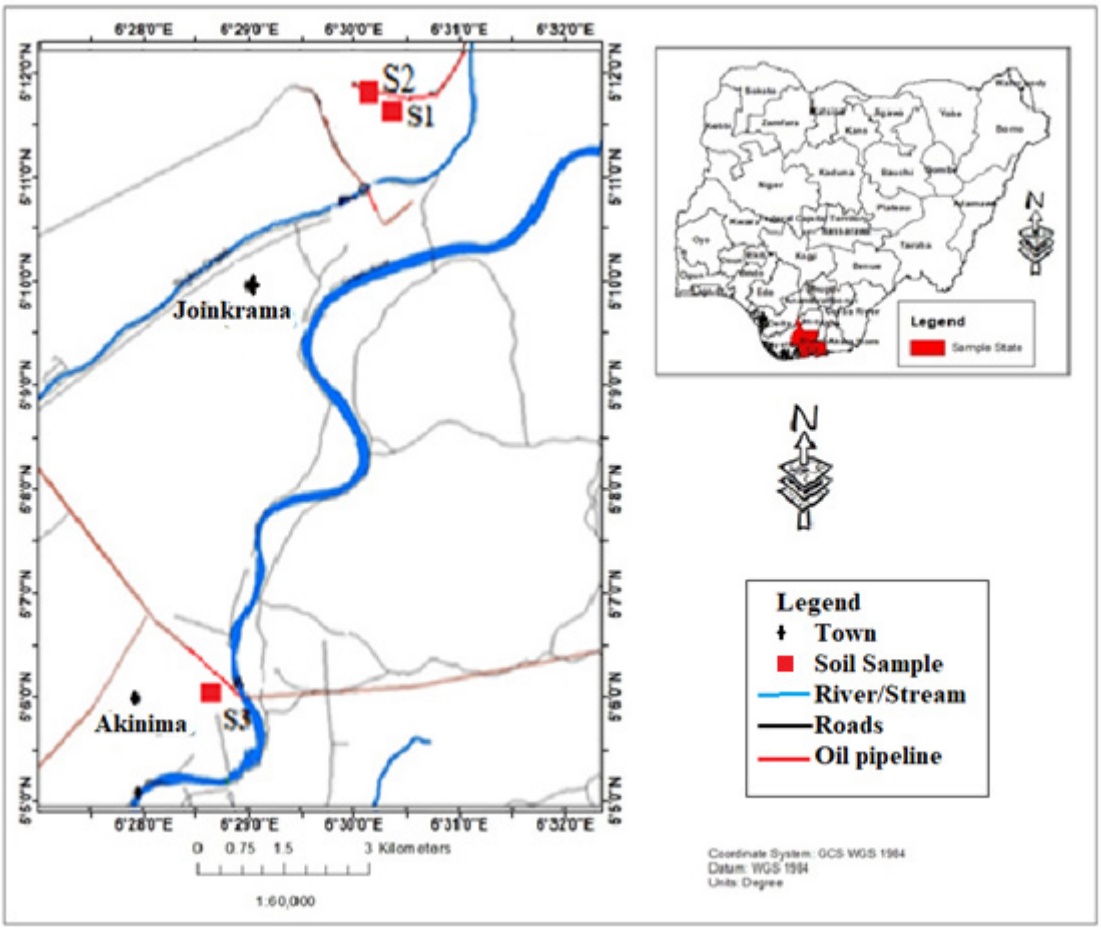

Figure 1. Study area map.

ed in Joinkrama 4, one in Akinima and Soil samples were collected from the outer surface and were analyzed in the laboratory for Polycyclic Aromatic Hydrocarbon, (PAHs), Total Petroleum Hydrocarbons (TPH) and Total Hydrocarbon Content (THC).

2.5 Limitation

In order to minimize the effect of cloud cover, in Landsat-8, this study is limited to the month of December 2021 as there is less cloud cover at this time of the year.

2.6 Data analysis/processing

PAH chemicals were analyzed using gas chromatography, TPH and phenol were measured using a photometer, and THC content was determined through spectrophotometer readings. These analytical techniques and instruments allowed for the accurate identification and quantification of these hydrocarbon compounds in various samples.

The oil spill data was in degrees, minutes and seconds and was imported into Microsoft Excel and converted to degree decimal before it was loaded into the Geographical Information System environment in Database Format to produce a sample location map using Arc GIS software. The Arc GIS spatial analyst extension was used to generate the thematic maps using Map Algebra in a raster calculator, and various vegetation indexes such as NDVI, SAVI, ARVI2, G-NIR and G-SWIR were derived. Finally, SPSS (Statistical Package for the Social Science) and IBM were used for statistical analysis such as Pearson correlation coefficient and T-test were done and Microsoft Excel was also used to plot the bar.

2.7 Vegetation indices

The use of Landsat imagery, specifically Landsat-5 and Landsat-8, is crucial for detecting oil spills and understanding their environmental impact through vegetation indices derived from broadband multispectral data. Five vegetation stress factors are employed in the study, utilizing the spectral bands of Landsat-5 and Landsat-8. For Landsat-8, the spectral bands used for vegetation indices are as follows: visible blue (0.450 to 0.515 μm), visible green (0.525 to 0.6 μm), visible red (0.630 to 0.68 μm), near-infrared (0.845 to 0.885 μm), and short-wave infrared I (1.56 to 1.66 μm), all with a resolution of 30 meters. In the case of Landsat-5, the vegetation indices are derived from the following spectral bands: visible blue (0.450 to 0.515 μm), visible green (0.525 to 0.6 μm), visible red (0.630 to 0.69 μm), near-infrared (0.77 to 0.90 μm), and short-wave infrared 1 (1.55 to 1.75 μm), also with a resolution of 30 meters. By analyzing these vegetation indices derived from Landsat imagery, researchers can assess the extent of oil spills and their impact on the environment, providing valuable insights for environmental studies.

Atmospheric correction refers to the process of adjusting the recorded satellite imagery to account for atmospheric effects and obtain accurate measurements of the Earth's surface. The equations for atmospheric correction of Landsat-8 imager from Digital Number (DN) to Top of Atmosphere (TOA) reflectance using reflectance rescaling coefficients from Landsat-8 metadata file are provided in Equations (1) and (2) [16-18].

Equation (1): TOA reflectance without correction for solar angle (ρλ') can be calculated using the formula:

$$p\lambda = MpQcal + Ap \quad (1)$$

Here, pλ represents TOA planetary reflectance, Mp is the band-specific multiplicative rescaling factor, Aρ is the band-specific additive rescaling factor, and Qcal refers to the quantized and calibrated standard product pixel values (DN).

Equation (2): TOA reflectance corrected for the sun angle can be calculated as follows:

$$p\lambda = (p\lambda) / \cos(\theta sz) = (p\lambda) / \cos(\theta se) \quad (2)$$

In Equation (2), θsz represents the solar zenith angle, while θse represents the solar elevation angle.

The Normalized Difference Vegetation Index (NDVI) is a commonly used spectral index that exhibits distinct characteristics for detecting vegetation stress. It utilizes the red band in the visible spectrum,

which is sensitive to chlorophyll content, and the near-infrared (NIR) band, which indicates healthy vegetation conditions. Equation (3) represents the calculation for NDVI [19,20].

$$NDVI = (RNIR - RRED) / (RNIR + RRED) \quad (3)$$

Here, RNIR represents the reflectance in the NIR band, and RRED represents the reflectance in the red band.

The Soil Adjusted Vegetation Index (SAVI) was developed by Huete [21] and Huete [22] to address noise present in NDVI due to canopy background and atmospheric conditions. SAVI incorporates an adjustment factor and is useful for correcting soil brightness and atmospheric effects [23];

$$SAVI = ((RNIR - RRED) / (RNIR + RRED + L)) \times (1 + L) \quad (4)$$

In Equation (4), L represents the adjustment factor, typically set to 0.5.

The Atmospheric Resistant Vegetation Index 2 (ARVI2) is designed to be resistant to atmospheric effects and sensitive to a wide range of chlorophyll concentrations. It is influenced by vegetation fraction and the rate of absorption of photosynthetic solar radiation. Equation (5) represents the calculation for ARVI2 [24,25]:

$$ARVI2 = -0.18 + 1.17 \times (RNIR - RRED / RNIR + RRED) \quad (5)$$

The Green-Near Infrared (G-NIR) index combines the green and near-infrared reflectance values to assess plant vigor and characterize vegetation structure. It has shown potential for discriminating between vegetation affected by oil spills and unaffected sites [26,27]:

$$G\text{-}NIR = (RGREEN - RNIR) / (RGREEN + RNIR) \quad (6)$$

In Equation (6), RGREEN represents the reflectance in the green band.

The Green-Short-Wave Infrared (G-SWIR) index has the ability to predict and sense nitrogen levels in plants [28] and can discriminate the moisture content of soil and vegetation. It may be useful for detecting changes in vegetation affected by oil spills [29]:

$$G\text{-}SWIR = (RGREEN - RSWIR) / (RGREEN + RSWIR) \quad (7)$$

In Equation (7), RSWIR represents the reflectance in the short-wave infrared (SWIR) band.

These equations and indices play crucial roles in analyzing satellite imagery and extracting valuable information about vegetation and environmental conditions.

3. Results and discussion

3.1 Assessment of oil spill's impact on the environment

The assessment of an oil spill's impact Joinkrama 4 and Akinima utilized the NDVI. **Tables 1 and 2** presented a comparison of NDVI spectral reflectance values between the oil spill site and a non-oil spill site. The results in **Figure 2** indicated the presence of unhealthy plants in the spill-affected area. The results revealed that the NDVI spectral reflectance values at the oil spill site were lower, indicating damage to the vegetation. **Figure 3** depicted the spectral reflectance, further emphasizing the significant extent of damage caused by the spill. The Oil Spill Site (OSS) exhibited a range of 0.0665 to 0.2622, while the Non-Oil Spill Site (NOSS) had a value of 0.4522. These findings demonstrate that the oil spill had a substantial adverse impact on the studied area's vegetation, as evidenced by the lower NDVI values and the presence of unhealthy plant growth.

The resulting SAVI values are then compared with historical data or a control area to identify regions where vegetation cover has been affected by the oil spill. SAVI proves effective in detecting oil spills because it provides a quantitative measure of the extent of the damage caused. The provided information indicates a negative impact on vegetation in the affected area due to the oil spill. Comparisons of SAVI values between the oil spill site and a non-oil spill site, as shown in **Tables 1 and 2**, further support the evidence of spill-induced damage in **Figure 4**. Spectral reflectance data in **Figure 5** illustrates that the oil spill site exhibits a lower SAVI range of 0.0333 to 0.1311, while the non-oil spill site displays a higher value of 0.2261. This disparity suggests that vegetation in the oil spill site is less healthy

compared to the non-oil spill site. Therefore, the presented information strongly indicates a significant negative impact of the oil spill on the vegetation in the affected area.

The study examined the health of vegetation in two distinct areas, one affected by an oil spill and the other untouched, using the Atmospheric Resistant Vegetation Index (ARVI). The analysis, presented in **Tables 1 and 2**, along with **Figure 6**, indicated the condition of vegetation in these areas. The color-coded images demonstrated that the regions affected by the oil spill exhibited unhealthy vegetation, while the non-oil spill area showed moderate vegetation. **Tables 1 and 2** were utilized to compare the ARVI values between the oil spill site and the non-oil spill site. The results derived from these tables were then used to generate **Figure 7**, which depicted the spectral reflectance of the oil spill site (OSS) and the non-oil spill site (NOSS). The range of the OSS values, ranging from –0.1022 to 0.1268, indicated the extent of vegetation damage caused by the oil spill. In comparison, the NOSS value of 0.3492 provided a reference point for evaluating the impact of the oil spill on vegetation in the area.

A comprehensive investigation of the influence of oil spills on vegetation stress through spectral reflectance in GNIR bands was conducted, as evident from the findings presented in **Tables 1 and 2** and **Figure 8**. These data depict the pre- and post-oil spill GNIR results, illustrating that the spills have induced stress and harm to the vegetation, resulting in changes in reflectance in both the green and NIR spectral bands. Moreover, the comparison of spectral reflectance between the oil spill site (OSS) and the non-oil spill site (NOSS) in **Figure 9**, provides further insights. The results demonstrate that reflectance values in the OSS range from –0.0479 to –0.1980, while the NOSS exhibits a reflectance of –0.3823. This comparison signifies that the presence of oil spills within the area significantly impacts the health of vegetation, leading to detectable changes in spectral reflectance that can be closely monitored. Consequently, the study underscores the significance of employing GNIR spectral reflectance as a means to identify and monitor the effects of oil spills on vegetation health. This knowledge can aid in the development of effective strategies to mitigate the damage caused by such incidents.

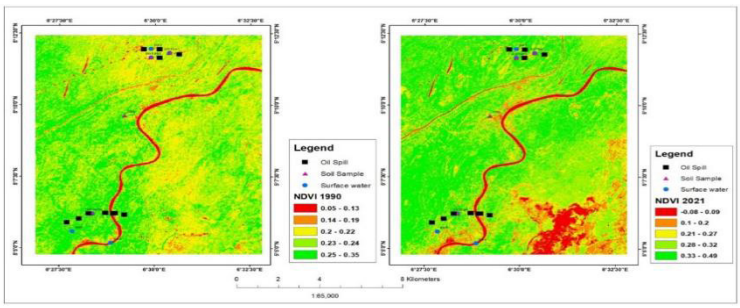

Figure 2. Vegetation analysis of normalized difference vegetation index (NDVI) 1990 and 2021.

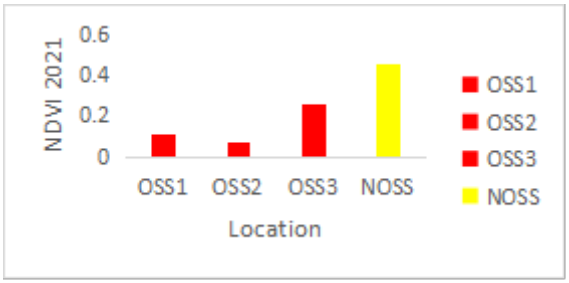

Figure 3. Normalized difference vegetation index for OSS and NOSS 2021.

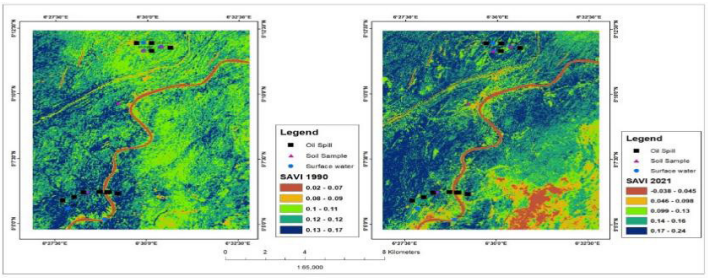

Figure 4. Vegetation analysis of soil adjusted vegetation index (SAVI) 1990 and 2021.

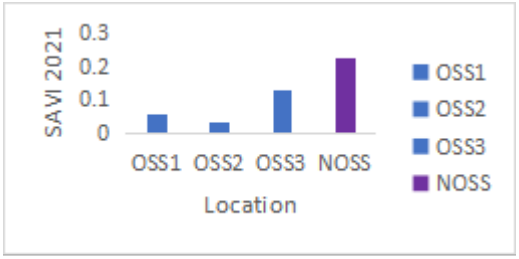

Figure 5. Vegetation analysis of soil adjusted vegetation index (SAVI) for OSS and NOSS 2021.

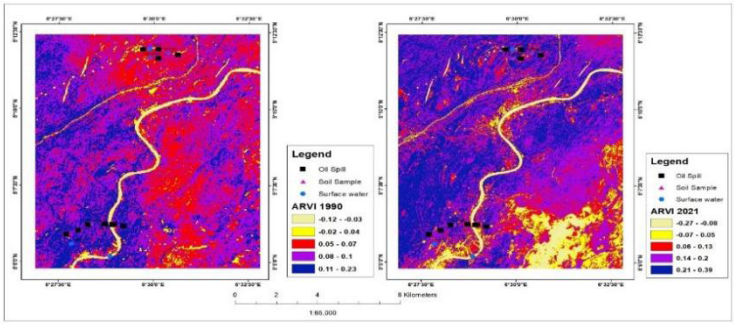

Figure 6. Vegetation analysis of atmospheric resistant vegetation index (ARVI) 1990 and 2021.

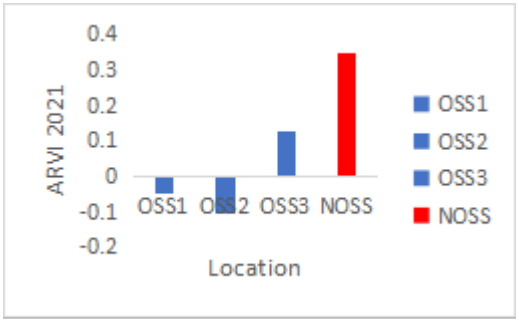

Figure 7. Vegetation analysis of atmospheric resistant vegetation index (ARVI) for OSS and NOSS 2021.

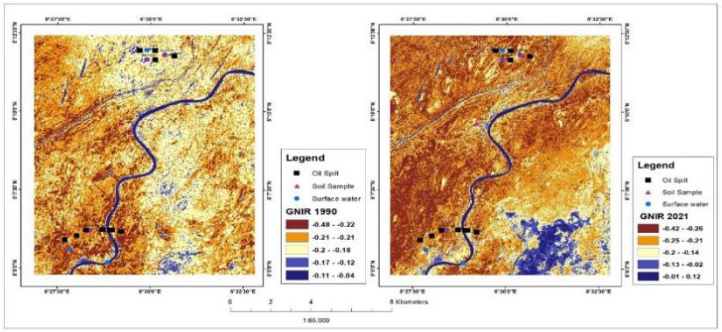

Figure 8. Vegetation analysis of green-near infrared (GNIR) 1990 and 2021.

Figure 9. Vegetation analysis of green-near infrared (GNIR) for OSS and NOSS 2021.

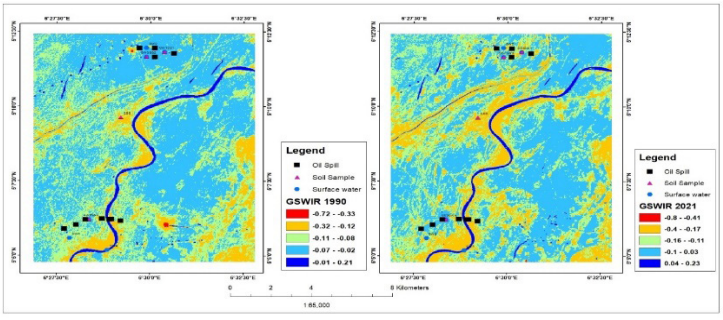

Figure 10. Vegetation analysis of green short wave infrared (GSWIR) 1990 and 2021.

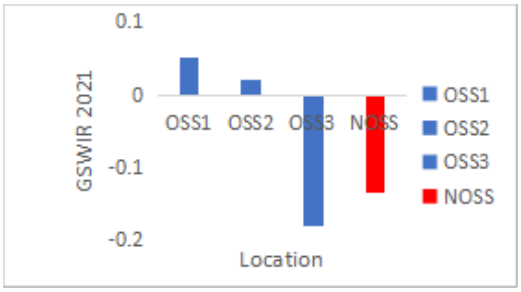

Figure 11. Vegetation analysis of green short wave infrared (GSWIR) for OSS and NOSS 2021.

The findings presented in **Tables 1 and 2** demonstrate the primary objective of the study, which was to evaluate how oil spills influence the well-being of vegetation by analyzing the spectral reflectance within the Green Short Wave Infrared (GSWIR) range. **Figure 10** reveals changes in GSWIR reflectance before and after the oil spill, indicating that the presence of the spill causes stress and harm to the vegetation, as evidenced by the altered reflectance. **Tables 4 and 5** compare the GSWIR reflectance between the oil spill site (OSS) and the non-oil spill site (NOSS). **Figure 11** illustrates that OSS 1 to OSS3 exhibit a range of values from 0.05717 to –0.1803, with OSS3 having a higher value than NOSS (–0.3823). This suggests that the presence of an oil spill has adversely affected the health of the vegetation in the area, resulting in changes in spectral reflectance in the Short Wave Infrared (SWIR) range. Thus, the study employed GSWIR spectral reflectance as a means to detect and monitor the impact of oil spills on vegetation health. The results underscore the necessity for effective measures to prevent oil spills and minimize their detrimental consequences on the environment.

Table 1. Vegetation indices spectral reflectance during the spill in soil sample 2021.

CODE	NDVI 2021	ARVI 2021	SAVI 2021	GSWIR 2021	GNIR 2021
OSS1	0.1115	–0.0495	0.0558	0.0517	–0.0479
OSS2	0.0665	–0.1022	0.0333	0.0214	–0.0104
OSS3	0.2622	0.1268	0.1311	–0.1803	–0.1980

Note: Oil spill site = OSS.

Table 2. Vegetation indices spectral reflectance in non-oil spill site 2021.

Vegetation indices	NOSS
NDVI	0.4523
ARVI	0.3492
SAVI	0.2261
GSWIR	–0.1332
GNIR	–0.3823

Note: Non-oil spill site = NOSS.

3.2 Pearson correlation coefficient analysis

Table 3 presents the findings of the Pearson correlation coefficient analysis, illustrating the relationship between various vegetation indices prior to and during an oil spill occurrence. The Pearson correlation coefficient assesses the linear connection between two variables and ranges from –1 (indicating a perfect negative correlation) to +1 (indicating a perfect positive correlation), with 0 representing no correlation. Based on the information provided, the Normalized Difference Vegetation Index (NDVI), Atmospheric Resistant Vegetation Index (ARVI), and Soil Adjusted Vegetation Index (SAVI) exhibit a strong positive correlation of r = 0.9229 before and during the oil spill event. This implies that these indices are highly associated and move in the same direction, suggesting their utility in monitoring vegetation changes during and after an oil spill. The statement further notes that the Green Short Wave Infrared (GSWIR) index demonstrates a strong positive correlation of r = 0.7559 before and during the oil spill event. Although this correlation is not as robust as the aforementioned indices, it still signifies a positive relationship between the variables. Lastly, the Green Near Infrared (GNIR) index reveals a strong positive correlation of r = 0.93649 before and during the oil spill event. This indicates a high correlation between GNIR and the other vegetation indices, making it suitable for monitoring vegetation changes throughout an oil spill event. Consequently, these correlations suggest that by combining different vegetation indices, one can effectively monitor vegetation changes before, during, and after an oil spill occurrence.

Table 3. Pearson correlation coefficient between vegetation indices before the spill and during the spill.

Vegetation indices before spill (1990) and during spill (2021)	r	Strength	Direction
NDVI	0.9229	Strong	positive
ARVI	0.9229	Strong	positive
SAVI	0.9229	Strong	positive
GSWIR	0.7559	Strong	positive
GNIR	0.9364	Strong	positive

The results from **Tables 4-7** indicate that there is a significant correlation between the Normalized

Difference Vegetation Index (NDVI) and the environmental parameters TPH, THC, and PAH in the affected oil spill site. Specifically, the results show a strong negative correlation (r = –0.7065) between NDVI and TPH, a strong positive correlation (r = 0.6968) between NDVI and THC, and a strong positive correlation (r = 0.5827) between NDVI and PAH. These correlations suggest that as the levels of TPH increase, the NDVI decreases, and as the levels of THC and PAH increase, the NDVI increases. This could indicate that higher levels of TPH negatively impact vegetation, while higher levels of THC and PAH positively impact vegetation in this particular oil spill site. However, it is important to note that correlation does not necessarily imply causation, and further research is needed to understand the specific mechanisms behind these relationships. Nonetheless, these findings could have important implications for understanding and mitigating the impacts of oil spills on vegetation in affected areas.

Table 4. Hydrocarbon results in soil.

Sample code	TPH	THC	PAH
Soil 1 (topsoil)	1.693	4.8	0.045
Soil 2 (topsoil)	1.736	4.1	0.03
Soil 3(topsoil)	1.691	4.82	0.043

Table 5. Pearson correlation coefficient between vegetation indices and TPH (topsoil).

2021	r	Strength	Direction
NDVI vs TPH	–0.7065	Strong	Negative
ARVI vs TPH	–0.7065	Strong	Negative
SAVI vs TPH	–0.7064	Strong	Negative
GSWIR vs TPH	0.4283	Weak	Positive
GNIR vs TPH	0.6840	Strong	Positive

Table 6. Pearson correlation coefficient between vegetation indices and THC (topsoil).

2021	r	Strength	Direction
NDVI vs THC	0.6958	Strong	Positive
ARVI vs THC	0.6958	Strong	Positive
SAVI vs THC	0.6958	Strong	Positive
GSWIR vs THC	–0.4147	Weak	Negative
GNIR vs THC	–0.6730	Strong	Negative

Table 7. Pearson correlation coefficient between vegetation indices and PAH (topsoil).

2021	r	Strength	Direction
NDVI vs PAH	0.5827	Strong	Positive
ARVI vs PAH	0.5827	Strong	Positive
SAVI vs PAH	0.5827	Strong	Positive
GSWIR vs PAH	–0.2765	Weak	Negative
GNIR vs PAH	–0.5570	Strong	Negative

3.3 T-test result for vegetation indices between the Oil Spill Site (OSS) and Non-Oil Spill Site (NOSS)

A dependent t-test was performed to compare the Normalized Difference Vegetation Index (NDVI) spectral reflectance between the Oil Spill Site (OSS) and Non-Oil Spill Site (NOSS), as indicated in **Table 8**. The results demonstrated a statistically significant difference between the two sites, with the NOSS mean surpassing the OSS mean. The t-test was conducted with a significance level (alpha) of $p < 0.05$, and the assumption of normally distributed difference scores was confirmed. The mean NDVI spectral reflectance for OSS was M = 0.1467 with a standard deviation of SD = 0.10250, while the mean for NOSS was M = 4.523 with a standard deviation of SD = 0.0000. The effect size was considered large, with d = 2.98, indicating a strong practical significance. Therefore, the findings imply that the presence of an oil spill negatively impacted vegetation health, resulting in lower NDVI spectral reflectance at the Oil Spill Site (OSS) compared to the Non-Oil Spill Site (NOSS). These results underscore the necessity for effective measures to prevent oil spills and minimize their environmental impact.

In **Table 9**, the results of a dependent t-test investigating the differences in the Atmospheric Resistant Vegetation Index (ARVI) between the Oil Spill Site (OSS) and Non-Oil Spill Site (NOSS) were presented. The research hypothesis aimed to determine whether the means of ARVI in OSS and NOSS were equal. The findings indicated a statistically significant difference between the mean ARVI scores of OSS and NOSS, with a t-value of 5.163 and a p-val-

ue less than 0.001. This suggests that the disparity between the means is unlikely to occur by chance. Furthermore, the effect size (d) was calculated as 2.98, demonstrating a substantial degree of practical significance. Thus, the results indicate that the mean ARVI for NOSS is significantly higher than the mean for OSS. It is important to note that the assumption of normally distributed difference scores was examined and met prior to conducting the analysis.

The data in **Table 10** show the results of a dependent t-test conducted to compare the Soil Adjusted Vegetation Index (SAVI) spectral reflectance at an Oil Spill Site (OSS) and a Non-Oil Spill Site (NOSS). The mean SAVI for OSS was 0.0734 with a standard deviation of 0.05122, while the mean SAVI for NOSS was 0.02261 with a standard deviation of 0.0000. The results of the dependent t-test indicated a statistically significant difference between the SAVI values for the OSS and NOSS ($t(3) = 5.164$, $p < 0.001$). The effect size was reported as large ($d = 2.98$), signifying a strong practical significance. Prior to conducting the t-test, it was confirmed that the assumption of normally distributed difference scores was satisfied. This assumption is crucial for the validity of the t-test results. Furthermore, an alpha level of $p < 0.05$ was employed, which is a common significance level in statistical testing. Consequently, the results suggest that the SAVI values were significantly higher at NOSS compared to OSS, indicating a potential discrepancy in vegetation health between the two sites.

Table 11 presents the outcome of a dependent t-test comparing the Green Short Wave Infrared (GSWIR) spectral reflectance at an Oil Spill Site (OSS) and a Non-Oil Spill Site (NOSS). The mean GSWIR for OSS was –0.0347 with a standard deviation of 0.07281, whereas the mean GSWIR for NOSS was –0.1332 with a standard deviation of 0.0000. The dependent t-test revealed a statistically significant difference between the SWIR values for OSS and NOSS ($t(3) = –1.34$, $p < 0.001$). The effect size was reported as large ($d = 0.77$), indicating a weak practical significance. It is noteworthy that the assumption of normally distributed difference scores was examined and satisfied prior to conducting the t-test. This assumption is critical for the validity of the t-test results. Additionally, an alpha level of $p < 0.05$ was employed, which is a common level of significance in statistical testing. Overall, the results suggest that the GSWIR values were significantly higher at NOSS compared to OSS, suggesting a potential disparity in the presence of oil or other contaminants between the two sites. However, the effect size was weak, implying that the practical significance of the difference might not be substantial.

The results depicted in **Table 12** demonstrate the use of a dependent t-test to examine the differences in Green Near Infrared (GNIR) spectral reflectance between an Oil Spill Site (OSS) and a Non-Oil Spill Site (NOSS). The findings indicated a statistically significant difference between OSS and NOSS, with a t-value of –5.180 and a p-value less than 0.001. This implies that the NOSS mean was significantly higher than the OSS mean for GNIR. The effect size was also computed, yielding a large effect size of $d = 3.0$. This indicates a strong degree of practical significance between the two groups. Prior to conducting the analysis, the assumption of normally distributed difference scores was examined, and the skew and kurtosis levels were found to be –1.46 and 0.00, respectively. These values were within the acceptable range for a t-test (i.e., skew < |2.0| and kurtosis < |9.0|; posten 1984), confirming the satisfaction of the assumption of normally distributed difference scores. Therefore, the results suggest a significant difference in GNIR spectral reflectance between OSS and NOSS, with NOSS exhibiting a higher mean than OSS.

4. Conclusions

The assessment of an oil spill's impact on vegetation in a specific area, utilizing the Normalized Difference Vegetation Index (NDVI), Atmospheric Resistant Vegetation Index (ARVI), Soil Adjusted Vegetation Index (SAVI), Green Short Wave Infrared (GSWIR), and Green Near Infrared (GNIR) spectral reflectance, revealed a significant negative impact on the health of vegetation due to the oil spill. The

Table 8. Paired samples statistics and Test for NDVI.

	Mean	N	Std. deviation	Std. error mean	Skew	Kurtosis	t
NOSS	0.4523	3	0	0	1.36	0.0000	5.164
OSS	0.1467	3	0.1025	0.05918			

Table 9. Paired samples statistics and tests for ARVI.

	Mean	N	Std. deviation	Std. error mean	Skew	Kurtosis	t
NOSS	0.3492	3	0.00000	0.00000	1.36	0.0000	5.163
OSS	–0.0083	3	0.11993	0.06924			

Table 10. Paired samples statistics and tests for SAVI.

	Mean	N	Std. error mean	Skew	Kurtosis	t
NOSS	0.2261	3	0.00000	1.36	0.0000	5.164
OSS	0.0734	3	0.02957			

Table 11. Paired samples statistics and tests for SWIR.

	Mean	N	Std. deviation	Std. error mean	Skew	Kurtosis	t
NOSS	–0.1332	3	0.00000	0.00000	–1.62	0.0000	–1.339
OSS	–0.0357	3	0.12611	0.07281			

Table 12. Paired samples statistics and tests for GNIR.

	Mean	N	Std. deviation	Std. error mean	Skew	Kurtosis	t
NOSS	–0.3823	3	0.00000	0.00000	–1.46	0.0000	–5.180
OSS	–0.0854	3	0.09927	0.05731			

comparisons between the oil spill site (OSS) and non-oil spill site (NOSS) consistently demonstrated lower vegetation health and damage in the OSS. The color-coded representations and spectral reflectance data provided visual evidence of unhealthy and stressed vegetation in the spill-affected area. The results from various statistical analyses, including dependent t-tests and Pearson correlation coefficients, further supported the findings by showing significant differences and relationships between vegetation indices and environmental parameters. Overall, the comprehensive findings suggest that the oil spill had a substantial adverse impact on the vegetation in the affected area. The lower values of NDVI, ARVI, SAVI, GSWIR, and GNIR reflectance at the oil spill site indicate damage and stress to the vegetation, while the healthier vegetation and higher reflectance values at the non-oil spill site serve as a reference point for comparison. The correlations between vegetation indices and environmental parameters provide insights into the relationship between oil spill characteristics and vegetation health. These findings highlight the importance of monitoring and mitigating the impacts of oil spills on vegetation. By utilizing remote sensing techniques and spectral reflectance analysis, it becomes possible to detect and monitor the extent of damage caused by oil spills. This knowledge can aid in the development of effective strategies for preventing and minimizing the detrimental consequences of oil spills on the environment and vegetation in affected areas.

Author Contributions

J. L.E developed the study, processed the data, and assisted with part of the writing, while E.E.D. assisted with writing and formatting. The final version was co-written by all authors.

Conflict of Interest

There is no conflict of interest.

References

[1] Okpobiri, O., Harry, A.A., 2022. Monitoring and detecting the impact of oil sabotage on land using multispectral imagery. International Journal of Multidisciplinary Research and Publications (IJMRAP). 4(9), 66-74.

[2] Kadafa, A.A., 2012. Oil exploration and spillage in the Niger Delta of Nigeria. Civil and Environmental Research. 2(3), 38-51.

[3] Okonkwo, C.N.P., Kumar, L., Taylor, S., 2015. The Niger Delta wetland ecosystem: What threatens it and why should we protect it? African Journal of Environmental Science and Technology. 9(5), 451-463.
DOI: https://doi.org/10.5897/AJEST2014.1841

[4] Environmental Assessment of Ogoniland [Internet]. Available from: http://www.zaragoza.es/contenidos/medioambiente/onu/issue06/1130-eng-sum.pdf

[5] Oyem, A., (2001). Christian call for action on Nigerian oil spill. Sage-Oxford's Christian Environmental Group.

[6] Egirani, D.E., Shehata, N., Ugwu, I.M., et al., 2021. Exposure, geochemical, and spatial distribution patterns of an oil spill in parts of the Niger Delta Region of Nigeria. Health and Environment. 2(1), 103-117.
DOI: https://doi.org/10.25082/HE.2021.01.005

[7] Egobueze, F.E., Rowland, E.D., Ebizimo, D.S., 2022. Multispectral imagery for detection and monitoring of vegetation affected by oil spills and migration pattern in Niger Delta Region, Nigeria. World Journal of Advanced Research and Reviews. 15(1), 447-458.
DOI: https://doi.org/10.30574/wjarr.2022.15.1.0682

[8] Van der Werff, H., Van der Meijde, M., Jansma, F., et al., 2008. A spatial-spectral approach for visualization of vegetation stress resulting from pipeline leakage. Sensors. 8(6), 3733-3743.
DOI: https://doi.org/10.3390/s8063733

[9] Guyot, G., Baret, F., Jacquemoud, S., 1992. Imaging spectroscopy for vegetation studies. Kluwer Academic Publishers: Dordrecht. pp. 145-165.

[10] Rowland, E.D., Okpobiri, O., 2021. Floodplain mapping and risks assessment of the Orashi River using remote sensing and GIS in the Niger Delta Region, Nigeria. Journal of Geographical Research. 4(2), 10-16.
DOI: https://doi.org/10.30564/jgr.v4i2.3014

[11] Rayment, R.A., 1965. Aspects of the geology of Nigeria—The stratigraphy of the cretaceous and cenozoic deposits. Ibadan University Press: Ibadan.

[12] Reijers, T., 2011. Stratigraphy and sedimentology of the Niger Delta. Geologos. 17(3), 133-162.

[13] Short, K.C., Stauble, A.J., 1967. Outline of geology of Niger Delta. AAPG Bulletin. 51(5), 761-779.

[14] Adewoyin, O.O., Joshua, E.O., Akinwumi, I.I., et al., 2017. Evaluation of geotechnical parameters using geophysical data. Journal of Engineering and Technological Sciences. 49(1), 95-113.

[15] Etu–Efeotor, J.O., 1997. Fundamentals of petroleum geology. Paragraphic: Port Harcourt.

[16] Jiang, Z., Huete, A.R., Didan, K., et al., 2008. Development of a two-band enhanced vegetation index without a blue band. Remote Sensing of Environment. 112(10), 3833-3845.
DOI: https://doi.org/10.1016/j.rse.2008.06.006

[17] Chavez, P.S., 1996. Image-based atmospheric corrections-revisited and improved. Photogrammetric Engineering and Remote Sensing. 62(9), 1025-1035.

[18] Rowland, E.D., Omonefe, F., 2022. Environmental monitory and impact assessment of solid waste dumpsite using multispectral imagery in Yenagoa, Bayelsa state, Nigeria. International Journal of Environmental Science and Technology. 19(2), 1007-1024.
DOI: https://doi.org/10.1007/s13762-021-03456-2

[19] Rouse, J.W.Jr., Haas, R.H., Schell, J.A., et al., 1973. Monitoring the Vernal Advancement and Retrogradation (Green Wave Effect) of Natural

Vegetation [Internet]. Available from: https://ntrs.nasa.gov/citations/19750020419

[20] Running, S.W., Justice, C.O., Salomonson, V., et al., 1994. Terrestrial remote sensing science and algorithms planned for EOS/MODIS. International Journal of Remote Sensing. 15(17), 3587-3620.
DOI: https://doi.org/10.1080/01431169408954346

[21] Huete, A.R., 1988. A soil-adjusted vegetation index (SAVI). Remote Sensing of Environment. 25(3), 295-309.

[22] Huete, A.R., Hua, G., Qi, J., et al., 1992. Normalization of multidirectional red and NIR reflectances with the SAVI. Remote Sensing of Environment. 41(2-3), 143-154.
DOI: https://doi.org/10.1016/0034-4257(92)90074-T

[23] Rondeaux, G., Steven, M., Baret, F., 1996. Optimization of soil-adjusted vegetation indices. Remote Sensing of Environment. 55(2), 95-107.
DOI: https://doi.org/10.1016/0034-4257(95)00186-7v

[24] Gitelson, A.A., Kaufman, Y.J., Merzlyak, M.N., 1996. Use of a green channel in remote sensing of global vegetation from EOS-MODIS. Remote sensing of Environment. 58(3), 289-298.
DOI: https://doi.org/10.1016/S0034-4257(96)00072-7

[25] Kaufman, Y.J., Tanre, D., 1992. Atmospherically resistant vegetation index (ARVI) for EOS-MODIS. IEEE Transactions on Geoscience and Remote Sensing. 30(2), 261-270.
DOI: https://doi.org/10.1109/36.134076

[26] Sripada, R.P., Heiniger, R.W., White, J.G., et al., 2006. Aerial color infrared photography for determining early in-season nitrogen requirements in corn. Agronomy Journal. 98(4), 968-977.
DOI: https://doi.org/10.2134/agronj2005.0200

[27] Adamu, B., Tansey, K., Ogutu, B., 2015. Using vegetation spectral indices to detect oil pollution in the Niger Delta. Remote Sensing Letters. 6(2), 145-154.
DOI: https://doi.org/10.1080/2150704x.2015.1015656

[28] Herrmann, I., Karnieli, A., Bonfil, D.J., et al., 2010. SWIR-based spectral indices for assessing nitrogen content in potato fields. International Journal of Remote Sensing. 31(19), 5127-5143.
DOI: https://doi.org/10.1080/01431160903283892

[29] Karnieli, A., Kaufman, Y.J., Remer, L., et al., 2001. AFRI—Aerosol free vegetation index. Remote Sensing of Environment. 77(1), 10-21.
DOI: https://doi.org/10.1016/S0034-4257(01)00190-0

BILINGUAL PUBLISHING GROUP

Journal of Geographical Research

https://journals.bilpubgroup.com/index.php/jgr

ARTICLE

Considering Regional Connectivity and Policy Factors in the Simulation of Land Use Change in New Areas: A Case Study of Nansha New District, China

Zehuan Zheng, Shi Xian*

School of Geographical Sciences and Remote Sensing, Guangzhou University-The University of Birmingham Joint Research Centre of Service Industries and Urban Development, Guangzhou University, Guangzhou, Guangdong, 510006, China

ABSTRACT

Numerous emerging development areas worldwide are receiving attention; however, current research on land use change simulation primarily concentrates on cities, urban clusters, or larger scales. Moreover, there is a limited focus on understanding the impact of regional connectivity with surrounding cities and policy factors on land use change in these new areas. In this context, the present study utilizes a cellular automata (CA) model to investigate land use changes in the case of Nansha New District in Guangzhou, China. Three scenarios are examined, emphasizing conventional locational factors, policy considerations, and the influence of regional connectivity with surrounding cities. The results reveal several key findings: (1) Between 2015 and 2021, Nansha New District experienced significant land use changes, with the most notable shifts observed in cultivated land, water area, and construction land. (2) The comprehensive scenario exhibited the highest simulation accuracy, indicating that Nansha New District, as an emerging area, is notably influenced by policy factors and regional connectivity with surrounding cities. (3) Predictions for land use changes in Nansha by 2030, based on the scenario with the highest level of simulation accuracy, suggest an increase in the proportion of cultivated and forest land areas, alongside a decrease in the proportion of construction land and water area. This study contributes valuable insights to relevant studies and policymakers alike.

Keywords: CA model; Land use change simulation; Nansha New District

*CORRESPONDING AUTHOR:

Shi Xian, School of Geographical Sciences and Remote Sensing, Guangzhou University-The University of Birmingham Joint Research Centre of Service Industries and Urban Development, Guangzhou University, Guangzhou, Guangdong, 510006, China; Email: geoshixian@gzhu.edu.cn

ARTICLE INFO

Received: 30 June 2023 | Revised: 28 July 2023 | Accepted: 4 August 2023 | Published Online: 15 August 2023

DOI: https://doi.org/10.30564/jgr.v6i3.5814

CITATION

Zheng, Z.H., Xian, S., 2023. Considering Regional Connectivity and Policy Factors in the Simulation of Land Use Change in New Areas: A Case Study of Nansha New District, China. Journal of Geographical Research. 6(3): 42-60. DOI: https://doi.org/10.30564/jgr.v6i3.5814

1. Introduction

Land use/land cover change (LUCC) is a significant consequence of human-induced alterations to the natural environment, carrying profound implications for global environmental change [1]. Consequently, understanding and predicting LUCC have become crucial focal points of research. Particularly in developing countries, rapid urbanization [2] has led to dramatic land use changes, intensifying the conflict between human activities and land resources. China, since its reforms and opening up, has experienced rapid urbanization and industrialization, positioning the Guangdong-Hong Kong-Macao Greater Bay Area as the world's fourth-largest bay area [3]. Against this backdrop, the release of the Chinese State Council's "Overall Plan for Guangzhou Nansha to Deepen Comprehensive Cooperation with Guangdong, Hong Kong, and Macao for the World" in 2022 has presented new opportunities. China's dynamic and swift urbanization has given rise to numerous emerging development areas, and among them, Nansha New District, situated in the heart of the Greater Bay Area, stands out as one of the most representative in recent years. The region has undergone rapid and substantial land use changes, largely influenced by policies and increased regional connectivity with surrounding cities. Considering these factors, Nansha New District serves as a typical and ideal case study for simulating land use changes in new development areas.

Commonly employed land use simulation models in existing studies include Markov chain models, system dynamics models, and CLUE-S (Conversion of land use and its effects at small region extent) models [4-7]. Many of these models are founded on the principles of the cellular automata (CA) model and the CLUE-S model, which have undergone further enhancements and refinements [8]. One notable advancement is the future land use simulation (FLUS) model developed by Liu, which effectively addresses uncertainties and complexities associated with interconversions between different land use types, demonstrating strong predictive capabilities in simulating land use patterns [9]. As complex system theory progresses and system simulation platforms are developed, the advantages of complex system simulation methods in land use change research become increasingly apparent [10]. Cellular automata (CA) has emerged as one of the most dominant models for land use simulation due to its remarkable ability to capture the interplay between natural and human-driven factors [1,5,11]. However, despite the prominence of CA models, existing studies on land use and land cover change (LUCC) have primarily focused on cities, urban agglomerations, or larger scales, with relatively fewer investigations specifically examining land use simulation within new areas [3,7,8,12,13]. The rapid and intense land use changes often observed in new areas within cities necessitate close monitoring and thorough understanding. When utilizing CA models for geographic simulation, researchers have found that the expansion of urban areas is influenced by a series of driving factors, including topographic conditions, transportation factors, and socio-economic development [14-16].

Traditional drivers of land use change have been extensively studied, encompassing natural factors, transportation factors, and location factors [17]. Among these, particular attention has been given to natural factors, including terrain conditions represented by the digital elevation model (DEM) [6,7,9,13,18-21], elevation [10,16,22,23], slope [6,7,10,12,13,16,18,19,21-23], and aspect [6,7,16,18], among others. Notably, slope stands out as one of the most significant topographic factors influencing urban sprawl [7].

In land use change studies, traffic factors encompass distance to major roads [13,18,21], motorways [10,18], the city center [13], regional centers [21,22], railways [21], and highways [21]. Additionally, researchers contend that accessibility factors, including public facilities [18] and industrial company density [18,21], play a pivotal role in shaping land use change. Moreover, both population density and the presence of public facilities [21,24] are acknowledged as influential factors in land use change dynamics. Furthermore, economic and social development factors are widely employed in land use change and simulation studies. These

factors consist of points of interest (POI) data [6,16,18,22], nighttime lighting (NTL) data [18], GDP [6,18-20], economic development indicators [18], population statistics [6,19,23,25], and population density metrics [13,16,18,20,23].

Scholars are increasingly recognizing the critical role of policy factors in comprehending land use change and simulation [6,25], especially in regions significantly influenced by such policies. Sarah Hasan et al., for instance, highlights the significance of diverse planning policy guidelines and regulations in shaping urban development [7]. In a separate study, Zhipeng Lai et al. utilizes two indicators, namely the Prime Farmland Protection Area and Ecological Sensitive Area, to assess the impact of spatially restricted zones on land use change [18]. Nonetheless, further explicit research is essential to thoroughly investigate the potential influence of government policies on land use [25,26].

Furthermore, there is a growing recognition of the substantial significance of inter-regional connectivity in urban development and land use change. Hence, it becomes imperative to investigate the impact of regional connectivity. Particularly, regional connectivity with surrounding cities acts as a quantitative indicator to assess the degree and quality of interconnectedness between a city and other surrounding cities [27,28], facilitating an analysis of the interconnectivity and interdependence among these urban centers. Moreover, by considering the total connectivity between cities [28-30], we can gauge the overall importance of a city network.

In summary, it is evident that the development of the Greater Bay Area is significantly shaped by both policies and regional connectivity with surrounding cities. Therefore, conducting a comprehensive analysis of land use changes in new areas, considering the influence of policy factors and inter-regional connectivity, becomes of paramount importance in understanding the dynamics of land cover changes and predicting future developments. However, it is important to note that there is a notable dearth of research specifically focusing on the influence of regional connectivity with surrounding cities and policy factors on land use change in new areas [2,6].

Based on this premise, the present study focuses on the Guangzhou Nansha New District within the context of the rapid development of the Guangdong-Hong Kong-Macao Greater Bay Area. Land cover data from 2015, 2018, and 2021 are utilized to construct three distinct scenarios in the cellular automata (CA) model: Scenario A considers conventional locational factors, scenario A + B incorporates policy factors, and scenario A + B+ C takes into account the influence of regional connectivity with surrounding cities on the study region. The research carefully analyzes the patterns and characteristics of land use changes in Nansha New District and subsequently employs the scenario that yields the highest accuracy of simulation to project its land use data for 2030. By investigating the patterns and influencing factors of land use changes in new areas, this study not only enhances our understanding but also provides empirical support for government policymaking, facilitating more sustainable land use planning in such regions.

2. Research data and methods

2.1 The study area and research data

In 2019, with the establishment of the Guangdong-Hong Kong-Macao Greater Bay Area as a national strategic zone, Guangzhou Nansha New District assumed a central and distinctive role as the sole national new district and comprehensive cooperation best practice zone in Guangdong Province (**Figure 1**). This strategic positioning placed Nansha New District at the geographical heart of the development, resulting in accelerated growth and significant land use changes. As a consequence, the region serves as an ideal research case for examining land use changes within new areas, particularly in the context of regional connectivity with surrounding cities and the influence of policy-driven factors.

The data utilized in this study consisted of five main components, as presented in **Table 1**. First-

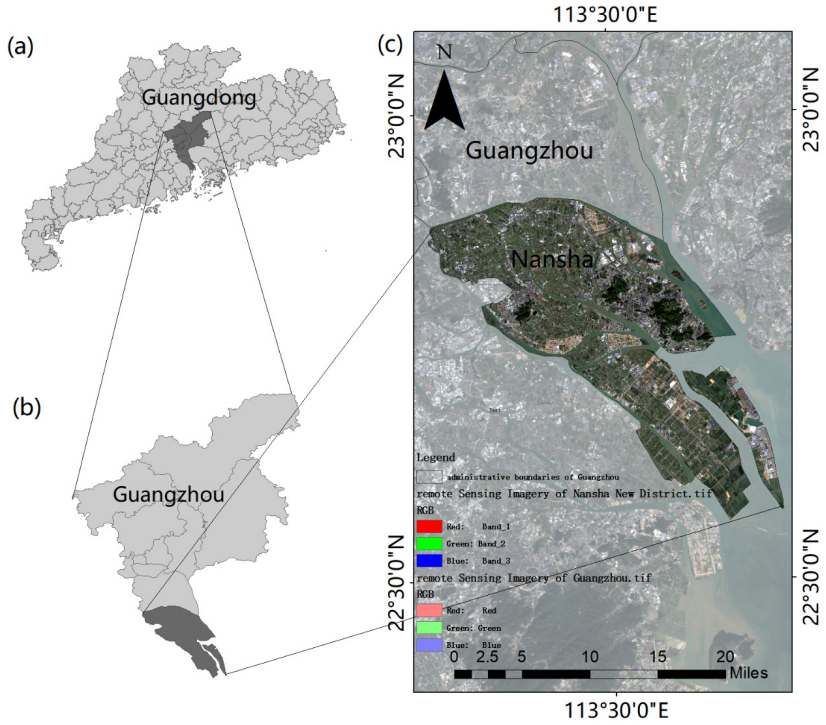

Figure 1. Location of Nansha New District.

Table 1. Data utilized in the study and the data source.

Setting of scenario driving factors			**Classification**	**Data type**	**Year**	**Data source**
			Land use data	Land use vector data	2015, 2018, 2021	https://doi.org/10.5281/zenodo.5816591
Scenario A + B + C	**Scenario A + B**	**Scenario A**	Data on natural environmental factors	DEM (including Slope)	2018	Resource and Environmental Science Data Center Network (http://www.resdc.cn/)
			Traffic elements and location data	Metro stations, regional centers, urban primary roads, urban secondary roads, provincial roads and highways	2018	Guangzhou Municipal Bureau of Planning and Natural Resources (http://ghzyj.gz.gov.cn/)
			Policy planning documents	The overall land use planning for Nansha New District (2006-2020).	2006 -2020	Guangzhou Planning and Natural Resources Bureau, Nansha Branch (http://www.gzns.gov.cn/)
			Socio-economic indicators	Economic activity indicators: total fixed assets, total production assets; static population indicators: total population at the end of the year, etc.	2018	Guangzhou City, Foshan City, Shenzhen City, Zhongshan City, Dongguan City, Zhuhai City Bureau of Statistics (https://lwzb.gzstats.gov.cn:20001/datav/admin/home/www_nj/)
			Data on indicators related to city connectedness	Geographical scale indicators: area, population, etc.; Location indicators: i.e. time and distance to the center of a large city; Other indicators: road passenger data, rail passenger data, frequency of place name buzzword searches, etc.	2018	Guangzhou, Foshan, Shenzhen, Zhongshan, Dongguan, Zhuhai Bureau of Statistics, Guangzhou Nansha New District Bureau of Statistics (http://www.gzns.gov.cn/), Guangzhou Planning and Natural Resources Bureau, Nansha Branch (http://www.gzns.gov.cn/)

ly, the land use data① for Nansha New District in Guangzhou City was collected for the years 2015, 2018, and 2021. The land use types in Nansha New District were classified into five major categories, namely cultivated land, forest land, grassland, water area, and construction land, in accordance with the national-level classification standard outlined in the Current Land Use Classification (GB/T21010-2017) by the Ministry of Land and Resources [31]. Secondly, the dataset included information on traffic elements and location data, encompassing metro stations, regional centers, urban primary roads, urban secondary roads, provincial roads, and highways. The European distance tool in ArcMap software was employed to calculate the shortest distance from each image element to the corresponding traffic element within Nansha New District. Subsequently, the traffic conditions were normalized using the raster calculator. Thirdly, the data encompassed natural environment factors, including a digital elevation model (DEM) with a resolution of 30 m, and slope data extracted from DEM. Fourthly, policy factors data involved dividing the study area into four functional areas: permitted construction area, conditional construction area, restricted construction area, and prohibited construction area. Weights were assigned to these functional areas using the analytic hierarchy process. Lastly, urban connectivity indicators incorporated various metrics, such as geographical scale, location, economic activity, static population, and other relevant indicators. Due to limited data availability regarding the regional connectivity between Nansha New District and surrounding cities, this study employed the regional connectivity between surrounding cities and Guangzhou City as an alternative measure for evaluating the regional connectivity of surrounding cities to Nansha New District.

① The source is the first Landsat-based annual land cover product (CLCD) in China released by Professors Jie Yang and Xin Huang of Wuhan University. The data format is raster data, including nine land types, namely, Cropland, Forest Shrub, Grassland, Water, Snow/Ice, Barren, Impervious and Wetland, with a spatial resolution of 30 m.

2.2 Research methods and data processing

Based on the land use data of Nansha New District for 2015, 2018, and 2021, this study employs the rate of change of land use types to quantify the extent of changes associated with specific land use types within the designated study area over the specified time frame [32]. The rate of change can take on positive or negative values, reflecting the corresponding increase or decrease in the land area occupied by the specific land use type, respectively.

Simulation of land use change trends based on CA model

The cellular automaton (CA) model is a powerful bottom-up approach known for its robust spatial computing capability. Recent research on CA applications has demonstrated its ability to simulate complex systems through the utilization of simple local transformation rules [5,33]. In this study, an extended exploratory investigation was conducted on the definition of CA, particularly focusing on neighborhood configuration and land use conversion rules. Subsequently, a land use evolution model was constructed by integrating artificial neural network techniques [5,7]. The CA model was employed in simulating scenarios of urban expansion pattern changes, with each scenario incorporating different driving factors. Three distinct scenarios were constructed: Scenario A, representing conventional locational factors; Scenario A + B, incorporating policy factors; and Scenario A + B + C, considering the influence of regional connectivity of surrounding cities on land use changes in the study area. Through the analysis of the interrelationships between land use change characteristics and the different driving factors during the years 2015, 2018, and 2021, the CA model yielded valuable insights.

The model scenarios and driving factors

This study aims to investigate the effects of multiple factors on land use dynamics in the Nansha New District. Three scenarios are examined, and cellular automata (CA) models are constructed for each scenario, incorporating factors sequentially as

follows: conventional locational factors (Scenario A), policy factors (Scenario A + B), and the influence of regional connectivity with surrounding cities on the study area (Scenario A + B + C). The specific setup of model scenarios and the associated driving factors are detailed as follows:

(1) ***Scenario A: Conventional locational factors***

Considering the land use development characteristics of Nansha New District and drawing from relevant studies and available data, the primary driving factors selected for the cellular automata (CA) model in the conventional locational factor scenario were topographic conditions and traffic factors. These factors encompass DEM data (including slopes extracted from DEM), distances to metro stations, regional centers, urban primary roads, urban secondary roads, provincial roads, and highways (please refer to **Table 1** for detailed information).

(2) ***Scenario A + B: Conventional locational factors overlaid with policy factors***

Against the backdrop of the Guangdong-Hong Kong-Macao Greater Bay Area development, policy factors significantly influence the land use changes in Nansha New District. The policy factors scenario (Scenario A + B) in this study considers the impact of functional area categories in planning policies as a crucial driving factor, while keeping the other driving factors consistent with Scenario A. In existing general urban planning documents, the construction land control area is primarily classified into four types: prohibited construction area, permitted construction area, restricted construction area, and conditional construction area (please refer to **Figure 5**). This research establishes the four types of functional areas based on the information provided in the Nansha District General Land Use Plan (2006-2020).

In Scenario A + B, varying degrees of influence on urban construction land are observed among different functional areas. These degrees of influence are quantified by assigning corresponding weights to each functional area, employing the expert grading method in conjunction with the analytic hierarchy process (AHP). The expert grade method involves statistical processing, analysis, and summarization of expert opinions obtained through anonymous solicitation. To determine ecological sensitivity weights for each factor, AHP is utilized, and the judgment matrix is constructed using the expert grade method to calculate the weights of each functional area.

(3) ***Scenario A + B + C: Conventional locational factors overlaid with policy factors and surrounding cities influence***

Within the context of urban cooperation in the Greater Bay Area, Nansha New District, positioned at the core of this region, is witnessing an increasing level of connectivity with surrounding cities. As a result, the land use changes in Nansha New District may be influenced by the extent of this connectivity. Thus, it is crucial to include the regional connectivity of surrounding cities as a driving factor in the cellular automata (CA) model. The interconnection and influence among cities serve as indicators reflecting the impact of urbanization in peripheral areas surrounding cities. Compared to Scenario A + B, Scenario A + B + C incorporates the driving factor of regional connectivity of surrounding cities while maintaining consistency with Scenario A + B in terms of the remaining driving factors. This addition aims to enhance the accuracy of land use simulation predictions in Nansha New District.

In this study, due to the availability of data regarding the regional connectivity of the surrounding cities in Nansha New District, Guangzhou city was chosen as the focal point for evaluating the city connectivity of these surrounding cities. Specifically, when computing the regional connectedness of cities neighboring Nansha New District, the study incorporated five adjacent cities, namely Foshan, Shenzhen, Zhongshan, Dongguan, and Zhuhai, as factors in the simulation calculation using a cellular automata (CA) model. The approach described by Lin et al. [30] was adopted in this study to calculate the node strength of each city (network node) within the city cluster network, thereby assessing the strength of city linkages using multiple indicators, as outlined in **Table 1**. In accordance with weighted network theory, the

city nodal strength is a representation of the sum of weights associated with a nodal bond [34-36]:

$$S_i = \sum_{j=1}^{n} C_{ij} r_{ij} (i \neq j) \quad (1)$$

S_i represents the node intensity of city i. n represents the total number of cities, C_{ij} represents the connectivity score between city i and city j, and r_{ij} represents the relationship between city i and city j. A value of 1 is assigned to r_{ij} if there is a relationship between the two cities, and a value of 0 if there is no relationship.

In this research, the selection of indicators was guided by domain knowledge and expert experience, encompassing several widely utilized socioeconomic indicators, namely gross economic product, fixed asset investment, and year-end resident population (as presented in **Table 1**). A higher average coefficient of determination generally indicates a more reliable dataset [37,38]. To effectively integrate the diverse data sources, an intelligent optimization algorithm known as the selective weighted combination method was employed in this study. Specifically, we utilized the well-established genetic algorithm proposed by Zhou et al. [39] for optimization purposes. This algorithm enabled us to obtain optimal weights and determine the coefficients of determination between different socioeconomic indicators. The adaptability function of the genetic algorithm was calculated as follows:

$$f(x) = \sum_{i=1}^{n} r_i / n \quad (2)$$

r_i represents the coefficient of determination between the weighted result and the ith socioeconomic indicator. n is the total number of indicators.

The final outcome reveals a significantly higher urban connectivity intensity when compared to any individual data source. The urban connectivity values between Nansha New District and the surrounding cities are presented in **Figure 6**. The final connectivity score (C_{ij}) between city i and city j can be expressed as follows:

$$C_{ij} = \sum_{k=1}^{t} W_k C_{ijk} \quad (3)$$

t is the total number of methods. C_{ijk} represents the result obtained from the kth method for the jth observation of the ith variable. W_k represents the weight assigned to the kth method. The sum of all weights, represented by ΣW, is equal to 1.

Accuracy assessment

To assess the accuracy of model simulations, previous studies have commonly employed overall accuracy (OA) and Kappa coefficients [33,40]. Additionally, scholars [41] proposed the factor of merit (FoM) as an alternative measure to evaluate simulation accuracy. FoM relies solely on the number of varying cells in the simulated process and offers a more robust assessment of simulation accuracy [13,16]. Building upon this, in this study, historical data was used for simulation, with the 2018 dataset serving as the initial input and the 2021 dataset used for verifying the validity of the CA model [1]. Kappa coefficient, overall accuracy (OA), and FoM were employed to evaluate the accuracy of the model. The Kappa coefficient and OA values range from 0 to 1, with higher values indicating greater classification accuracy achieved by the model. A Kappa coefficient above 0.80 is typically considered indicative of very high simulation accuracy [4,6,9]. As for FoM, values exceeding 0.2 are suggested to indicate an extremely usable model [21,22,42].

3. Simulation results and analysis

3.1 Characteristics and trend analysis of land use change

As discussed in the methodology section, the changes in land area of different land types in Nansha New District were first calculated for the period from 2015 to 2021 (see **Figure 2**).

The findings of the study revealed several noteworthy trends (see **Figure 2**). Firstly, there was a gradual decrease in the area of cultivated land, forest land, and water area in Nansha New District over the specified period. Cultivated land accounted for more than half of the total area during 2015-2021 and served as the predominant land type in the district. However, its proportion experienced a year-on-year decline, with the proportion in 2021 being approximately 1.5 percentage points lower than that

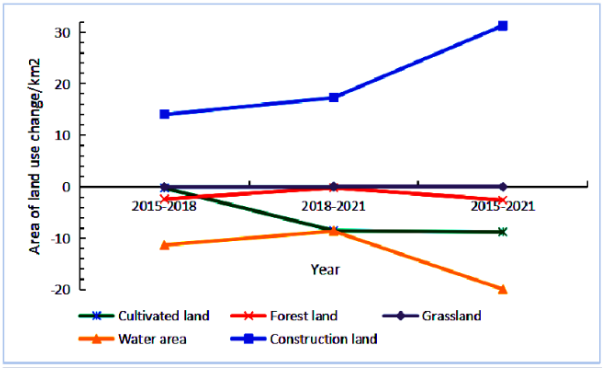

Land use type/km^2

Year	2015	2018	2021
Cultivated land	314.03	313.78	305.25
Forest land	23.58	21.19	20.99
Grassland	0.12	0.07	0.1
Water area	133.18	121.88	113.28
Construction land	115.58	129.58	146.86

Figure 2. Land use changes in Nansha New District, Guangzhou (2015-2021).

in 2015. The proportion of forest land also exhibited a decreasing trend during the same period. Additionally, the water area saw a reduction between 2015 and 2021, accounting for more than one-fifth of the total area in 2015 and less than one-fifth in 2021. In contrast, the area of construction land exhibited a steady increase, while the area of grassland initially decreased and then showed an upward trend. Construction land accounted for less than one-fifth of the total area in 2015 and surpassed one-fourth in 2021, representing more than one-fourth of the overall growth between 2015 and 2021. In 2015, construction land was primarily concentrated in the eastern and western townships, but it gradually expanded towards the central and northern areas near the center of Guangzhou city after 2015. The proportion of grassland area demonstrated a decrease followed by an increase during the period from 2015 to 2021. During the development and construction of Nansha New District from 2015 to 2021, a considerable amount of cultivated land and water area were converted to meet the demands of urban construction.

To illustrate the changes in land use types within the Nansha New District from 2015 to 2021, this study employs a land use transition matrix to depict the interconversion of land use types in the research area (see **Figure 3** and **Table 2**). The findings indicate that the conversion of land to other use types during the 2015-2021 period is relatively limited. Specifically, between 2015 and 2018, the most significant land use conversion occurred from cultivated land to other use types, followed by water area. Almost half of the grassland area was transformed into construction land, and forest land was predominantly converted to cultivated land, with over 10 percent of the total forest area transitioning to cultivated land, and only a minimal proportion transitioning to construction land. Water area conversions were primarily towards cultivated land, while construction land conversions were limited, not exceeding 0.2 percent. During the 2018-2021 period, the land use conversions remained consistent with those observed in the 2015-2018 period. Notably, there was a significant conversion of construction land to cultivated land. Furthermore, the proportion of water area transitioning to cultivated land decreased from nearly 7.43 percent during 2015-2018 to nearly 4.52 percent during 2018-2021, whereas the proportion of water area transitioning to construction land increased from about 2.23 percent during 2015-2018 to about 3.45 percent during 2018-2021. The examination of the land use transition matrix for 2015-2021 further supports the aforementioned results, indicating that the conversion of larger land areas to construction land predominantly affected cultivated land and water area. Specifically, during the period 2015-2021, about 7.64 percent of the total area of cultivated land was converted to construction land. Similarly, roughly 5.56 percent of the water area underwent a transition to construction land. It is worth noting that this study also reveals a trend of gradual increase in the proportion of cultivated land and water area transitioning to construction land. These findings substantiate the negative impact of urban construction demand on cultivated land and water area during the 2015-2021 period.

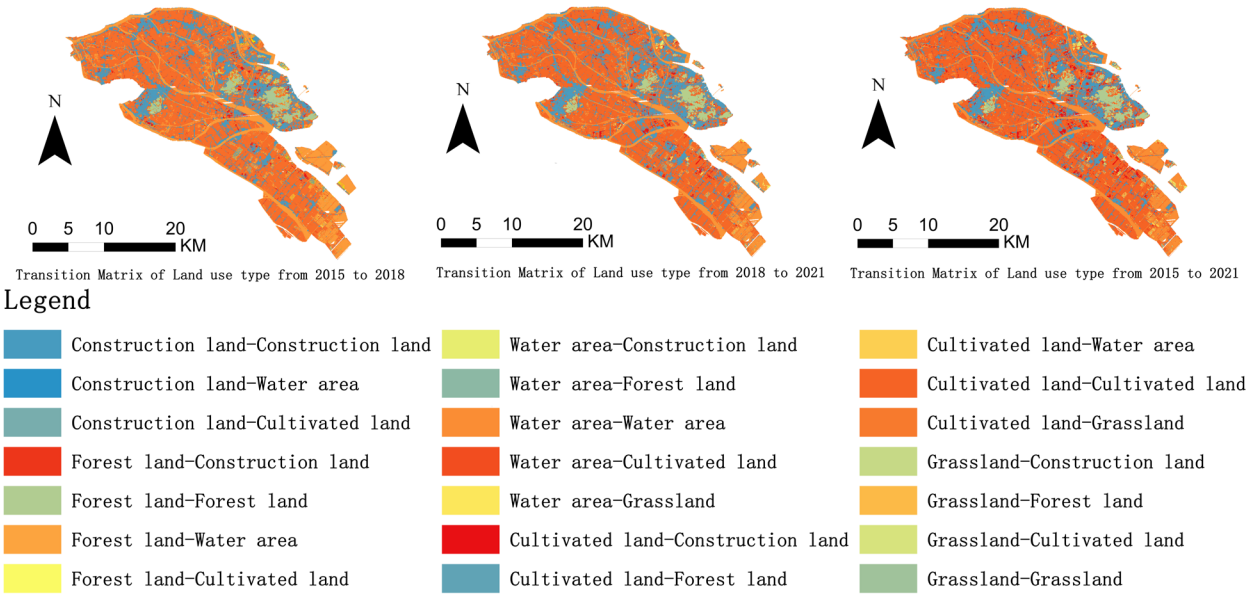

Figure 3. Transition matrix of land use type in Nansha New District from 2015 to 2021.

Table 2. Transition matrix of land use type in Nansha New District from 2015 to 2021.

	Land use type	2018					
		Grassland (km^2)	Cultivated land (km^2)	Construction land (km^2)	Forest land (km^2)	Water area (km^2)	Total (km^2)
2015	Grassland (km^2)	0.06	0.00	0.06	0.00		0.12
	Cultivated land (km^2)	0.01	301.33	11.11	0.22	1.37	314.03
	Construction land (km^2)			115.37		0.22	115.58
	Forest land (km^2)		2.54	0.07	20.97		23.58
	Water area (km^2)	0.01	9.90	2.97	0.00	120.29	133.18
	Total (km^2)	0.07	313.78	129.58	21.19	121.88	586.50
	Land use dynamic (%)	–14.22	–0.03	4.04	–3.38	–2.83	
		2021					
2018	Grassland (km^2)	0.05	0.00	0.02	0.00		0.07
	Cultivated land (km^2)	0.01	298.83	13.18	0.74	1.01	313.78
	Construction land (km^2)		0.02	129.40		0.16	129.58
	Forest land (km^2)		0.90	0.05	20.24		21.19
	Water area (km^2)	0.04	5.51	4.21	0.01	112.11	121.88
	Total (km^2)	0.10	305.25	146.86	20.99	113.28	586.50
	Land use dynamic (%)	15.81	-0.91	4.44	–0.31	–2.35	
		2021					
2015	Grassland (km^2)	0.04	0.01	0.08	0.00		0.12
	Cultivated land (km^2)	0.02	287.24	23.99	0.61	2.17	314.03
	Construction land (km^2)		0.02	115.25		0.32	115.58
	Forest land (km^2)		3.06	0.14	20.37	0.01	23.58
	Water area (km^2)	0.05	14.93	7.41	0.01	110.78	133.18
	Total (km^2)	0.10	305.25	146.86	20.99	113.28	586.50
	Land use dynamic (%)	–2.57	–0.47	4.51	–1.83	–2.49	

3.2 The calculated results for the main driving factors in the three scenarios

In this study, three distinct scenarios were considered in developing the CA models, and the calculation of the main driving factors for each scenario is presented as follows:

The calculated results for the main driving factors in Scenario A

In Scenario A, the driving factors for the CA model consisted of conventional locational factors, including topographic conditions and traffic factors, with the normalized values presented in **Figure 4**.

The calculated results for the main driving factors in Scenario A + B

The calculation results, derived from the implementation of the expert grade method and analytic hierarchy process (AHP), demonstrated that the weights assigned to the permitted construction area, conditional construction area, restricted construction area, and prohibited construction area were 0.538, 0.242, 0.145, and 0.075, respectively (refer to **Figure 5**). Among the functional areas considered, the permitted construction area exhibited the highest weight value, signifying its significant influence on the allocation of construction land within Nansha New District. Conversely, the prohibited construction area had the lowest weight value, indicating its minimal impact on the dynamics of construction land within Nansha New District.

The calculated results for the main driving factors in Scenario A + B + C

Based on the data provided in **Figure 6**, the results indicate that Nansha New District displayed the highest level of connectivity with Shenzhen, surpassing a threshold of 0.6. Furthermore, Foshan City exhibited a connectivity degree exceeding 0.5. In contrast, Zhongshan, Dongguan, and Zhuhai demonstrated comparatively lower levels of connectivity with Nansha New District.

By utilizing the Euclidean distance tool, this study calculated the distances between the cell centers of Nansha New District and its surrounding

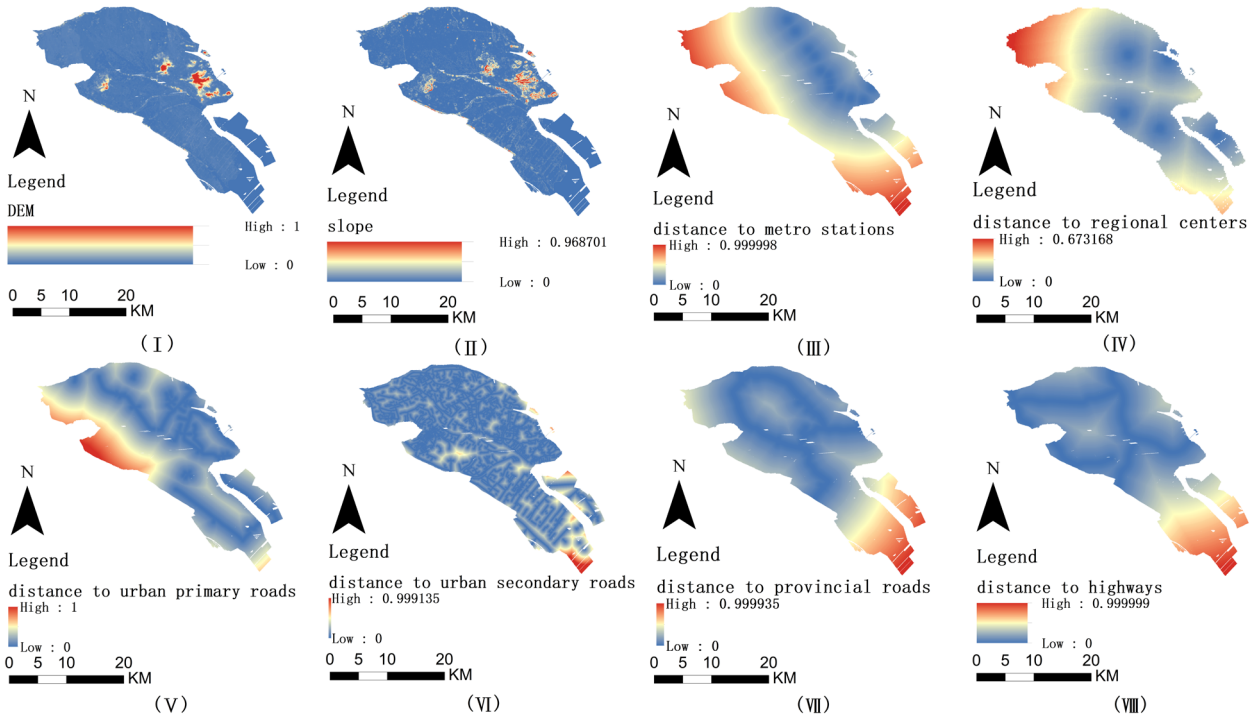

Figure 4. Driving factors used for scenario A: (I) DEM; (II) slope; (III) distance to metro stations; (IV) distance to regional centers; (V) distance to urban primary roads; (VI) distance to urban secondary roads; (VII) distance to provincial roads; (VIII) distance to highways.

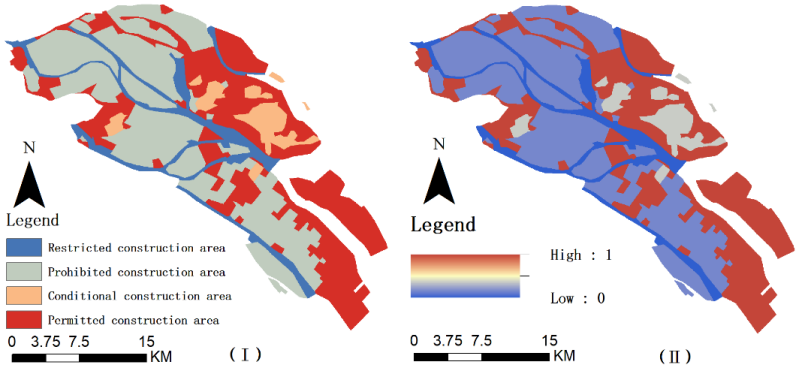

Weights of the four functional areas in Nansha New District	
Functional Areas	**Weights**
Permitted construction area	0.538
Conditional construction area	0.252
Restricted construction area	0.145
Prohibited construction area	0.075

Figure 5. Driving factors used for scenario A + B: (I) Planning map of different functional areas in Nansha New District; (II) Degree of land use impact of different functional areas.

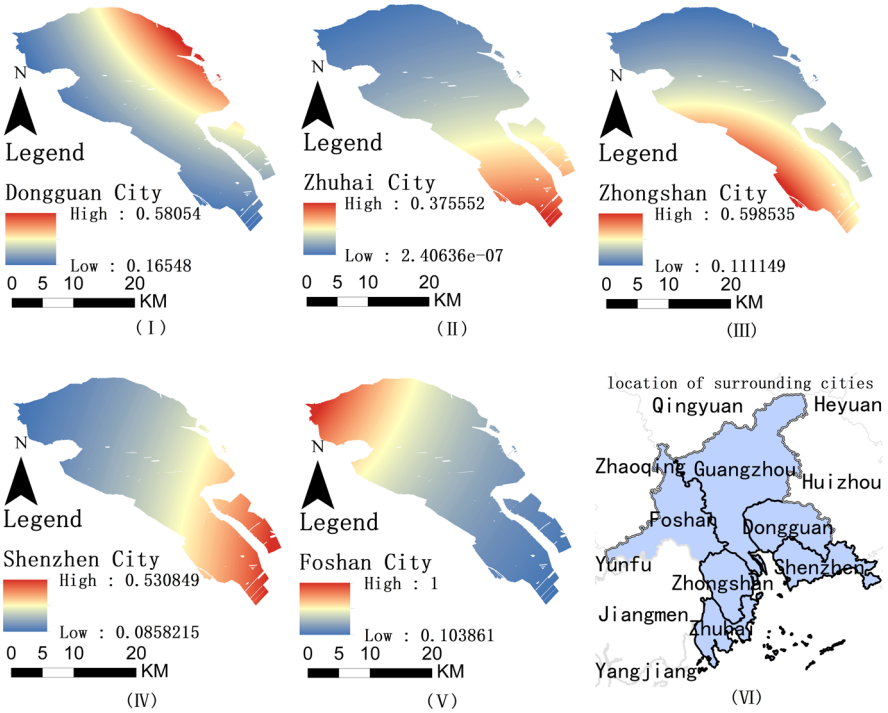

Regional connectivity between surrounding cities and Nansha New District of Guangzhou	
City	**Connectivity intensity**
Shenzhen	0.066896
Zhuhai	0.043393
Dongguan	0.047352
Foshan	0.058144
Zhongshan	0.035301

Figure 6. Driving factors used for scenario A + B + C: (I-VI indicate Dongguan City, Zhuhai City, Zhongshan City, Shenzhen City, Foshan City and location of surrounding cities, respectively).

cities. These distances were then combined with the level of city connection to generate **Figure 6**.

The results provide the following insights:

Industrial Development Structure: The land use patterns in Nansha New District exhibit a stronger influence from areas that closely align with its industrial structure.

Economic Development Level: The land use in Nansha New District is more influenced by cities with a stronger economic base. These cities act as development poles, facilitating the exchange of various factors such as human flow, logistics, and capital flow with neighboring urban clusters, fostering positive interactions.

Transportation Accessibility and Population Mobility: Areas with higher levels of traffic accessibility and greater population mobility exert a stronger influence on the land use patterns of Nansha New District.

3.3 Simulation results of land use changes using the CA Model and the accuracy assessment

The land use change simulation in Nansha New District in 2021 was conducted using the cellular automata (CA) model, with the 2018 land use data serving as the baseline. Three distinct scenarios, namely A, A + B, and A + B + C, were established to simulate the land use patterns. These scenarios incorporated conventional locational factors (Scenario A), policy factors (Scenario A + B), and regional connectivity with surrounding cities (Scenario A + B + C). The simulation results depicting the land use changes in Nansha New District in 2021 under the three different scenarios are presented in **Figure 7** and **Table 3**.

In this study, the processed data were utilized as input for the CA model to simulate and predict the land use change trend of Nansha New District from 2015 to 2021. The findings (refer to **Figure 7** and **Table 3**) revealed that the highest overall accuracy (OA) of the model was achieved when considering the overlay of conventional locational factors, related policy factors, and influence factors of regional

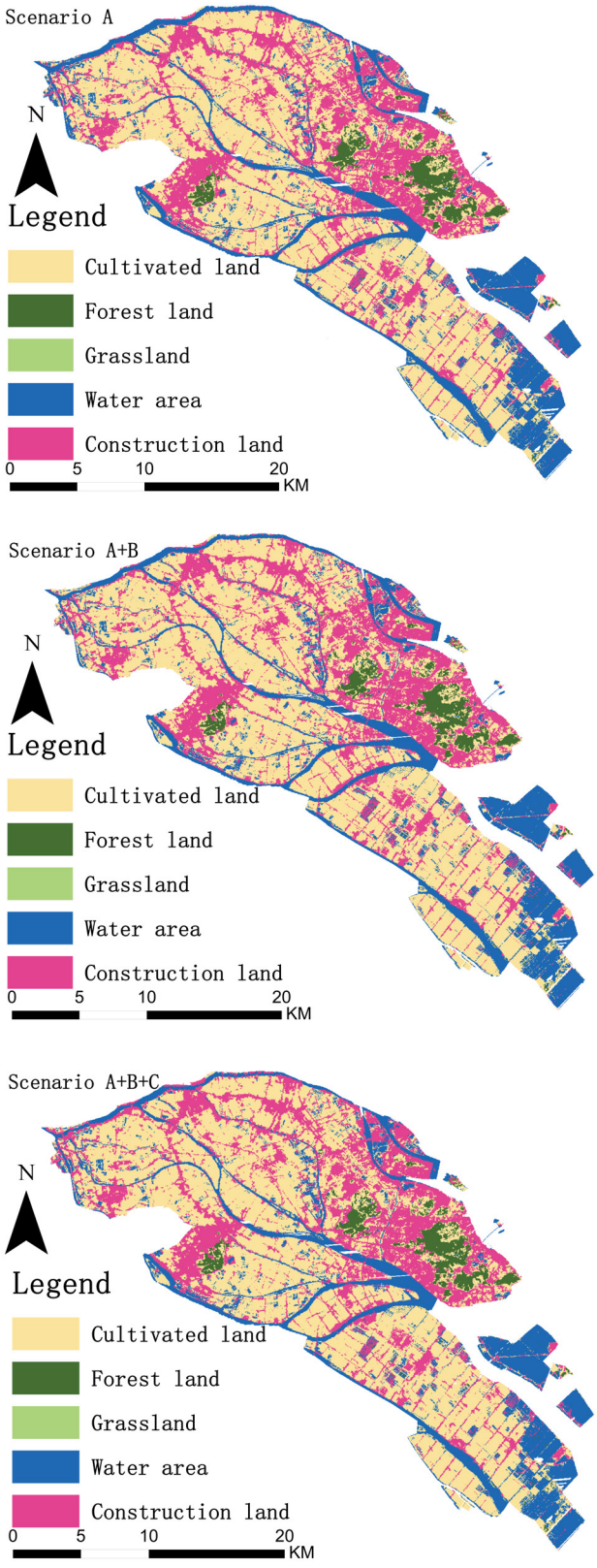

Figure 7. Simulated land use in Nansha New District, Guangzhou in 2021 under scenario A; A + B; A + B + C.

Table 3. Simulation results of land use changes and the accuracy assessment.

Scenario Type	**A**		**A + B**		**A + B + C**	
	Area (km^2)	Percentage (%)	Area (km^2)	Percentage (%)	Area (km^2)	Percentage (%)
Cultivated land	305.25	52.05	305.25	52.05	305.25	52.05
Forest land	20.99	3.58	21.02	3.58	21.03	3.59
Grassland	0.08	0.01	0.08	0.01	0.07	0.01
Water area	113.31	19.32	113.28	19.31	113.28	19.31
Construction land	146.86	25.04	146.86	25.04	146.86	25.04
Accuracy of land use types in Nansha New District in 2021 for three scenarios						
Scenario type	**A**		**A + B**		**A + B + C**	
Overall accuracy (OA)	0.8933		0.898		0.899	
Kappa coefficient	0.8304		0.8372		0.8394	
FoM accuracy value	0.0554		0.0565		0.0516	

connectivity with surrounding cities simultaneously. This scenario yielded an OA of 0.8990, a Kappa coefficient of 0.8394, and a factor of merit (FoM) of 0.0516. The changes in OA values and Kappa coefficients were more pronounced in Scenario A+B compared to Scenario A, suggesting that policy factors exerted a significant influence on land use change in Nansha New District. However, the changes in OA values and Kappa coefficients in Scenario A + B + C showed subtle variations, which were not as significant as the changes from Scenario A to Scenario A + B, indicating that the influence of regional connectivity of surrounding cities on land use change in Nansha New District was not as prominent as that of policy factors. Nevertheless, the combined OA values and Kappa coefficients indicated that the simulation accuracy of Scenario A + B + C considering multiple driving factors was the highest (refer to **Table 3**).

In this study, we examined the impact of policy factors and regional connectivity with surrounding cities on the land use dynamics of Nansha New District, a burgeoning development area. Our findings revealed that policy factors played a more prominent role in shaping land use changes. When analyzing the simulated area and proportion of different land use types in Nansha New District in 2021 under various scenarios, significant changes were observed in forest land, grassland, and water area. Notably, when considering the overlay of conventional locational factors, policy factors, and the influence of regional connectivity with surrounding cities, the proportion of forest land area was the highest, reaching 3.5858% of the total land area. In contrast, the area occupied by grassland was the smallest, representing only 0.0114% of the land. Regarding water area, the largest proportion was observed when solely considering the conventional location factors, accounting for 19.3197% of the total land area.

3.4 Future land use prediction of Nansha New District in 2030

Based on the significant findings mentioned above, Scenario A + B + C, which encompassed the integration of conventional locational factors, policy factors, and the influence of regional connectivity with surrounding cities, exhibited the highest accuracy in the model simulation. Consequently, this scenario was chosen for predicting the characteristics of land use change in Nansha New District for the year 2030. Using the CA model, the study simulated and predicted the expected land use types in Nansha New District for 2030.

Based on the predicted results (**Figure 8**), several notable observations can be made regarding the anticipated land use changes in Nansha New District between 2021 and 2030. Firstly, the proportion of cultivated land area is projected to increase from 52.05% in 2021 to 53.24% in 2030. Secondly, there

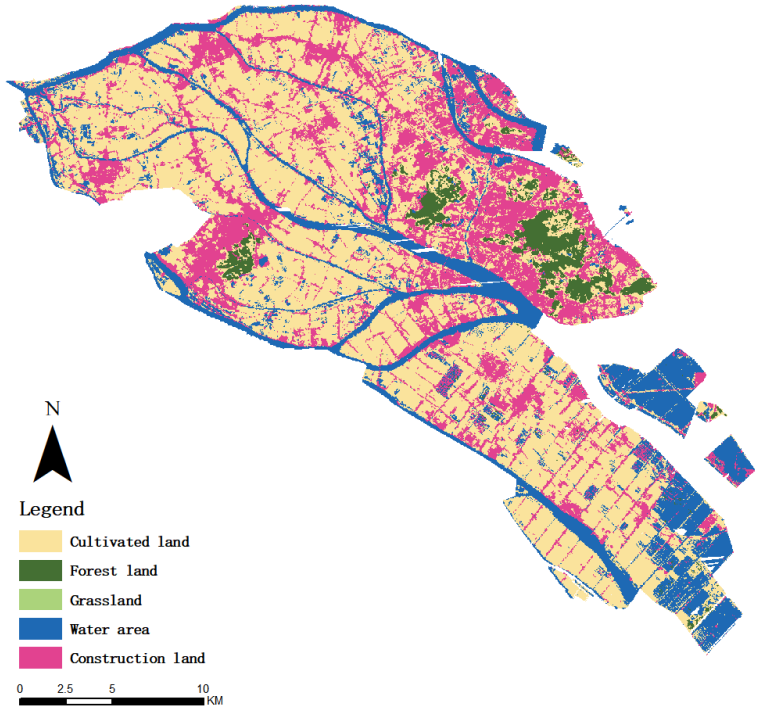

Area and proportion of land use types in Nansha New District in 2030

Land Use Type	Area (km)^2	Percentage(%)
Cultivated land	312.26	53.24
Forest land	21.08	3.59
Grassland	0.09	0.02
Water area	111.16	18.95
Construction land	141.91	24.2

Figure 8. Land use predicted results of Nansha New District in 2030.

is a minor decrease expected in the proportion of water area, declining from 19.31% in 2021 to 18.95% in 2030. Thirdly, the proportion of construction land area is predicted to decline, decreasing from 25.04% in 2021 to 24.2% in 2030. Additionally, the proportion of forest land area is projected to exhibit a marginal increase, rising from 3.58% in 2021 to 3.59% in 2030. Lastly, the proportion of grassland area is anticipated to remain relatively stable, with no significant changes expected during the specified period.

4. Conclusions and discussion

The rapid and profound urbanization in China has given rise to numerous new development areas. However, existing research primarily focuses on land use change simulation at the city, urban cluster, or larger scales, offering limited insights into simulating land use change within newly emerging areas. Moreover, there is a notable scarcity of studies that simultaneously consider conventional locational factors, the influence of regional connectivity with surrounding cities, and policy factors on land use change within these new areas. This paper aims to address and critically discuss the limitations identified in the aforementioned relevant studies. Utilizing a case study of Nansha New District in China and employing the CA model, this study simulated the land use changes in Nansha New District for the years 2015, 2018, and 2021, while also predicting its changes in 2030. The CA model was constructed under three scenarios: conventional locational factors alone, conventional locational factors combined with policy factors, and conventional locational factors integrated with policy factors and regional connectivity of the surrounding cities. The latter two scenar-

ios were specifically designed to elucidate the impact of policy factors and regional connectivity on land use changes within Nansha New District. The findings revealed that: (1) significant changes in various land uses in Nansha New District during the period from 2015 to 2021, particularly in cultivated land, water area, and construction land. (2) Comparing the predicted land use data for 2030, generated from the comprehensive model with the highest simulation accuracy, with the current land use status in 2021, it was observed that the proportion of cultivated land and forest land area increased, while the proportion of construction land and water area decreased. The proportion of grassland area showed insignificant changes.

By examining the land use data from 2015, 2018, and 2021, along with the predicted land use data for 2030, several key observations emerge regarding the land use dynamics in Nansha New District. Firstly, the dynamic development of new areas often leads to rapid and significant land use transformations within relatively small areas. Secondly, cultivated land holds a prominent proportion in the current land use pattern; however, it is currently facing challenges such as gradual fragmentation and declining intensification. This fragmentation and declining productivity pose significant obstacles to agricultural activities in Nansha New District, highlighting the impact of urbanization on agricultural land. Furthermore, the expansion of construction land is noteworthy, particularly at the expense of cultivated land. The current distribution of construction land exhibits fragmentation and disorderly spreading, particularly in the eastern part of the district. The predicted spatial distribution of construction land in 2030, especially in relation to the four industrial zones highlighted in the Urban Development Plan of Nansha New District, requires more attention in future planning evaluations.

In the future development of Nansha New District, to formulate policies that effectively address land-use challenges arising from rapid development, decision-makers should promote high-quality development in Nansha New District through enhanced coordination between human activities and land utilization. To address the problem of cultivated land fragmentation, a comprehensive approach focusing on the binding role of policies and regulations is essential. Timely planning evaluation is crucial, and greater attention should be given to the protection of basic farmland and cultivated land. Strictly penalizing violations of the law involving construction on cultivated land should be prioritized. Additionally, leveraging the advantages of regional connectivity with neighboring cities is vital. Mitigating the haphazard expansion of urban construction land requires emphasizing compact land use and effective land use planning. Key strategies include promoting mixed land use, optimizing the integration of above and below-ground space, and exploring untapped urban land potential. Innovative modes of land use planning and management, including evaluating the alignment between planning policies and actual site layout, can enhance the effectiveness of planning decisions.

This study provides support for the argument that policy factors and regional connectivity with surrounding cities exert a substantial influence on the development of new areas. Three scenarios were investigated in this research, each considering different influential factors. The findings reveal that the scenario achieving the highest overall model accuracy was the comprehensive model, which simultaneously considers conventional locational factors, relevant policy factors, and the influence of regional connectivity with surrounding cities. This indicates that policy factors and regional connectivity with surrounding cities significantly impact the land use change in Nansha New District as an emerging area. The study holds noteworthy theoretical and empirical significance, contributing to a comprehensive understanding of the driving forces behind land use changes within flourishing new areas, especially in the context of regional association and cooperation strategies.

Admittedly, this study selected only a limited number of factors as conventional locational factors, and the approximation of the connectivity of

surrounding cities to Nansha New District based on their connectivity to Guangzhou might introduce some inaccuracies in the results. Additionally, the consideration of only functional areas in the CA model when analyzing policy factors might be further improved by incorporating additional factors for a more comprehensive analysis to enhance simulation accuracy in future studies. Nevertheless, this research may offer valuable implications for simulating land use change in similar rapidly developing new areas, and it provides valuable insights for policymakers.

Author Contributions

Zehuan Zheng: Conceptualization, methodology, Formal analysis, Data Curation, Writing-Original draft preparation, Writing-Review; Editing.

Shi Xian: Conceptualization, Writing-Review; Editing.

Conflict of Interest

Declaration of no conflict of interest.

Funding

This research received was funded by the National Natural Science Foundation of China (Grant No. 42271217) and the Guangdong Planning Office of Philosophy and Social Science (Grant No.GD-21CGL15).

References

[1] Liu, X., Hu, G., Ai, B., et al., 2018. Simulating urban dynamics in China using a gradient cellular automata model based on S-shaped curve evolution characteristics. International Journal of Geographical Information Science. 32(1), 73-101.
DOI: https://doi.org/10.1080/13658816.2017.1376065

[2] Liu, X., Li, X., Shi, X., et al., 2010. Simulating land-use dynamics under planning policies by integrating artificial immune systems with cellular automata. International Journal of Geographical Information Science. 24(5), 783-802.
DOI: https://doi.org/10.1080/13658810903270551

[3] Zhou, R., Lin, M., Gong, J., et al., 2019. Spatio-temporal heterogeneity and influencing mechanism of ecosystem services in the Pearl River Delta from the perspective of LUCC. Journal of Geographical Sciences. 29(5), 831-845.
DOI: https://doi.org/10.1007/s11442-019-1631-0

[4] Beroho, M., Briak, H., Cherif, E.K., et al., 2023. Future scenarios of land use/land cover (LULC) based on a CA-markov simulation model: Case of a Mediterranean watershed in Morocco. Remote Sensing. 15(4), 1162.
DOI: https://doi.org/10.3390/rs15041162

[5] Li, X., Yang, Q., Liu, X., 2007. Genetic algorithms for determining the parameters of cellular automata in urban simulation. Science in China Series D: Earth Sciences. 50(12), 1857-1866.
DOI: https://doi.org/10.1007/s11430-007-0127-4

[6] Lin, W., Sun, Y., Nijhuis, S., et al., 2020. Scenario-based flood risk assessment for urbanizing deltas using future land-use simulation (FLUS): Guangzhou Metropolitan Area as a case study. Science of the Total Environment. 739, 139899.
DOI: https://doi.org/10.1016/j.scitotenv.2020.139899

[7] Hasan, S., Shi, W., Zhu, X., et al., 2020. Future simulation of land use changes in rapidly urbanizing South China based on land change modeler and remote sensing data. Sustainability. 12(11), 4350.
DOI: https://doi.org/10.3390/su12114350

[8] Li, D., Li, X., Liu, X., et al., 2012. GPU-CA model for large-scale land-use change simulation. Chinese Science Bulletin. 57(19), 2442-2452.
DOI: https://doi.org/10.1007/s11434-012-5085-3

[9] Liu, X., Liang, X., Li, X., et al., 2017. A future land use simulation model (FLUS) for simulating multiple land use scenarios by coupling human and natural effects. Landscape and Urban Planning. 168, 94-116.
DOI: https://doi.org/10.1016/j.landurbplan.2017.09.019

[10] Liu, X., Li, X., Shi, X., et al., 2012. A multi-

type ant colony optimization (MACO) method for optimal land use allocation in large areas. International Journal of Geographical Information Science. 26(7), 1325-1343.
DOI: https://doi.org/10.1080/13658816.2011.635594

[11] van Vliet, J., Hurkens, J., White, R., et al., 2012. An activity-based cellular automaton model to simulate land-use dynamics. Environment and Planning B: Planning and Design. 39(2), 198-212.
DOI: https://doi.org/10.1068/b36015

[12] Xiong, N., Yu, R., Yan, F., et al., 2022. Land use and land cover changes and prediction based on multi-scenario simulation: A case study of Qishan County, China. Remote Sensing. 14(16), 4041.
DOI: https://doi.org/10.3390/rs14164041

[13] Xu, X., Zhang, D., Liu, X., et al., 2022. Simulating multiple urban land use changes by integrating transportation accessibility and a vector-based cellular automata: A case study on city of Toronto. Geo-spatial Information Science. 25(3), 439-456.
DOI: https://doi.org/10.1080/10095020.2022.2043730

[14] Liu, X., Li, X., Shi, X., et al., 2010. Simulating land-use dynamics under planning policies by integrating artificial immune systems with cellular automata. International Journal of Geographical Information Science. 24(5), 783-802.
DOI: https://doi.org/10.1080/13658810903270551

[15] Wu, F., 2002. Calibration of stochastic cellular automata: The application to rural-urban land conversions. International Journal of Geographical Information Science. 16(8), 795-818.
DOI: https://doi.org/10.1080/13658810210157769

[16] Zhang, J., Hou, Y., Dong, Y., et al., 2022. Land use change simulation in rapid urbanizing regions: a case study of Wuhan urban areas. International Journal of Environmental Research and Public Health. 19(14), 8785.
DOI: https://doi.org/10.3390/ijerph19148785

[17] Chen, C., Liu, Y., 2021. Spatiotemporal changes of ecosystem services value by incorporating planning policies: A case of the Pearl River Delta, China. Ecological Modelling. 461, 109777.
DOI: https://doi.org/10.1016/j.ecolmodel.2021.109777

[18] Lai, Z., Chen, C., Chen, J., et al., 2022. Multi-scenario simulation of land-use change and delineation of urban growth boundaries in county area: A case study of Xinxing County, Guangdong Province. Land. 11(9), 1598.
DOI: https://doi.org/10.3390/land11091598

[19] Liao, W., Liu, X., Xu, X., et al., 2020. Projections of land use changes under the plant functional type classification in different SSP-RCP scenarios in China. Science Bulletin. 65(22), 1935-1947.
DOI: https://doi.org/10.1016/j.scib.2020.07.014

[20] Li, L., Huang, X., Yang, H., 2023. Scenario-based urban growth simulation by incorporating ecological-agricultural-urban suitability into a future land use simulation model. Cities. 137, 104334.
DOI: https://doi.org/10.1016/j.cities.2023.104334

[21] Zhai, Y., Yao, Y., Guan, Q., et al., 2020. Simulating urban land use change by integrating a convolutional neural network with vector-based cellular automata. International Journal of Geographical Information Science. 34(7), 1475-1499.
DOI: https://doi.org/10.1080/13658816.2020.1711915

[22] Yao, Y., Liu, X., Li, X., et al., 2017. Simulating urban land-use changes at a large scale by integrating dynamic land parcel subdivision and vector-based cellular automata. International Journal of Geographical Information Science. 31(12), 2452-2479.
DOI: https://doi.org/10.1080/13658816.2017.1360494

[23] Liu, L., Yu, S., Zhang, H., et al., 2023. Analysis of land use change drivers and simulation of different future scenarios: Taking Shanxi Province

of China as an example. International Journal of Environmental Research and Public Health. 20(2), 1626.
DOI: https://doi.org/10.3390/ijerph20021626

[24] Zhang, D., Liu, X., Wu, X., et al., 2019. Multiple intra-urban land use simulations and driving factors analysis: a case study in Huicheng, China. GIScience & Remote Sensing. 56(2), 282-308.
DOI: https://doi.org/10.1080/15481603.2018.1507074

[25] Arficho, M., Thiel, A., 2020. Does land-use policy moderate impacts of climate anomalies on lulc change in dry-lands? An empirical enquiry into drivers and moderators of LULC change in Southern Ethiopia. Sustainability. 12(15), 6261.
DOI: https://doi.org/10.3390/su12156261

[26] Kolb, M., Galicia, L., 2018. Scenarios and story lines: Drivers of land use change in southern Mexico. Environment, Development and Sustainability. 20(2), 681-702.
DOI: https://doi.org/10.1007/s10668-016-9905-5

[27] Fan, T., 2006. Improvements in intra-European inter-city flight connectivity: 1996-2004. Journal of Transport Geography. 14(4), 273-286.
DOI: https://doi.org/10.1016/j.jtrangeo.2005.08.006

[28] Allard, R.F., Moura, F., 2016. The incorporation of passenger connectivity and intermodal considerations in intercity transport planning. Transport Reviews. 36(2), 251-277.
DOI: https://doi.org/10.1080/01441647.2015.1059379

[29] Yang, Y., Li, D., Li, X., 2019. Public transport connectivity and intercity tourist flows. Journal of Travel Research. 58(1), 25-41.
DOI: https://doi.org/10.1177/0047287517741997

[30] Lin, J., Wu, Z., Li, X., 2019. Measuring inter-city connectivity in an urban agglomeration based on multi-source data. International Journal of Geographical Information Science. 33(5), 1062-1081.
DOI: https://doi.org/10.1080/13658816.2018.1563302

[31] GB/T 21010-2017 (GBT21010-2017). Current land use classification [Internet]. China National Standardization Administration. Available from: https://www.chinesestandard.net/PDF/English.aspx/GBT21010-2017

[32] Yan, J., Zhang, Y., Liu, L., et al., 2002. Land use and landscape pattern change: A linkage to the construction of the Qinghai-Xizang Highway. Journal of Geographical Sciences. 12(3), 253-265.
DOI: https://doi.org/10.1007/bf02837543

[33] Liu, X., Li, X., Anthony, G.O.Y., 2006. Multi-agent systems for simulating spatial decision behaviors and land-use dynamics. Science in China Series D: Earth Sciences. 49(11), 1184-1194.
DOI: https://doi.org/10.1007/s11430-006-1184-9

[34] Barrat, A., Barthelemy, M., Pastor-Satorras, R., et al., 2004. The architecture of complex weighted networks. Proceedings of the National Academy of Sciences of the United States of America. 101(11), 3747-3752.
DOI: https://doi.org/10.1073/pnas.0400087101

[35] Batty, M., 2018. The new science of cities. The MIT Press: Cambridge.

[36] Newman, M.E., 2004. Analysis of weighted networks. Physical Review E. 70(5), 056131.
DOI: https://doi.org/10.1103/PhysRevE.70.056131

[37] Onnela, J.P., Saramäki, J., Hyvönen, J., et al., 2007. Analysis of a large-scale weighted network of one-to-one human communication. New Journal of Physics. 9(6), 179.
DOI: https://doi.org/10.1088/1367-2630/9/6/179

[38] Opsahl, T., Agneessens, F., Skvoretz, J., 2010. Node centrality in weighted networks: Generalizing degree and shortest paths. Social Networks. 32(3), 245-251.
DOI: https://doi.org/10.1016/j.socnet.2010.03.006

[39] Zhou, Z.H., Wu, J., Tang, W., 2002. Ensembling neural networks: Many could be better than all. Artificial Intelligence. 137(1-2), 239-263.

DOI: https://doi.org/10.1016/S0004-3702(02)00190-X

[40] Li, X., Yeh, A.G.O., 2002. Neural-network-based cellular automata for simulating multiple land use changes using GIS. International Journal of Geographical Information Science. 16(4), 323-343.
DOI: https://doi.org/10.1080/13658810210137004

[41] Pontius Jr, R.G., Walker, R., Yao-Kumah, R., et al., 2007. Accuracy assessment for a simulation model of Amazonian deforestation. Annals of the Association of American Geographers. 97(4), 677-695.
DOI: https://doi.org/10.1111/j.1467-8306.2007.00577.x

[42] Gerard, B.M.H., 1998. Error propagation in environmental modelling with GIS. CRC Press: Boca Raton.

BILINGUAL PUBLISHING GROUP

Journal of Geographical Research

https://journals.bilpubgroup.com/index.php/jgr

ARTICLE

Spatial Agglomeration and Diffusion of Population Based on a Regional Density Function Approach: A Case Study of Shandong Province in China

Xiaohan Zhao*, *Yanbin Chen*

College of Geography and Environment, Shandong Normal University, Jinan, Shandong, 250358, China

ABSTRACT

Population density functions have long been used to describe the spatial structure of regional population distributions. Several studies have been conducted to examine the population distribution in Shandong Province, China, but few have applied regional density functions to the analysis. Therefore, based on the 2000, 2010, and 2020 population censuses, this study used monocentric and polycentric regional density functions to study the characteristics of population agglomeration and diffusion in Shandong. This is followed by an in-depth discussion based on population growth rate data and hot- and cold-spot analyses. The results showed that the Shandong Province population was spatially unevenly distributed. Population growth rates were higher in urban centers and counties, with more significant changes in population size in the eastern coastal areas than in the inland areas. As verified in this study, the logarithmic form of the single-center regional density function R^2 was greater than 0.8, which was in line with the population spatial structure of Shandong Province. During the study period, the estimated population density of the regional center and the absolute value of the regional population density gradient both increased, indicating a clear and increasing trend of centripetal agglomeration of regional centers over the study period. Overall, the R^2 value of the multicenter region density function was higher than that of the single-center region density function. The polycentric regional density function showed that the population density gradient of some centers had a downward trend, which reflected the spatial development trend of outward diffusion in these centers. Meanwhile, the variation in the estimated population density and the population density gradient exhibited differences in the central population distribution patterns at different levels.

Keywords: Regional density functions; Population spatial structure; Shandong Province

*CORRESPONDING AUTHOR:

Yanbin Chen, College of Geography and Environment, Shandong Normal University, Jinan, Shandong, 250358, China; Email: ychen@sdnu.edu.cn

ARTICLE INFO

Received: 5 July 2023 | Revised: 10 August 2023 | Accepted: 14 August 2023 | Published Online: 18 August 2023

DOI: https://doi.org/10.30564/jgr.v6i3.5826

CITATION

Zhao, X.H., Chen, Y.B., 2023. Spatial Agglomeration and Diffusion of Population Based on a Regional Density Function Approach: A Case Study of Shandong Province in China. Journal of Geographical Research. 6(3): 61-80. DOI: https://doi.org/10.30564/jgr.v6i3.5826

1. Introduction

Population is the most dynamic and active element in the process of urban development, and its spatial distribution in cities has always been an important part of urban geography research [1-3]. The spatial structure of a population refers to the tendency of the population to agglomerate or diffuse within a given region, which can, to a certain extent, reveal the strength or weakness of the region's socioeconomic activities [4]. With the increasingly significant spatial reconfiguration of the inner city, studying population distribution within the city has become increasingly vital [5]. Population spatial structures have far-reaching implications for regional transport planning [6], risk assessment and policy decisions [5], public safety, and crisis management [7]. Therefore, this study helps understand the characteristics of the regional spatial structure and its evolutionary trends, thus providing a reference for regional spatial organization and restructuring.

Researchers have a long history of studying regional spatial structures from the perspective of population spatial distributions. In 1951, Clark pioneered the Distance Decay Model, which suggests that population density tends to decrease with increasing distance from urban centers [8]. Since then, population density functions have been used as effective tools to characterize urban spatial structures. On this basis, scholars such as Tanner, Sherratt, McDonald, Suits, Mason and others have proposed various models of population density in monocentric cities [9], which have resulted in significant achievements in the study of urban population spatial structures. However, these studies only depicted population distribution at the city level. Parr highlighted in the mid-1980s that the decaying characteristics of population density with distance in suburban and rural areas outside cities did not conform to a negative exponential model but were closer to a Pareto function. He also proposed a unified functional form to describe the characteristics of population density across regions [10]. Later, Barkley [11], Wang [4], and others applied different forms of monocentric regional population density models to explore the fitting of the regional population density distribution and analyze the regional spatial structure and its evolutionary characteristics. However, compared to urban population density models, the research results are still relatively limited. With the innovation of information technology, restructuring of economic space, and development of transport infrastructure, the trend toward urban polycentricity is becoming increasingly evident. The existence of multiple centers with specialized economic, social, and cultural functions, as well as the interaction between the centers, makes monocentric models no longer suitable for describing contemporary urban structures [12]. Therefore, scholars have questioned the application of monocentric models [13] and have begun to apply polycentric regional density functions to explain the spatial structural characteristics and evolutionary trends of regional population density. Heikkila et al. [14] proposed three models of population density distribution in polycentric urban areas, followed by Small and Song [15], Bontjie [1], McMillen, McDonald [16] and Joseph [17] who applied polycentric regional density functions to Los Angeles, Western Europe, Chicago, and Port-au-Prince.

Research into population density models in China began in the late 1990s. This research focused on fitting regional optimal population density models based on census data and summarizing the characteristics of regional spatial structure evolution. Zhou Chunshan and Xu Xueqiang were the first to apply a monocentric city population density model to illustrate the urban population density development process in Guangzhou [18]. Later, Wang and Zhou [19] and Luo and Wei [20] simulated the population density distribution in Beijing and Nanjing, respectively, under monocentric conditions. Along with rapid urbanization and industrialization in China, the spatial variation in population density has taken on new characteristics, and the regional spatial structure has gradually changed to a complex polycentric structure. Consequently, scholars have begun to explore the spatial structure of polycentric cities and population spatial distribution. Wang and Meng [21]

used Shenyang as the study object and were the first to investigate the polycentric population density distribution structure in Chinese cities. Feng Jian and Zhou Zhouxing conducted a systematic study on the multi-core population density model in Beijing [22]. Wu Wenyu and Ma Xiya used Shanghai as the study object to analyze the characteristics of the polycentric structure of population distribution from 1990 to 2000 [23]. Jiang Li and Wu Shoulong measured the change in population spatial distribution in Guangzhou [24], and the results demonstrated a good fit for the polycentric model. Subsequently, the analysis of polycentric structures gradually expanded to regional areas, including the Beijing-Tianjin-Hebei metropolitan area [25], Yangtze River Delta urban agglomeration [26] and Huanghuaihai Plain [27]. In terms of research regions, most studies focused on more economically developed large cities or hotspot regions. There has been less exploration of regions than cities in terms of the volume of literature. In contrast to Western scholars' systematic analysis of population density models and improved testing of model applications, the analysis of population density models in the Chinese geographical circle primarily uses the existing population density model to conduct empirical research on a specific region, with few theoretical innovations. Moreover, Chinese scholars mostly base their calculations on the Euclidean distance. The Euclidean distance characterizes the straight-line distance, which differs from the actual distance in reality and does not accurately reflect a real situation. When applying the regional density function, the shortest vehicular route between two places, provided by Amap (https://www.amap.com/), was adopted to describe the distance, which is more relevant to a real situation than the Euclidean distance.

In terms of population and economic output, Shandong is one of the largest provinces in China and is characterized by an uneven level of development within the region. In previous studies, scholars have discussed the population distribution in Shandong Province, starting from the structure index [28,29], population gravity center [28,29], shift-share analysis [28] and spatial autocorrelation analysis [29,30]; however, few studies have used regional density functions for analysis. Population density patterns are important features of regional economies and societies [31]. The optimization of the spatial distribution of the population can have a significant impact on the structure and layout of various factors, such as the economy, culture, and industry, helping to promote regional economic development and improve people's quality of life. Viewing the growing importance of the population spatial structure and rapid urbanization and continuous economic restructuring in Shandong Province in recent years, it is particularly essential to utilize the regional density function to study its population distribution and spatial structure, evolution pattern and regional spatial structure's variation trend.

In summary, this study analyzed the population density characteristics of Shandong Province from 2000 to 2020 based on county data. It used the Inverse Distance Weighted method to clarify the spatial relationship of population distribution. Subsequently, the spatial structure of Shandong Province and its evolutionary characteristics were shown by applying monocentric and polycentric regional density functions, respectively. The spatial agglomeration and diffusion of the population in Shandong Province were discussed in depth based on the population growth rate and hot and cold spot analysis. Analyzing the spatial structure of Shandong Province from the standpoint of the regional density function provides a new perspective on the study of spatial structure, which can be compared with the results obtained from other methods. Simultaneously, the evolutionary characteristics and development trend of Shandong Province's population spatial structure can be examined, as well as the problems that hamper its long-term development process and the law of urban agglomeration development can be better understood. This can provide a basis for urban planners to rationally guide regional population distribution, optimize resource allocation, make scientific spatial planning decisions, and serve as a reference for other urban agglomerations in China.

2. Materials and methods

2.1 Study area

Shandong Province is located in the economically developed eastern coastal region of China, downstream of the Yellow River, the second-longest river in China, and between the two state-level urban agglomerations: the Beijing-Tianjin-Hebei region, and the Yangtze River Delta urban agglomerations. To the east, it is separated from the Korean Peninsula and Japan by the sea. Its eastern part is dominated by hills, while the central part has many mountains, and the southwest and northwest are mostly plains (**Figure 1**), with a total land area of 156,700 km^2. According to data from the 7th National Census, the number of people living in Shandong Province exceeded 100 million, ranking second in China in terms of total population. Simultaneously, the gross national product of Shandong Province is expected to reach 728 million yuan in 2020, ranking third in China. Shandong Province is veritable in terms of its population and economy. As an uncommon province in China where a province is developed as an urban agglomeration, the Shandong Peninsula Urban Agglomeration is one of the important urban agglomerations proposed in the National 14th Five-Year Plan for development and growth and is also the core of the national strategy to promote new urbanization and economic development [32]. To respond positively to the national planning objectives, Shandong Province specified in the "Outline of the 14th Five-Year Plan for National Economic and Social Development of Shandong Province and Vision 2035" that the institutional mechanism for the coordinated development of the whole region should be promoted in an integrated manner. Optimizing and improving the regional spatial structure is the key to achieving coordinated regional development [33], which must be based on an in-depth understanding of the spatial structure of population density and its evolutionary characteristics in Shandong Province.

2.2 Methods

The regional density function is an important means to study the spatial structure of the regional population and its evolution trend. Since its introduction, many scholars have extended its application and supplemented its amendments, achieving rich research results. Given that the acquisition of population data is relatively convenient and reliable and the mathematical form of the regional density function is quite simple, this study also chose this method to model the population agglomeration and diffusion characteristics of Shandong Province.

(i) Monocentric regional density function

The regional density function is used to describe how population density varies with distance from the central city, and is an effective tool for studying the characteristics of population agglomeration and diffusion [13]. Following Alperovich, the following four forms of monocentric area density functions (**Table 1**) were validated by some scholars [4]:

The monocentric regional density function as-

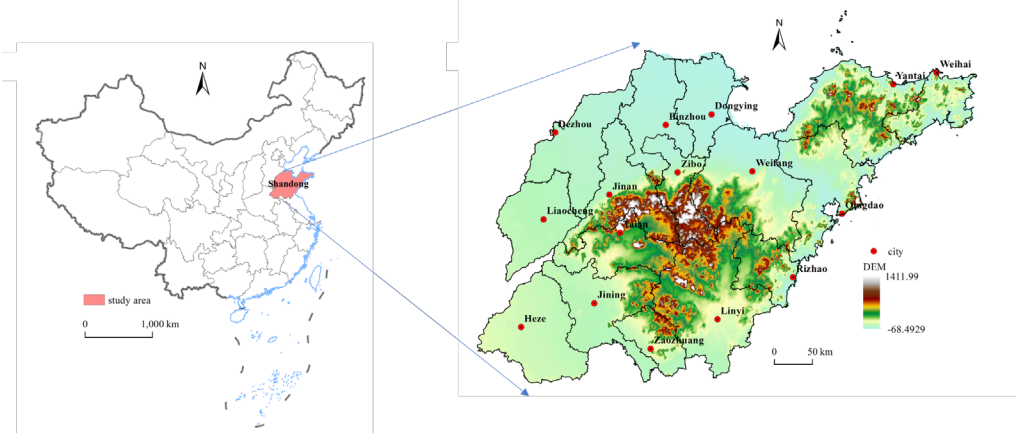

Figure 1. Location and topography of Shandong Province.

Table 1. Monocentric regional density functions and the parameters.

Models	Function used in regression	Original function	X variable	Y variable	Restrictions	Meanings of parameters
Linear	$D_r = a + br$	Same	r	D_r	None	*r* is the distance between the area and the regional center, D_r is the population density at distance *r* from the regional center, and *a* and *b* are parameters to be estimated.
Logarithmic	$D_r = a + b\ln r$	Same	$\ln r$	$_D$r	$r \neq 0$	
Power	$\ln D_r = a + b\ln r$	$D_r = ar^b$	$\ln r$	$\ln D_r$	$r \neq 0$ and $D_r \neq 0$	
Exponential	$\ln(D_r) = a + br$	$D_r = ae^{br}$	r	$\ln D_r$	$D_r \neq 0$	

sumes that there is only one central city in the region. Therefore, when discussing the form of the monocentric regional density function, it is first necessary to divide Shandong Province into a number of monocentric metropolitan areas. In this study, we referred to Wang Fahui's approach for delineating urban influence ranges [4] and used the urban areas of the central cities in the region as the core to delineate their zones of influence. The delineation of the zone of influence was based on the gravity model:

$$I_i = C_i \,/\, r_{ij}^{\beta} \tag{1}$$

where C_i is the population size of city *i*; r_{ij} is the distance between regional unit *j* and city *i*; I_{ij} indicates the degree to which regional unit *j* is influenced or radiated by city *i*; and β is the distance friction coefficient, where the empirical value of $\beta = 2.1$ is taken from the gravity model used by Yang Qi in his study of inter-regional passenger flows in China [34]. A central city is an attributed city of regional unit *j* if its radiation or influence on regional unit *j* is the greatest among all central cities.

(ii) Polycentric regional density function

The monocentric regional density function only considers the influence of a single central city when analyzing the regional population distribution [25]. It is believed that the population density at the same distance from the center is the same, regardless of the direction [17], which has some limitations when analyzing the trend of population density changes in polycentric regions. Therefore, it is essential to consider the impact of multiple centers in the region on the population distribution to more accurately interpret the characteristics of regional population agglomeration and dispersion. The polycentric regional density function was used to reveal the distribution and trend of regional population density under the combined effect and influence of multiple centers. Heikkila et al. argued that if multiple centers are in competition and division of labor with each other, and there is both substitutability and complementarity, then the polycentric density function may formally take the form of a merger of multiple monocentric density functions. Based on this, they proposed three models for the distribution of population density in polycentric urban areas [14]. Assumptions regarding the impact of multiple centers on population distribution range from full substitution to full complementation. Given the fact that most scholars deem the impact of each center in the region to be between complete substitution and complementation [38] and the actual situation in Shandong Province, this study selected the exponential model to test Shandong Province. Its functional form is:

$$D_r = \sum_{i=1}^{n} a_i e^{b_i r_i} \tag{2}$$

where D_r is the population density at distance *r* from the regional center, *n* represents the number of regional centers, r_i is the distance from the region to each center, and a_i and b_i are parameters specific to regional center *i*.

(iii) Inverse Distance Weighted (IDW) Interpolation

To clearly reflect the spatial relationship of the population distribution in Shandong Province, this study applied the IDW method to analyze the regional population density distribution. The IDW is one of the most commonly used methods for interpolating spatial information. It is based on the "first law of geography", which assumes that the parameter values of observations closer to the prediction point are

more similar than those further away from the prediction point [36]. Therefore, the IDW method assigns more weight to observations that are closer to the predicted points [37]. The equation for this method is as follows:

$$Z = \sum_{i=1}^{n} \frac{Z_i}{d_i^p} / \sum_{i}^{n} d_i^p \tag{3}$$

where Z is the estimated value, Z_i is the i (i = 1,...,n) sample value, d_i represents the distance, and p is the power of the distance, which was chosen based on the minimum mean absolute error criterion. The default setting is p = 2, at which point the corresponding method is called inverse distance squared interpolation [38].

(iv) Cold and hotspot analysis

Cold and hotspot analysis is one of the methods used for global aggregation testing. It identifies high- and low-value clusters of regional elements at different spatial locations by calculating the Getis-Ord G_i^* statistics for each element in the dataset. That is, it identifies the spatial distribution pattern of cold and hot spots in the study area [39]. The equation [40] is as follows:

$$G_i^* = \frac{\sum_{j=1}^{n} W_{ij} x_j}{\sum_{j=1, j\neq i}^{n} x_j} \tag{4}$$

where G_i^* is the Getis-Ord G_i^* statistic. x_j is the elemental attribute value at location j; n is the total number of districts and counties; and W is the spatial weighting matrix. When the G_i^* value is positive and significant, it indicates that the values around the detected points are relatively high and belong to the high-value spatial agglomeration (hot spot area); a negative and significant G_i^* value indicates that the values around the detected points are relatively low and belong to the low-value spatial agglomeration (cold spot area); a G_i^* value of zero indicates that the result was randomly generated and not statistically significant. A significance test was performed on the obtained G_i^* values to identify cold and hot spots at the confidence intervals.

2.3 Data sources

In this study, resident population data for 2000, 2010, and 2020 were selected as the population data. Compared to the household population indicator, the resident population indicator more accurately reflects the total number of people residing in a region over a certain time period and can more accurately indicate the true size of a region's population [41]. Resident population figures for 2000, 2010, and 2020 were obtained from the fifth, sixth, and seventh national census bulletins, respectively, published by each municipality.

For the administrative division data, the land area data of the county administrative area were used to calculate the regional population density, and the data were derived from the Baidu Encyclopedia of the corresponding county. The administrative divisions of Shandong Province underwent adjustments and changes during the study period. To ensure continuity and comparability of the data, this study used the 2020 administrative divisions as the standard and matched the statistics for 2000 and 2010. This included correction and matching of the names used in 2020 for county-level administrative units that had been renamed and adjusted, adjustment of the zoning of newly established districts and counties according to the streets and towns under their jurisdiction in 2020, and merging or splitting of county-level units with boundary adjustments and changes according to boundary changes. In addition, non-administrative areas, such as high-tech zones and economic and technological development zones in each municipality were consolidated according to the area in which they were located.

Data used to measure the distance between the two regions were obtained from Amap (https://www.amap.com/). This study selected the shortest vehicle route between the county or municipal government of the two administrative regions to represent the distance between each region.

3. Results and discussions

3.1 Population distribution characteristics of Shandong Province

Statistical characteristics of the population distribution

An analysis of regional population density can reveal the basic characteristics of regional population distribution and reflect regional differences in population distribution [27]. According to the population density distribution map of Shandong Province from 2000 to 2020 (**Figure 2**), the population of Shandong Province was spatially unevenly distributed, with obvious differences between districts and counties. Areas with high population densities were more dispersed, with multiple densely populated circles in local areas. In contrast, areas with low population densities were characterized by faceted contiguity. Specifically, the population density was lower in the northern part of Shandong Province and higher in the eastern coastal, central, and southern regions. Peak population density areas were concentrated in the urban areas of the cities, with the northern and southern districts of Qingdao having extremely high population densities, forming two polarized centers with population densities of over 10,000 persons per square kilometer in all years. The other regions with higher population densities (Lixia District in Jinan, Zhangdian District in Zibo, Licang District in Qingdao and Zhifu District in Yantai) were almost all between 5,000 and 10,000 persons per square kilometer, a far cry from the two districts in Qingdao. There were sharp differences in population density between urban areas and districts and counties outside urban areas, presenting a clear decay from urban areas to the periphery of the city. Most population densities in the districts and counties outside the city are less than 1,000 persons per square kilometer. In addition, the population density varied significantly between districts and counties in Shandong Province (**Table 2**). For example, in 2000, the minimum population density was only 97 persons/square kilometer, whereas the maximum reached 14,918 persons/

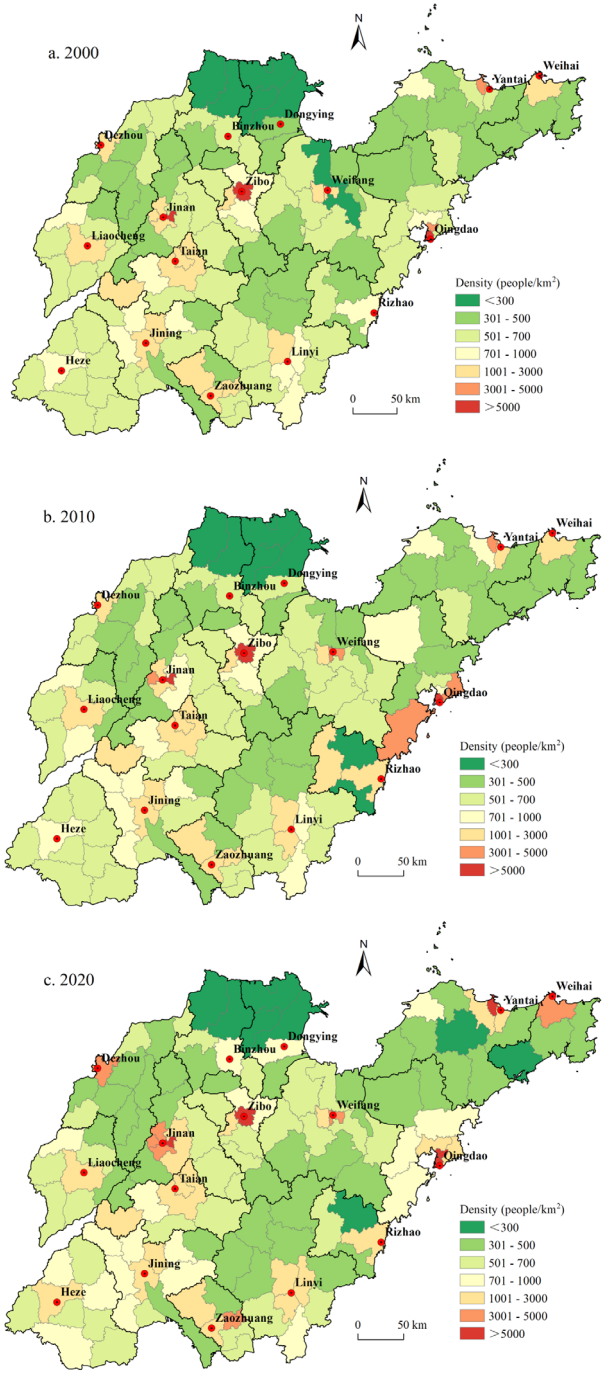

Figure 2. Population density distribution map of Shandong Province.

square kilometer, a difference of nearly 150 times. Specifically, in terms of spatial changes in population distribution, with the exception of Heze City and the peripheral districts and counties of Qingdao City, where there was a widespread increase in population density, there was little change in the distribution of all classes of population density over the study pe-

Table 2. The descriptive statistics of population density in Shandong Province.

Year	Population density (person/km^2)			
	Maximum	Minimum	Average	Standard deviation
2000	14918	97	1010	1889
2010	18162	109	1168	2246
2020	17411	108	1280	2337

Year	Number of counties by population density(person/km^2)						
	< 300	300-500	500-700	700-1000	1000-3000	3000-5000	> 5000
2000	7	38	52	15	18	2	4
2010	7	36	45	19	20	5	4
2020	8	41	34	20	21	6	6

riod, and the pattern of population distribution was relatively stable.

From the perspective of temporal changes in population density, both the mean and standard deviation of population density in Shandong Province showed an increasing trend (**Table 2**). This indicates that the population density of Shandong Province has grown over the past 20 years, and regional differences have increased. This is demonstrated by the minimum population density in Shandong Province (Hekou District, Dongying City) increasing from 97 persons/km^2 in 2000 to 108 persons/km^2 in 2020; the average population density increasing from 1010 to 1280 persons per square kilometer over a period of 20 years; and the number of areas with a population density greater than 1,000 persons per square kilometer rising from 24 in 2000 to 33 (**Table 2**), with new areas including Licheng District in Jinan, Laoshan District in Qingdao, Laishan District in Yantai, Donggang District in Rizhao, Luozhuang District, and Hedong District in Linyi. There was a marked change in the districts and counties with population density values between 500 and 700 persons/km^2, with several of them having increased to 700-1000 persons/km^2 in 2020.

In summary, the densely populated areas of Shandong Province are concentrated in economically developed areas with superior natural geography. Economically developed areas with accelerating levels of urbanization are attracting growing population concentrations from outlying districts and counties, making the local population density significantly higher than that of other districts and counties. The influence of the natural geographical environment on population distribution can be observed in the topography of the terrain. The flatter terrain favors the growth of local crops, which in turn leads to higher population densities [42]. In the south-central region of Shandong Province, mountainous and hilly terrain is widespread, transportation is inconvenient, and economic development is relatively slow, making the population more dispersed [43]. The Yellow River Delta region of Dongying and Binzhou, although located on the plain, is plagued by seawater erosion and serious land salinization, making reclamation and renovation difficult; therefore, it is sparsely populated. The topography of the Jiaodong Peninsula is predominantly hilly and complex; thus, the population is mostly concentrated in gently sloping coastal areas [28]. Coupled with the advantageous geographical location of the Shandong Peninsula urban agglomeration, convenient waterway transportation, earlier development, and higher levels of economic development and urbanization than in inland areas, this has led to the movement of the surrounding population to coastal areas, resulting in significant differences between the surrounding districts and counties [44]. In addition, the areas along the axes of the main railway lines (Jiaoji, Beijing-Shanghai, Beijing-Kowloon and Xinshi lines) are also areas of high population density.

Spatial characteristics of population distribution

The IDW results (**Figure 3**) demonstrated that,

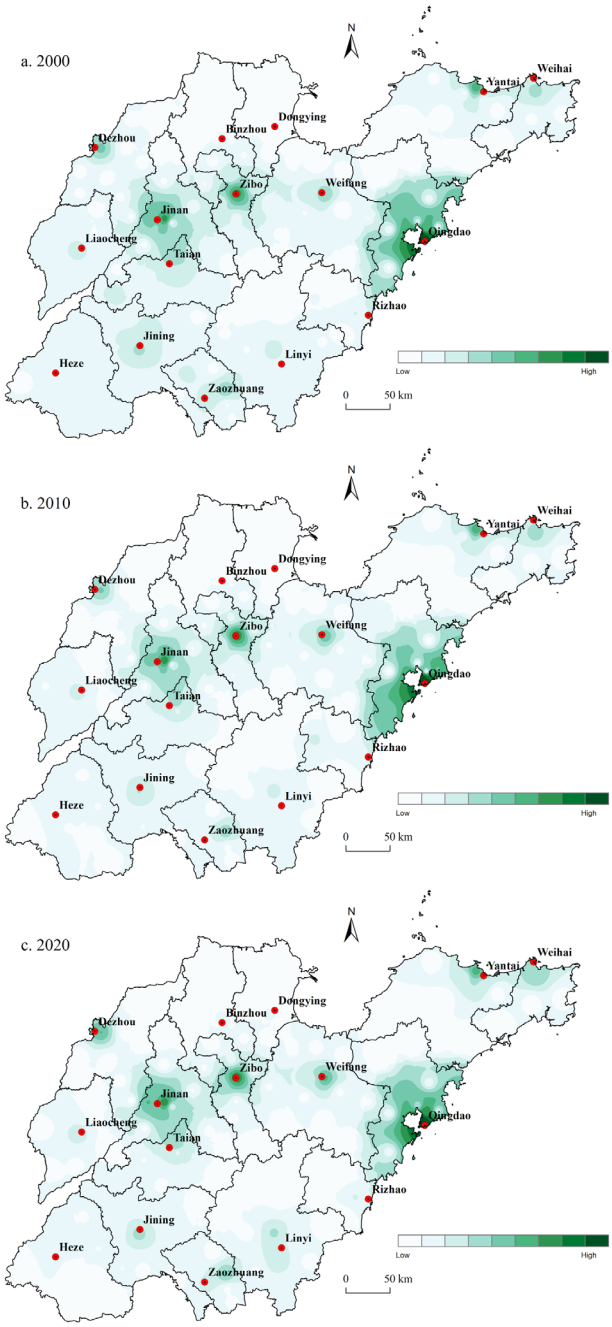

Figure 3. Population density distribution map of Shandong Province based on IDW.

in general, the areas with high and low values did not vary significantly during the study period. The divergence in population density was evident, showing a trend of local concentration in high-value areas and a contiguous distribution in low-value areas. A spatial distribution pattern was formed, with Jinan, Qingdao, Zibo, Weifang, Yantai, and Dezhou as local high-value areas, whereas other areas were low-value areas for a long time. Meanwhile, several high-value areas tended to diffuse from the center to the periphery, presenting a certain circular structure. Moreover, degradation of the high- and low-value areas occurred in almost all outer districts of the city during the study period. This could indicate a developmental tendency of the population to concentrate on the central city.

Overall, the results based on the IDW revealed the stable existence of six statistically significant high population density areas within Shandong Province, indicating a polycentric spatial structure characteristic of regional population distribution. The six densely populated areas centered on the Jinan, Qingdao, Zibo, Weifang, Yantai, and Dezhou centers can serve as the six population density centers in Shandong Province. This finding provided a basis for the application of the polycentric regional density function to analyze the characteristics of regional population agglomeration and diffusion.

3.2 Agglomeration and diffusion of the population in Shandong Province

Analysis based on the monocentric regional density functions

According to the results of the IDW, there are six statistically significant population density centers in Shandong province, namely Jinan center (Lixia District, Shizhong District, Huaiyin District, Tianqiao District, Licheng District), Qingdao center (Shinnan District, Hebei District, Laoshan District, Licang District), Zibo center (Zichuan District, Zhangdian District, Zhoucun District), Yantai center (Zhifu District, Fushan District, Muping District, Leshan District), Weifang center (Weicheng District, Hanting District, Fangzi District, Kuiwen District) and Dezhou center (Decheng District). Considering the need for computation, this study chose the shortest route between the other district and county governments and the regional center government, plus one kilometer as the distance from the regional center; and thus, the impact area was divided. Combined with the results of the influence zone division, this study fits four forms of density functions for the Ji-

nan, Qingdao, Zibo, Yantai, Weifang, and Dezhou centers. The results demonstrated (**Table 3**) that the logarithmic model exhibited high goodness of fit in all six regions. Therefore, a logarithmic model was selected for analysis of the study area.

The intercept *a* and slope *b* of the regional density function represent the estimated population density at the center of the region and the regional population density gradient, respectively. By observing the fitted lines of density functions based on the logarithmic model for the Jinan, Qingdao, Zibo, Yantai, Weifang, and Dezhou centers over the study period (**Figure 4**), the absolute values of the intercept *a* and slope *b* increased in all six regions from 2000 to 2020, and the growth in the Jinan and Dezhou centers was prominent from 2010 to 2020, while the growth in the remaining four population density centers was relatively stable over the two decades, with the Qingdao and Dezhou centers rising particularly rapidly. An increase in the intercept reflects an increase in population density in the urban areas of the central city, while an increase in the slope indicates that population density decreases more rapidly as the distance to the central city increases. This indicates a clear and increasing trend of centripetal agglomeration in the six regions over the 20-year period. Districts closer to the center not only have a higher population density but also a faster growth rate in population density than more distant districts. After analyzing the census data, this study suggests that the rapid increase

Table 3. Regression results of monocentric regional density functions.

Region	Function form	*a*			*b*			R^2		
		2000	2010	2020	2000	2010	2020	2000	2010	2020
Jinan	Linear	786.652	919.785	1085.737	–2.793*	–3.767*	–5.605*	0.226	0.235	0.238
	Logarithmic	1310.016	1624.713	2145.855	–187.243	–251.158	–372.169	0.801	0.811	0.822
	Power	7.123	7.321	7.556	–0.216	–0.248	–0.309	0.687	0.694	0.685
	Exponential	6.517	6.619	6.676	–0.003*	–0.004*	–0.005*	0.190	0.193	0.179
Qingdao	Linear	1860.429*	2478.311*	3037.079*	–14.989*	–24.340*	–30.040*	0.409	0.443	0.502
	Logarithmic	3163.444	4045.571	4738.781	–617.727	–834.934	–958.835**	0.921	0.945	0.929
	Power	8.053	8.353	8.577	–0.409	–0.458**	–0.471*	0.920	0.901	0.837
	Exponential	7.261	7.598	7.900	–0.011*	–0.016*	–0.018*	0.511	0.575	0.683
Zibo	Linear	1203.035	1356.848	1469.173	–13.461	–16.179	–18.770*	0.873	0.895	0.850
	Logarithmic	1328.238	1533.722	1730.581	–194.064**	–241.313	–297.126	0.780	0.856	0.917
	Power	7.264	7.419	7.546	–0.242**	–0.271**	–0.310**	0.655	0.718	0.768
	Exponential	7.150	7.275	7.343	–0.018	–0.020	–0.021	0.830	0.874	0.854
Yantai	Linear	567.085**	716.164**	841.868*	–1.030*	–2.778*	–4.409*	0.059	0.238	0.308
	Logarithmic	629.576**	813.582**	988.158**	–36.753*	–81.059*	–126.524*	0.155	0.421	0.528
	Power	6.507	6.686	6.860	–0.075*	–0.139*	–0.200*	0.167	0.364	0.397
	Exponential	6.317	6.507	6.581	–0.002*	–0.005*	–0.006*	0.066	0.192	0.193
Weifang	Linear	562.077	621.762	689.244	–1.242**	–0.937*	–2.967*	0.283	0.041	0.307
	Logarithmic	560.444	742.276	924.003	–16.906*	–47.690*	–110.551**	0.115	0.184	0.735
	Power	6.330	6.593	6.807	–0.035*	–0.076*	–0.162**	0.130	0.174	0.603
	Exponential	6.328	6.398	6.463	–0.002*	–0.001*	–0.004*	0.294	0.038	0.251
Dezhou	Linear	2358.959*	2904.270*	4286.715*	–52.823*	–67.412*	–106.679*	0.937	0.942	0.939
	Logarithmic	2383.428**	2932.550**	4334.992**	–542.267**	–690.924**	–1094.709**	0.993	0.994	0.993
	Power	7.771	7.979	8.365	–0.468**	–0.515**	–0.648**	0.986	0.988	0.985
	Exponential	7.745	7.956	8.325**	–0.045*	–0.050*	–0.063*	0.924	0.933	0.919

Note: The significance level of parameter estimates without labeling is p = 0.001; * indicates that the parameter estimates are not significant, and ** indicates that the significance level of parameter estimates is p = 0.01.

in population density in the centers of Jinan and Qingdao is mainly due to the large influx of people from other areas. The population of the urban area in Jinan is large, and the growth of its population density is closely related to its special status as the capital city of the province. The population density in the Jinan center rose faster from 2010 to 2020, and this study speculates on the following reasons: In 2017, Shandong Province clarified the strategic concept of the conversion of old and new kinetic energy, and Jinan city actively responded to the requirements by developing a number of new industries. The objective demand for economic structure optimization and policy support led to the migration of talent to Jinan. In addition, in 2020, Jinan proposed a "strong provincial capital" strategy and zero-threshold settlement policy, which also contributed to rapid growth in population density. Qingdao, the most developed leading city in the Jiaodong Economic Circle and an important national coastal center city, is well placed in terms of economic output, employment opportunities, social security, and infrastructure. Simultaneously, Qingdao hosted various major events, such as the Shanghai Cooperation Organization summit, and the city's influence increased significantly. The reform of the household registration system and the relaxation of settlement and access conditions also provided conditions for population agglomeration, which undoubtedly attracted the population of the surrounding districts and counties. As far as the other three centers are concerned, Zibo has a long history of industry and is an old industrial area that has developed based on its resources. This, coupled with its emphasis on the transformation and upgrading of traditional industries and its focus on the tertiary sector during its development in recent years, has allowed the region to flourish. Yantai is strategically located and is an important land and sea transportation hub in Northeast Asia and the Circum-Bohai Sea Economic Zone. Relying on its excellent port conditions, the city is actively cultivating and growing its hub economy. Simultaneously, as one of the "three cores" of Shandong Province's comprehensive pilot zone for the conversion of old and new kinetic energy, it is developing well. Weifang ranks among the top cities in Shandong Province in terms of geographical area, population, and total economic scale, and has a strong industrial base as a traditional industrial and agricultural city. It relies on the Weifang Port to actively develop its port economy. In recent years, Weifang has been optimizing and upgrading its industrial system, improving its modern industrial system, and continuously increasing its investment in innovative cities with certain advantages. The transport location and natural conditions provide a good foundation for the development of Dezhou. Relying on its superior transportation location, the Dezhou center has taken the lead in development, driven by the synergistic development of the Beijing-Tianjin-Hebei Region. As a large national transportation hub, Dezhou is developing at a relatively rapid pace. In addition, rich mineral resources exist underground in Decheng District. The Dezhou Power Plant of Huaneng International Power Co., Ltd., the second largest thermal power plant in China, is located in the Decheng District, which also attracts the population of surrounding districts and counties to work there [45]. Although the Zibo, Yantai, Weifang, and Dezhou centers also have a certain floating population, they are inferior to the Jinan and Qingdao centers.

Furthermore, it can be observed from **Figure 4** that the growth rate varied considerably between the different areas in the hinterlands of the Qingdao and Dezhou centers. The growth in population density was very significant in proximity to the Qingdao and Dezhou centers, whereas the growth in areas further away from them was slow. This is in line with the "core growth-hinterland stagnation" pattern of Barkley et al. [11]. In contrast, the growth patterns of the remaining centers were more moderate, and although the areas closer to the center continued to grow faster than those away from it, the difference in growth rates was more moderate than that in the two centers mentioned above. These two growth patterns reflect the difference between the development of the central city and that of its hinterland. Qingdao's economy is large and has an extremely strong agglomeration effect. It has a large development gap

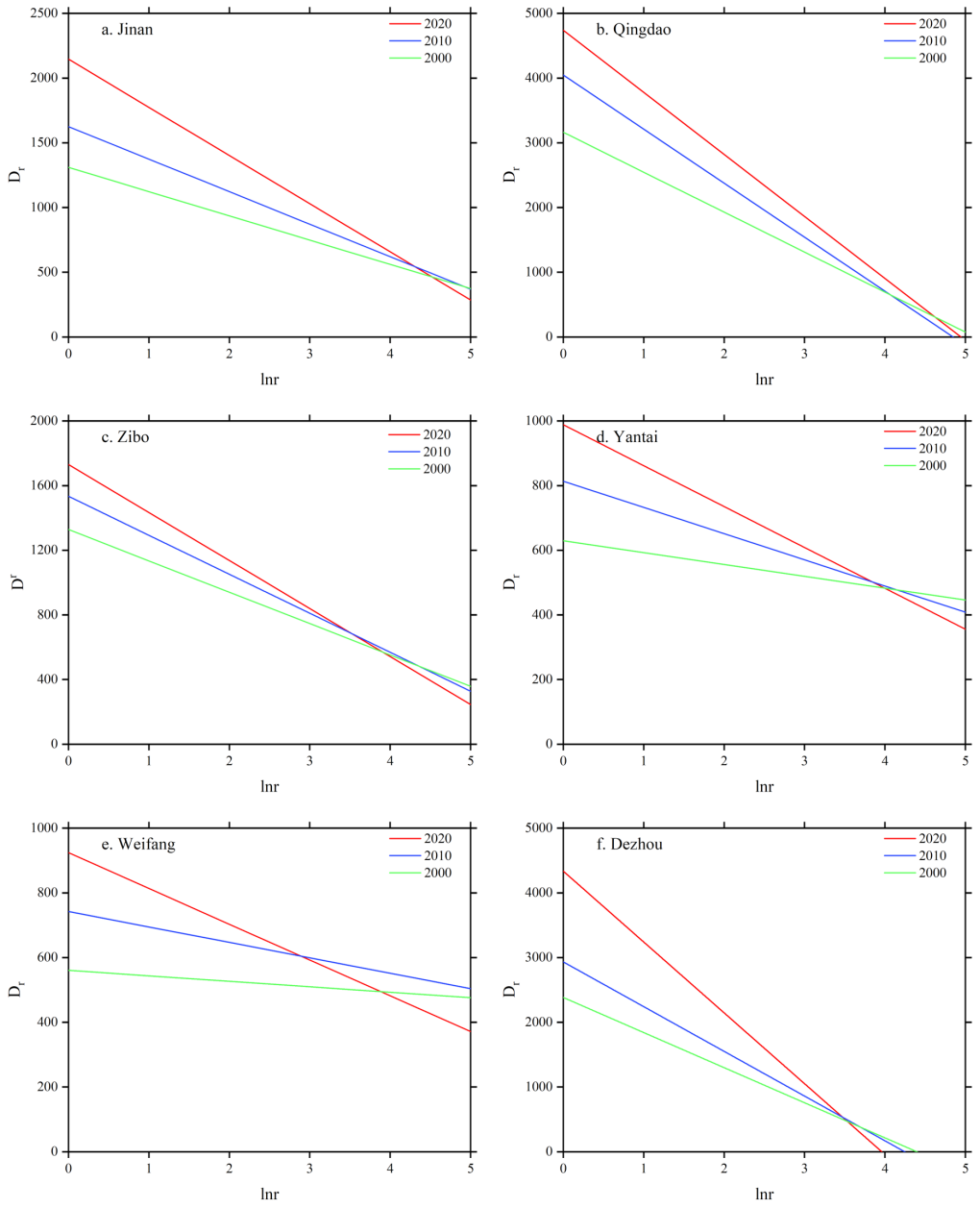

Figure 4. Growth patterns in different population density centers.

with the surrounding districts and counties, and the city of Qingdao does not have a strong radiation drive. The lack of large-scale, complete industrial chains and high-level modern industrial enterprises in the Jiaodong Peninsula makes it difficult to stimulate economic development in the hinterland [46]. The stronger polarization effect led to a larger difference in population density between the central area and peripheral districts and counties. The reason for the large difference in population density between the center of Dezhou and the periphery is the low level of economic development in Dezhou as a whole. Compared to other county-level regions, Decheng District has a high degree of development. In Dezhou city, the center has a comparative advantage. In addition, most new infrastructure is concentrated in cities and counties, which increases the development gap [47]. The center of Jinan has a well-developed economy, excellent service facilities and, thanks to the integration construction of the Jinan metropolitan area, Jinan and its neighboring cities have reached the standard of a "one-hour economic circle" with

convenient transportation [48]. The diffusion effect has also led to higher population densities in neighboring areas, with stronger spatial correlations between regional units [42]. In addition, **Figure 4** shows that the population density in Jinan center is lower than that in Qingdao center. This study speculates that this is because of the rapid development of Qingdao in recent years, with Jinan, the provincial capital city, being overwhelmed by Qingdao, and the increasing competition gap. Compared to Jinan, the gap between the centers of Zibo, Yantai, and Weifang and the peripheral areas is smaller. The common reason for this is that the economic development of the districts and counties within the sphere of influence of these three centers is at a similar level. The centers do not have a strong population concentration capacity, but their relatively rapid economic development has attracted a certain population from the surrounding districts and counties. Together with the proximity of these three centers to the cities of Jinan and Qingdao, their development is inevitably influenced by the two powerhouses, limiting their polarization and diffusion effects.

Analysis based on the polycentric regional density functions

The determination of regional density centers was based on the above analysis of the characteristics of the population density distribution in Shandong Province. Six population density centers were used for the monocentric regional density function analysis: Jinan, Qingdao, Zibo, Yantai, Weifang, and Dezhou. According to the IDW, the most prominent centers were Jinan, Qingdao, and Zibo. The polycentric regional density function followed the six centers mentioned above, and the models were fitted and compared separately for different numbers of centers. The fit results for the polycentric population density model are presented in **Table 4**.

The polycentric population density model based

Table 4. Comparison of the fitting results of the polycentric population density model.

Center	Year	Model 1		Model 2		Model 3		Model 4	
		a	b	a	b	a	b	a	b
	2000	641.290	–0.002	1538.991	–0.482	1359.701	–0.356	1319.043	–0.324
Jinan	2010	1020.603	–0.007	1459.236	–0.114	1467.612	–0.124	1444.702	–0.100
	2020	3223.348	–0.568	2154.727	–0.111	2137.374	–0.094	2138.823	–0.096
	2000	3216.818	–0.068	3138.012	–0.080	3144.400	–0.080	3144.892	–0.080
Qingdao	2010	4267.686	–0.046	3932.811	–0.065	3918.105	–0.066	3928.841	–0.066
	2020	4789.047	–0.044	4551.754	–0.051	4570.155	–0.051	4568.794	–0.051
	2000	775.341	–0.050	855.579	–0.044	846.112	–0.045	846.598	–0.045
Zibo	2010	1016.212	–0.040	1053.177	–0.045	1044.845	–0.047	1024.394	–0.049
	2020	998.269	–0.006	1284.258	–0.051	1267.076	–0.052	1267.173	–0.052
	2000			498.867	0.000	241.642	–0.272	234.610	–0.236
Yantai	2010			504.216	0.000	528.988	0.000	486.983	–0.268
	2020			504.531	0.000	805.472	–0.309	771.650	–0.273
	2000					504.355	0.000	504.311	0.000
Weifang	2010					486.365	–0.547	568.621	–0.001
	2020					538.579	–0.001	534.415	–0.001
	2000							3972.119	–0.716
Dezhou	2010							2940.236	-0.162
	2020							7021.046	-0.577
	2000	0.887		0.958		0.958		0.968	
R^2	2010	0.888		0.955		0.946		0.962	
	2020	0.920		0.937		0.940		0.961	

on the exponential form fits better and is generally more applicable than the monocentric model, with R^2 values above 0.9 in all years of the study period. This indicates that the exponential model can better explain the structure of the population density distribution in Shandong Province, which has formed a polycentric population density spatial structure, and the relationship between population density centers is between complete substitution and complementation. Model 1 used three centers, Jinan, Qingdao, and Zibo, all of which had R^2 values exceeding 0.88, indicating that these three centers explained, to a large extent, the distribution of population density in Shandong Province. By 2020, the R^2 value reached 0.92, indicating that these three centers had an increasingly strong influence on regional population density distribution and could dominate regional population density distribution. Model 2 added the Yantai center, and the R^2 value further increased to over 0.93. The explanatory power of the model was further enhanced, indicating that these four centers could fully explain the regional population density distribution. However, between 2000 and 2020, the R^2 values showed a decreasing trend, indicating that other population density centers in the region continued to develop and had an increasingly significant impact on the regional population density distribution, while the explanatory power of the Yantai center on the overall regional population density distribution decreased. Models 3 and 4 added the Weifang and Dezhou centers, respectively, and the results demonstrated that the two centers also had an impact on the regional population density distribution; however, there was no significant change in R^2 values, indicating that the Weifang and Dezhou centers made a relatively limited contribution to the degree of model interpretation.

Changes in the estimated values of *a* and *b* reflect the characteristics of regional population agglomeration and diffusion at different stages. The estimates of regional population density *a* showed that all six centers had an upward trend in their population density estimates. This reflected the overall trend of population concentration in Shandong Province toward urban areas. In terms of changes in *b* value of the population density gradient, both the Jinan and Qingdao centers exhibited a decrease in the *b* value during the study period, demonstrating continuous outward population diffusion. This reflected the spatially evolving characteristics of the population structure of the center's growth-based diffusion pattern, where the center's population density increased while the population density gradient decreased. This indicated that Jinan and Qingdao grew stronger as centers while driving the development of other districts and counties within their spheres of influence, with a high degree of center development. The Zibo, Yantai, and Weifang centers displayed a generally weak upward trend, with the population density gradient increasing but not changing significantly. This reflected the centripetal concentration pattern of the population and the fact that the three areas were relatively "weak" centers. The population density gradient in the Dezhou center demonstrated a decline followed by an increase, indicating that the Dezhou center had not yet shown a strong agglomeration ability from 2000 to 2010. The regional population distribution was mainly dominated by centers such as Jinan, Qingdao, and Zibo, while the agglomeration effect gradually emerged after 2010, displaying a trend of population agglomeration toward the center.

3.3 Further discussion on population agglomeration and diffusion

To further explore the spatial variation pattern of population dispersion in Shandong Province, we first visualized the population growth rate during the study period using ArcGIS, and the results are shown in **Figure 5**. Overall, there were significantly more areas with positive population growth rates from 2000 to 2010 than from 2010 to 2020, and the areas with higher population growth rates were broadly concentrated in the central districts and counties of the cities. Specifically, from 2000 to 2010, the population growth rate in the western region of Shandong Province was higher than that in the eastern region, with a contiguous positive regional distribution of

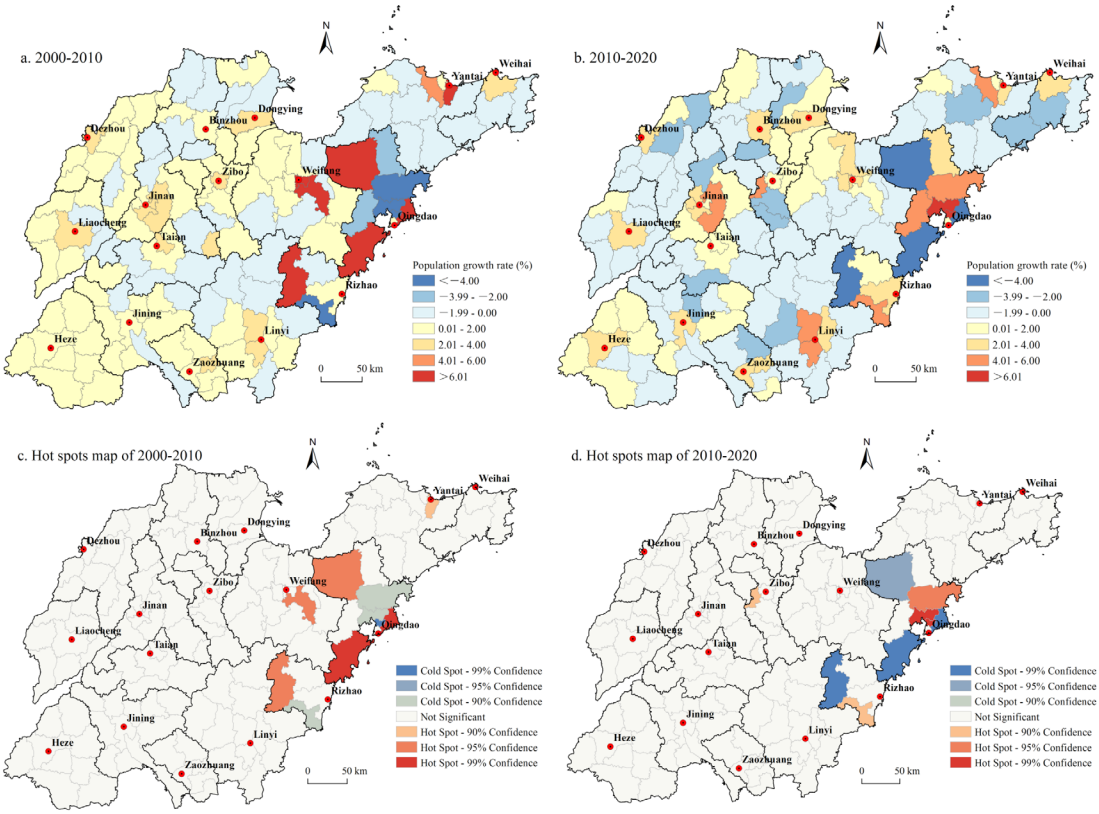

Figure 5. Population growth rate map and distribution map of hot and cold spots in Shandong Province.

growth rates. However, the eastern regions of Pingdu City, Kuiwen District, Fangzi District, Laoshan District, Huangdao District, Laishan District and Ju County had the highest population growth rates. The regions with the lowest population growth rates, namely Jimo, Chengyang, Licang, and Lanshan, were also located in the eastern part of Shandong Province. This indicated that the population growth rate varied more among districts and counties in the eastern region and less among districts and counties in the western region. For the period 2010-2020, regions with negative population growth rates constituted the majority. The population growth rate between city center districts and peripheral districts increased further. This reflected a further strengthening of population agglomeration and a more pronounced polarization effect of the centers. It is worth noting that most of the regions with the highest growth rates in the period 2000-2010 had growth rates of less than –4% in the period 2010-2020. In contrast, the regions with the lowest growth rates in the period 2000-2010 almost all saw their growth rates increase above 4% in the period 2010-2020.

Based on the characteristics of the population growth rate of each county and district in Shandong Province, this study further explored the agglomeration and diffusion characteristics using cold and hot spot analyses. As shown in **Figure 5c**, the spatial variations in the cold and hot spot areas from 2000 to 2010 were small, with more hot spot areas than cold spot areas. Specifically, there are six hotspot areas, mainly in the eastern part of Shandong Province, including Pingdu City, Fangzi District, Laoshan District, Huangdao District, Leshan District, and Juxian County. There are four cold spots: Jimo District, Chengyang District, Licang District, and Lanshan District, which are more concentrated than the hot spots. **Figure 5d** shows that there was some replacement of cold and hot spot zones in 2010-2020 compared with those in 2000-2010. Four cold spot zones—Pingdu City, Laoshan District, Huangdao District, and Ju County—were hot spot zones during the last time period. There are five hotspot zones: the Zhoucun, Lanshan, Jimo, Chengyang, and Licang

Districts. Except for Zhoucun District, the other four districts were cold spots during the last time period.

In summary, the population agglomeration effect in the central districts and counties of Shandong Province was increasing. Variations in population size were more significant along the eastern coastal area than in the inland area, and the phase of population growth rates along the eastern coastal area was more evident over the study period.

4. Conclusions and limitations

4.1 Conclusions

This study analyzed the distribution of population density in counties in Shandong Province based on data from the 2000, 2010, and 2020 censuses. To directly reflect the spatial relationship of the population distribution, this study used the IDW. On this basis, the monocentric and polycentric regional density functions were applied to study the characteristics of population agglomeration and diffusion in Shandong Province, and the changes in the population growth rate and variations in cold and hot spots were further analyzed over a twenty-year period. The results indicated that the spatial distribution of the population in Shandong Province was uneven, with obvious differences in population size and changes between districts and counties. With urban areas as the center of population concentration, a multi-center spatial structure was formed, and six central cities dominated the spatial distribution trend of regional population density, including Jinan, Qingdao, Zibo, Yantai, Weifang, and Dezhou centers. Methodological and conclusive differences between monocentric and polycentric regional density functions were compared. The polycentric regional density function exhibited a better fit and was more applicable than the monocentric model. The results of the monocentric regional density function analysis showed a clear and increasing trend toward the centripetal agglomeration of regional centers over the study period, but the ability to agglomerate and the difference in the rate of population growth between the center and hinterland differed. Conversely, the polycentric regional density function reflected that some of the centers displayed a spatial trend of diffusing outward, and that different levels of centers exhibited different patterns of population agglomeration and diffusion. The spatial statistical analysis of population density growth further validated the polycentric density function. The multicenter regional density function reflected the trend of population density change more accurately and precisely because of the comprehensive consideration of the influence of multiple centers on the distribution of population density.

4.2 Limitations

The study of the characteristics of regional population density distribution is important for identifying the characteristics of regional spatial structure development. In this study, monocentric and polycentric regional density functions were discussed, and the analysis and comparison were relatively complete. However, this study only started with demographic data, as a more diverse range of socioeconomic data was required for a comprehensive analysis of the regional spatial structure. Simultaneously, the distribution of the population density is influenced by economic, social, and natural factors, and further exploration of the mechanisms that influence the spatial structure of the population is needed. In addition, this study was based on county data and did not discuss the spatial structure of the population of Shandong Province in sufficient detail; a more comprehensive study could be conducted in the future using data from smaller-scale geographical units.

Author Contributions

Conceptualization (Chen YB). Methodology (Chen YB, Zhao XH). Software (Chen YB, Zhao XH). Formal analysis (Zhao XH). Resources (Zhao XH). Data curation (Zhao XH). Writing of the original draft (Zhao XH). Writing, reviewing, and editing (Chen YB). Visualization (Zhao XH). Supervision (Chen YB).

Conflict of Interest

There is no conflict of interest.

Funding

This research was funded by the Shandong Provincial Natural Science Foundation (grant number ZR202102240088).

References

[1] Bontje, M., 2001. Dealing with deconcentration: population deconcentration and planning response in polynucleated urban regions in Northwest Europe. Urban Studies. 38(4), 769-785.
DOI: https://doi.org/10.1080/00420980120035330

[2] Salvati, L., Carlucci, M., 2016. In-between stability and subtle changes: Urban growth, population structure, and the city life cycle in Rome. Population Space and Place. 22(3), 216-227.
DOI: https://doi.org/10.1002/psp.1877

[3] Kabisch, N., Haase, D., Haase, A., 2012. Urban Population development in Europe, 1991-2008: The examples of Poland and the UK. International Journal of Urban and Regional Research. 36(6), 1326-1348.
DOI: https://doi.org/10.1111/j.1468-2427.2012.01114.x

[4] Wang, F.H., 2001. Regional density functions and growth patterns in major plains of China, 1982-1990. Papers in Regional Science. 80(2), 231-240.
DOI: https://doi.org/10.1007/PL00013624

[5] Jia, P., Qiu, Y.L., Gaughan, A.E., 2014. A fine-scale spatial population distribution on the high-resolution gridded population surface and application in Alachua County, Florida. Applied Geography. 50, 99-107.
DOI: https://doi.org/10.1016/j.apgeog.2014.02.009

[6] Murray, A.T., Davis, R., Stimson, R.J., et al., 1998. Public transportation access. Transportation Research Part D: Transport and Environment. 3(5), 319-328.
DOI: https://doi.org/10.1016/S1361-9209(98)00010-8

[7] Li, J.G., Li, J.W., Yuan, Y.Z., et al., 2019. Spatiotemporal distribution characteristics and mechanism analysis of urban population density: A case of Xi'an, Shaanxi, China. Cities. 86, 62-70.
DOI: https://doi.org/10.1016/j.cities.2018.12.008

[8] Clark, C., 1951. Urban population densities. Journal of Royal Statistics Society. 114(4), 490-496.
DOI: https://doi.org/10.2307/2981088

[9] Cheng, L., 2014. Zhong guo qu yu ren kou mi du mo xing ji jing ji zeng zhang de kong jian mo shi (Chinese) [Regional population density function and spatial patterns of economic growth in China] [Ph.D.'s thesis]. Changchun: Northeast Normal University. p. 8-9.

[10] Parr, J.B., 1985. A population—density approach to regional spatial structure. Urban Studies. 22(4), 289-303.
DOI: https://doi.org/10.1080/00420988520080531

[11] Barkley, D.L., Henry, M.S., Bao, S., 1996. Identifying "Spread" versus "Backwash" effects in regional economic areas: A density functions approach. Land Economics. (72), 336-357.

[12] Limtanakool, N., Dijst, M., Schwanen, T., 2007. A theoretical framework and methodology for characterising national urban systems on the basis of flows of people: Empirical evidence for France and Germany. Urban Studies. 44(11), 2123-2145.
DOI: https://doi.org/10.1080/00420980701518990

[13] Subasinghe, S., Wang, R., Murayama, Y., 2022. Modelling spatial pattern of population distribution in 50 largest cities in the world: A geospatial approach. IOP Conference Series: Earth and Environmental Science. 1109(1), 012065.
DOI: https://doi.org/10.1088/1755-1315/1109/1/012065

[14] Heikkila, E., Gordon, P., Kim, J., et al., 1989. What happened to the CBD—distance gradient? Land values in a polycentric city. Environment and Planningn A. 21(2), 221-232.

[15] Small, K.A., Song, S., 1994. Population and employment densities: Structure and change. Journal of Urban Economics. 36, 292-313.

DOI: https://doi.org/10.1006/juec.1994.1037

[16] McMillen, D.P., McDonald, J.F., 1998. Suburban subcenters and employment density in metropolitan Chicago. Journal of Urban Economics. 43(2), 157-180.
DOI: https://doi.org/10.1006/juec.1997.2038

[17] Joseph, M., Wang, F.H., 2010. Population density patterns in Port-au-Prince, Haiti: A model of Latin American city? Cities. 27(3), 127-136.
DOI: https://doi.org/10.1016/j.cities.2009.12.002

[18] Zhou, Ch.S., Xu, X.Q., 1997. Guang zhou shi ren kou kong jian fen bu te zheng ji yan bian qu shi fen xi (Chinese) [Population distribution and its change in Guangzhou city]. Tropical Geography. 17(1), 53-60.

[19] Wang, F.H., Zhou, Y.X., 1999. Modelling urban population densities in Beijing 1982-90: Suburbanisation and its causes.Urban Studies. 36(2), 271-287.
DOI: https://doi.org/10.1080/0042098993600

[20] Luo, J., Wei, Y.D., 2006. Population distribution and spatial structure in transitional Chinese cities: A study of Nanjing. Eurasian Geography and Economics. 47(5), 585-603.
DOI: https://doi.org/10.2747/1538-7216.47.5.585

[21] Wang, F.H., Meng, Y., 1999. Analyzing urban population change patterns in Shenyang, China 1982-90: Density function and spatial association approaches. Geographic Information Sciences. 5(2), 121-130.
DOI: https://doi.org/10.1080/10824009909480521

[22] Feng, J., Zhou, Y.X., 2003. Jin 20 nian lai bei jing dou shi qu ren kou zeng zhang yu fen bu (Chinese) [The growth and distribution of population in Beijing Metropolitan Area (1982-2000)]. Journal of Geographical Sciences. 58(6), 903-916.
DOI: https://doi.org/10.11821/xb200306014

[23] Wu, W.Y., Ma, X.Y., 2006. Duo zhong xin cheng shi ren kou mo xing ji mo ni: Yi shang hai wei li (Chinese) [Polycentric population density functions and modelling: The case of Shanghai]. Modern Urban Research. 21(12), 39-44.
DOI: https://doi.org/10.3969/j.issn.1009-6000.2006.12.008

[24] Jiang, L., Wu F.L., 2013. Guang zhou ren kou kong jian fen bu bian dong yu duo zhong xin cheng shi kong jian jie gou yan hua ce du (Chinese) [Guangzhou population spatial distribution and polycentricity spatial structure evolution]. Tropical Geography. 33(2), 147-155.
DOI: https://doi.org/10.13284/j.cnki.rddl.002318

[25] Sun, T.Sh., Li, G.P., Lu, M.H., 2009. Jing jin ji dou shi quan ren kou ji ju yu kuo san ji qi ying xiang yin su: Ji yu qu yu mi du han shu de shi zheng yan jiu (Chinese) [Concentration and decentralization of population in the Beijing-Tianjin-Hebei metropolitan region and its determinants: A regional density function approach]. Acta Geographica Sinica. 64(8), 956-966.
DOI: https://doi.org/10.11821/xb200908007

[26] Liu, N.Q., Deng, M., 2018. Duo zhong xin jie gou mo shi yu zhang san jiao cheng shi qun ren kou kong jian fen bu you hua (Chinese) [Urban spatial structure and optimization of population distribution in Yangtze River Delta Region]. Review of Industrial Economics. 27(4), 91-103.
DOI: https://doi.org/10.19313/j.cnki.cn10-1223/f.2018.04.007

[27] Hong, Sh.M., Hao, J.M., 2018. Huang huai hai ping yuan ren kou kong jian jie gou ji qi yan bian te zheng yan jiu (Chinese) [Spatial structure of population and characteristics of evolution in Huang-Huai-Hai Plain]. Resource Development & Market. 34(11), 1526-1532+1557.
DOI: https://doi.org/10.3969/j.issn.1005-8141.2018.11.008

[28] Dong, L.F., Wang, L.L., Shao, J.H., et al., 2012. Jin 20 nian lai shan dong sheng ren kou fen bu kong jian ge ju ji qi yan bian te zheng fen xi (Chinese) [Population spatial distribution pattern and evolution characteristics of Shandong province in recent 20 years]. Territory & Natural Resources Study. 138(3), 11-13.
DOI: https://doi.org/10.16202/j.cnki.tnrs.2012.03.031

[29] Li, W.X., Sun, X.H., 2007. Ji yu GIS de shan dong sheng ren kou zhong xin qian yi yan jiu (Chinese) [Study of the migration of population

gravity center in Shandong Province based on GIS]. Journal of Shandong Normal University. 99(3), 83-86.
DOI: https://doi.org/10.3969/j.issn.1001-4748.2007.03.026

[30] Wang, J., Yang, X.H., Shi, R.X., 2012. Shan dong sheng ren kou kong jian fen bu ge ju de duo chi du fen xi (Chinese) [Spatial distribution of the population in Shandong Province at multi-scales]. Progress in Geography. 31(2), 176-182.
DOI: https://doi.org/10.11820/dlkxjz.2012.02.006

[31] McDonald, J.F., 1989. Econometric studies of urban population density: A survey. Journal of Urban Economics. 26(3), 361-385.
DOI: https://doi.org/10.1016/0094-1190(89)90009-0

[32] Liu, Zh.D., Luo, Sh.F., Lin, Zh.W., et al., 2021. Shan dong sheng ren kou cheng zhen hua de shi kong te zheng ji kong jian xiao ying yan jiu (Chinese) [Study on spatial-temporal characteristics and spatial effects of population urbanization in Shandong Province]. Qu Journal of Qufu Normal University (Natural Science). 47(4), 112-119.

[33] Li, Ch.P., 2015. Xin xi liu shi jiao de shan dong sheng cheng shi wang luo te zheng yan jiu (Chinese) [City network structure of Shandong Province based on information flow]. Journal of Arid Land Resources and Environment. 29(12), 51-56.
DOI: https://doi.org/10.13448/j.cnki.jalre.2015.399

[34] Yang, Q., 1990. Qu yu ke liu fen bu mo xing de yan jiu (Chinese) [A model for interregional trip distribution in China]. Acta Geographica Sinica. 45(3), 264-274.
DOI: https://doi.org/10.11821/xb199003002

[35] Wang, F.H., 2014. Quantitative methods and socio-economic applications in GIS. CRC Press: Boca Raton. pp. 127.

[36] Ohlert, P.L., Bach, M., Breuer, L., 2023. Accuracy assessment of inverse distance weighting interpolation of groundwater nitrate concentrations in Bavaria (Germany). Environmental Science and Pollution Research. 30(4), 9445-9455.
DOI: https://doi.org/10.1007/s11356-022-22670-0

[37] Ghorbani, Z., Sexton, A., Van Loon, L.L., et al., 2023. Biogeochemical prospecting for gold at the Yellowknife City Gold Project, Northwest Territories, Canada: Part 2-Robust statistical analysis. Applied Geochemistry. 149, 105559.
DOI: https://doi.org/10.1016/j.apgeochem.2023.105559

[38] Ashraf, M., Loftis, J.C., Hubbard, K.G., 1997. Application of geostatistics to evaluate partial weather station networks. Agricultural and Forest Meteorology. 84(3), 255-271.
DOI: https://doi.org/10.1016/S0168-1923(96)02358-1

[39] Zhang, K., Wang, Zh.R., 2023. LTPP data-based investigation on asphalt pavement performance using geospatial hot spot analysis and decision tree models. International Journal of Transportation Science and Technology. 12(2), 606-627.
DOI: https://doi.org/10.1016/j.ijtst.2022.06.007

[40] Ord, J.K., Getis, A., 1992. The analysis of spatial association. Geogrphical Analysis. 24(3), 189-206.
DOI: https://doi.org/10.1111/j.1538-4632.1992.tb00261.x

[41] Tan, M.H, Li, X.B., Lu, C.H., et al., 2008. Urban population densities and their policy implications in China. Habitat International. 32(4), 471-484.
DOI: https://doi.org/10.1016/j.habitatint.2008.01.003

[42] Li, P., Xu, Y.T., 2011. Shan dong sheng ren kou kong jian fen bu te zheng fen xi (Chinese) [Characteristic study on the spatial distribution of Shandong Population]. Ludong University Journal (Natural Science Edition). 27(3), 274-278.
DOI: https://doi.org/10.3969/j.issn.1673-8020.2011.03.021

[43] Mao, Q.Zh., Long, Y., Wu, K., 2015. Zhong guo ren kou mi du shi kong yan bian yu cheng zhen hua ge ju chu tan—cong 2000 nian dao 2010 nian (Chinese) [Spatial-temporal changes of population density and exploration on urbanization pattern in China: 2000-2010]. City Planning Review. 39(2), 38-43.

[44] Zhang, P.F., Xu, Y.T., 2019. Ji yu GIS de shan dong sheng ren kou fen bu shi kong ge ju ji ying

xiang yin su fen xi (Chinese) [Spatial temporal pattern and influencing factors of population distribution in Shandong Province based on GIS]. Anhui Agricultural Science Bulletin. 25(9), 158-162.
DOI: https://doi.org/10.3969/j.issn.1007-7731.2019.09.063

[45] Pang, Y., Lian, H., Wang, L., 2019. De zhou shi xian yu cheng zhen hua shui ping ce du ji qi fen yi yan jiu (Chinese) [Study on the measurement and dissimilarity of urbanization level of Dezhou County]. City. 227(2), 53-60.

[46] Zhu, Y., 2021. Ke xue gou jian jiao dong ban dao jing ji quan yi ti hua zhan lue ge ju (Chinese) [Scientifically constructing an integrated strategic pattern of the Jiaodong Peninsula economic circle]. China Journal of Commerce. 830(7), 12-14.
DOI: https://doi.org/10.19699/j.cnki.issn2096-0298.2021.07.012

[47] Gao, Q., 2019. De zhou cheng zhen hua fa zhan bu ping heng bu chong fen wen ti qian xi (Chinese) [Analysis of unbalanced and inadequate urbanization development in Dezhou]. Modern Economic Information. 14, 498.

[48] Cai, Y.J., 2021. Ji yu duo yuan shu ju de ji nan dou shi quan tong cheng hua jin cheng ji qi ying xiang yin su yan jiu (Chinese) [Research on the process and influencing factors of urban integration of Jinan Metropolitan Area based on multi-source data] [Master's thesis]. Jinan: Shandong Normal University. p. 22.

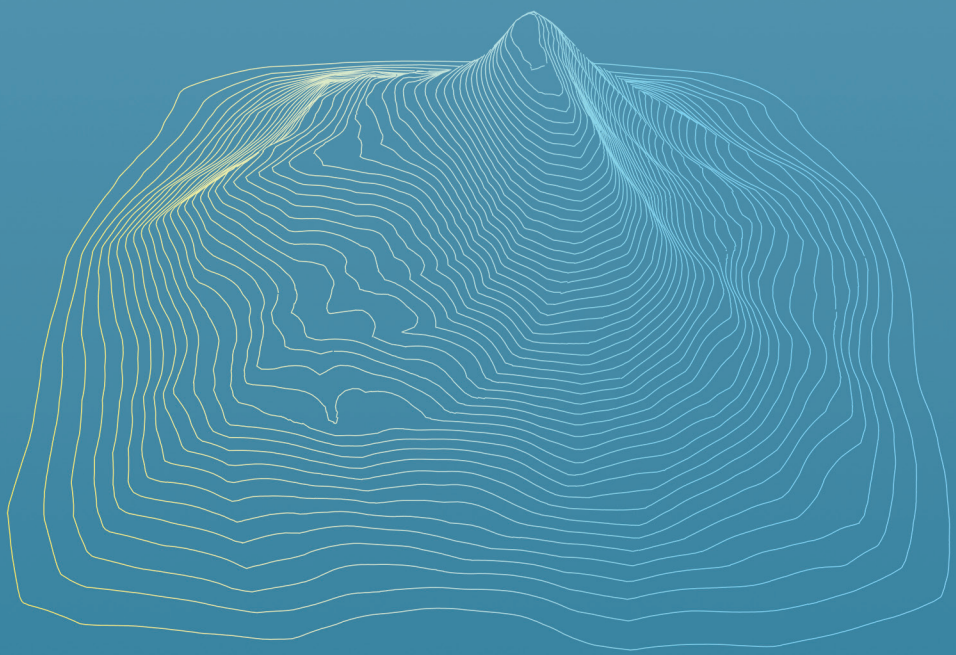

BILINGUAL PUBLISHING GROUP
Tel:+65 65881289
E-mail: contact@bilpublishing.com
Website:https://journals.bilpubgroup.com

2630-5070 03
9 772630 507235